ABSTRACT

Title of Document: MEASUREMENTS AND ANALYSIS OF EXTINCTION IN VITIATED FLAME SHEETS

Justin Wade Williamson, Doctor of Philosophy, 2009

Directed By: Professor André Marshall, Department of Fire Protection Engineering

Accidental fires present many challenging hazards to people and property. The thermal and toxic effects of fires are significantly affected by the ventilation conditions supplied to the fire. Vitiation is a consequence of limited ventilation, where the products of combustion mix with the unburned reactants prior to reaction. Vitiation results in diluting and preheating the reactants, significantly enhancing the behavior of the fire. An interesting effect of vitiation is the increased propensity of the flame to experience extinction, either locally or globally. Likewise, there are other factors that can increase the propensity for extinction, including losses due to incomplete chemical kinetics, radiation, and conduction. These extinction events have a direct impact on the thermal and toxic hazards associated with accidental fires by creating holes in the reaction surface. This research provides a detailed analysis of local flame extinction by examining the behavior of counterflow flames undergoing kinetic losses, radiation losses, and vitiation. A thorough review of flame extinction

theory was conducted to determine the appropriate parameters necessary for characterizing local flame extinction conditions. Simple scaling arguments are presented to demonstrate that each of these parameters is significant in accidental fires. Counterflow methane-air diffusion flames have been studied experimentally and numerically with OPPDIF to systematically examine the effects of each parameter on local flame extinction. Furthermore, a model is presented, which uses reactant composition and temperature in the vicinity of the flame, net radiation losses from the flame, and the local scalar dissipation rate as inputs to model local extinction conditions. The proposed model is suitable for integration into Computational Fluid Dynamics (CFD) codes used to predict the hazards associated with accidental fires.

MEASUREMENTS AND ANALYSIS OF EXTINCTION IN VITIATED FLAME SHEETS

By

Justin Wade Williamson

Dissertation submitted to the Faculty of the Graduate School of the
University of Maryland, College Park, in partial fulfillment
of the requirements for the degree of
Doctor of Philosophy
2009

Advisory Committee:
Associate Professor André Marshall, Chair
Associate Professor Christopher Cadou, Dean's Representative
J.L. Bryan Professor James Quintiere
Assistant Professor Peter Sunderland
Associate Professor Arnaud Trouvé

Acknowledgements

This work was supported by the National Institute of Standards and Technology (Grant 70NANB4H1089) and managed by Dr. Jiann Yang, Fire Metrology Group Leader of the NIST Building and Fire Research Laboratory. I would also like to acknowledge Dr. Filippo Gavelli from Exponent for the internship opportunity they provided.

Many people have directly contributed to the success of this work. I would like to thank the professors and staff of the Department of Fire Protection Engineering for their varied contributions to this research. Primarily among them, I would like to acknowledge my advisors Professors André Marshall, Arnaud Trouvé, James Quintiere, and Peter Sunderland for their valued guidance in all stages of my research and professional development. Mr. Sigfried Dobrotka deserves accolades for the work done to develop the counterflow burner used in this study. This research was also a product of the collaborative efforts of the ventilation limited compartment fire research group, including substantial contributions from Dr. Yunyong Utiskul, Mr. Zhixin Hu, Mr. Vivien Lecoustre, and Mr. Mizukami Tensei. I would also like to thank Dr. Xiaobo Yao, Dr. Carlos Cruz and Mr. Praveen Narayanan for the productive and insightful discussions we have shared.

Finally, I must acknowledge my wife, Marjorie Williamson, for her patience, dedication and support throughout. Her contributions are immeasurable.

Table of Contents

List of Tables

List of Figures

Nomenclature

a	Dimensionless Flame Temperature
A	Arrhenius Rate Model Pre-exponential Factor (s^{-1})
a_g	Global Strain Rate (s^{-1})
a_t	Turbulent Strain Rate (s^{-1})
b	Reaction Order Constant
B	Mean Beam Length Corrector Factor
c	Reaction Order Constant
c_p	Constant Pressure Specific Heat (J/kg-K)
d	Separation Distance (m)
D	Pool Diameter (m)
Da	Damköhler Number
D_{th}	Thermal Diffusivity (m^2/s)
E	Activation Energy (J/mol)
F	Dimensionless Radiant Loss Parameter
f_v	Soot Volume Fraction (ppmv)
H	Enthalpy Deficit Parameter
Le	Lewis Number, $D_{th}/D = Sc/Pr$
l_f	Arrhenius Modeled Radiant Loss
l_t	Turbulent Integral Length Scale (m)
$\dot{m}''_\infty$	Reference Fuel Mass Flux (kg/m^2)
$\dot{q}'''_{rad}$	Local Radiative Energy Loss (W/m^3)
$\dot{q}''_{rad}$	Integral Radiative Energy Loss (W/m^2)
$\dot{q}'''_{gen}$	Local Energy Production (W/m^3)
$\dot{q}''_{gen}$	Integral Flame Energy Production (W/m^2)
$\dot{Q}$	Total Energy Release Rate (W)
R	Ideal Gas Constant (J/K-mol)
r_s	Stoichiometric Oxygen to Fuel Mass Ratio
Re_t	Turbulent Reynolds Number
t_{chem}	Characteristic Chemical Time (s)
t_{mix}	Characteristic Mixing Time (s)
T	Temperature (K)
T_a	Activation Temperature, E/R (K)
T_c	Critical Flame Temperature (K)
T_u	Unburned Reactant Mixing Temperature (K)
$u_{0,\max}$	Mean Centerline Velocity at the Flame Tip (m/s)
u'	RMS Velocity Fluctuation (m/s)

U	Inlet Velocity (m/s)
U_r	Velocity Ratio
V_k	Kolmogorov Velocity Scale (m/s)
x	Stream-Wise Location (m)
Y	Mass Fraction
Z	Mixture Fraction

Symbols

β	Zel'dovich Number
χ	Scalar Dissipation Rate (s^{-1})
δ_{gen}	Reaction Zone Integral Length Scale
Δh_c	Heat of Combustion from Fuel Consumption (J/kg)
Δh_{O_2}	Heat of Combustion from O_2 Consumption (J/kg)
ΔT_0	Temperature Increase at the Flame Tip (K)
ϕ	Equivalence Ratio
φ	Variable Density Correction Factor
γ	Radiant Loss Sensitivity to Temperature
Γ	Radiative Fraction
η_k	Kolmogorov Length Scale (m)
κ	Planck Mean Absorption Coefficient (m^{-1})
ν	Kinematic Viscosity (m^2/s)
Θ	Temperature Ratio
ρ	Density (kg/m^3)
∂	Partial Derivative
∇	Gradient

Subscripts

BS	Burke-Schumann Flame Temperature
crit	Extinction Condition
F	Fuel Property
gen	Energy Generation
O_2	Oxidizer Property
rad	Net Radiative Loss
st	Evaluated at Stoichiometric Mixture Fraction

Superscripts

amb	Ambient Condition
rad	Corrected for Radiation Losses
ref	Reference Condition
+	OPPDIF Parameter Space
∞	Local Vitiated Reactant Property

Chapter 1: Introduction

1.1 Background and Motivation

1.1.1 Accidental Fires

Accidental fires present profound hazards to people and property. The heat produced by accidental fires can result in significant thermal property damage and personal injury, while the smoke produced by accidental fires can also have significant toxic effects. Fire protection professionals are often interested in predicting the hazards of these fires to people and property, to support the development of adequate protection [1]. One of the predictive tools commonly used by fire protection professionals are Computational Fluid Dynamics (CFD) codes that can incorporate combustion and heat transfer among many other phenomena [2]. These codes have advanced in parallel with computational power, and further improvements in computer technology warrant increasing the complexity of the models used therein. Particularly in the area of combustion, early CFD codes capable of simulating full-scale accidental fires used simplified methods to predict the combustion behavior of the fire. Over-simplified combustion models can produce non-physical results depending on the implementation of the model. The errors associated with these non-physical behaviors can greatly impact the prediction of heat release and toxic products of combustion from fires. Knowledge of this weakness has led to the development of more robust models for combustion. The research detailed

in this document will provide insight to support the enhancement of current combustion models based on theories developed from fundamental combustion research pertaining to local flame extinction. This research is presented with the hope of improving the accuracy of hazard predictions, both thermal and toxic, from CFD codes.

One classical accidental fire configuration is the unconfined fire, where there is a fuel source in an unperturbed open environment [3]. The unconfined fire produces heat and smoke in rates that are dependent on the size of the fuel source. When the fuel reacts with the surrounding air, the products of combustion increase in temperature and convect upward based on buoyancy. This buoyancy-induced flow drives the entrainment of fresh air from the surroundings to react with the fuel, resulting in a stable self-sustaining fire. Observations of small-scale unconfined fires on the order of the size of a candle indicate that the reaction of the fuel and air is complete as indicated by very small quantities of soot released as smoke. As the scale of the unconfined fire is increased, the proportion of sooty smoke released increases dramatically. Scaling of turbulent unconfined fires demonstrates that more than enough air is entrained to completely oxidize the fuel, but some fraction of the fuel does not react completely [1]. This incomplete combustion is obvious by observations of large quantities of black sooty smoke, and also the presence of carbon monoxide (CO) and other unburned hydro-carbons (UHC) [4]. It is clear that if CFD codes are to accurately predict the combustion behavior of these large, unconfined fires, the combustion models built into the code must be able to account for an incomplete

reaction of fuel for large-scale fires, while maintaining the capability to predict nearly complete reactions for small-scale fires.

The compartment fire is a classical accidental fire configuration in which a fire is enclosed within a compartment with limited ventilation for the fire [5,6]. The compartment fire behaves differently from an unconfined fire, based primarily on the limited ventilation caused by the compartment. Conversely, an unconfined fire has no restriction for entraining air. The buoyancy of hot products of combustion controls the rate at which an unconfined fire entrains air, and the unconfined fire easily entrains many times the mass of air required to burn the fuel completely. This is not necessarily the case with compartment fires. Buoyancy still drives the flow of gases in and out of the compartment, but the geometry of the ventilation can significantly restrict the flow of gases. In compartments, the fire may not entrain enough air to burn the fuel completely. Products of combustion may also remain within the compartment to interact with the fire. These ventilation effects have been studied at length, and they have a profound impact on the fire behavior [5,6]. Among the effects of ventilation-limited combustion is increased production of CO, soot and unburned fuel, as well as a reduction in the production of heat, with the possibility of global extinction of the fire. Each of these effects has a major impact on the predictability of hazards resulting from compartment fires. It is clear that if CFD codes are to accurately predict the behavior of compartment fires, the combustion models built into the code must be able to account for an incomplete reaction of fuel based on the level of ventilation available, as well as the interaction of the fire with the product gases inside the compartment.

The unconfined fire and the compartment fire are just two examples of how accidental fires can demonstrate dramatically different behaviors based on scale and ventilation. Likewise, there are many other configurations that will show various changes in behavior based on variation of key parameters. It is also important to recognize that some CFD codes are generalized to the point that they are used in all of these configurations, without requiring modification of the code. This is an important feature of CFD simulation of fire that makes it useful over a huge range of input parameters. Therefore, any modifications to the combustion model must use local and instantaneous parameters that are readily available in the CFD code, and not global parameters that are dependent on configuration or time-averaged conditions.

1.1.2 Flame Vitiation

The analysis of accidental fires poses a complex, highly coupled multi-physics problem. The environmental conditions affecting fire behavior are strongly influenced by the fire itself, particularly in the compartment fire configuration. One example of this coupled, multi-physics behavior is vitiation, where products of combustion re-circulate and mix with reactants. Vitiation is characterized by reduced reactant concentration and increased reactant temperature. In the case of small, unconfined accidental fires, the oxidizer stream is pure air at ambient temperature while the fuel stream is pure gaseous fuel at a characteristic vapor temperature. However, oxidizer stream vitiation is common in under-ventilated fires, which often occur in compartments as illustrated in Figure 1. As the drawing on the left side of Figure 1 illustrates, the flame height in a compartment fire can easily extend into the smoke layer. Any oxidizer that reacts in this region must be transported through products of

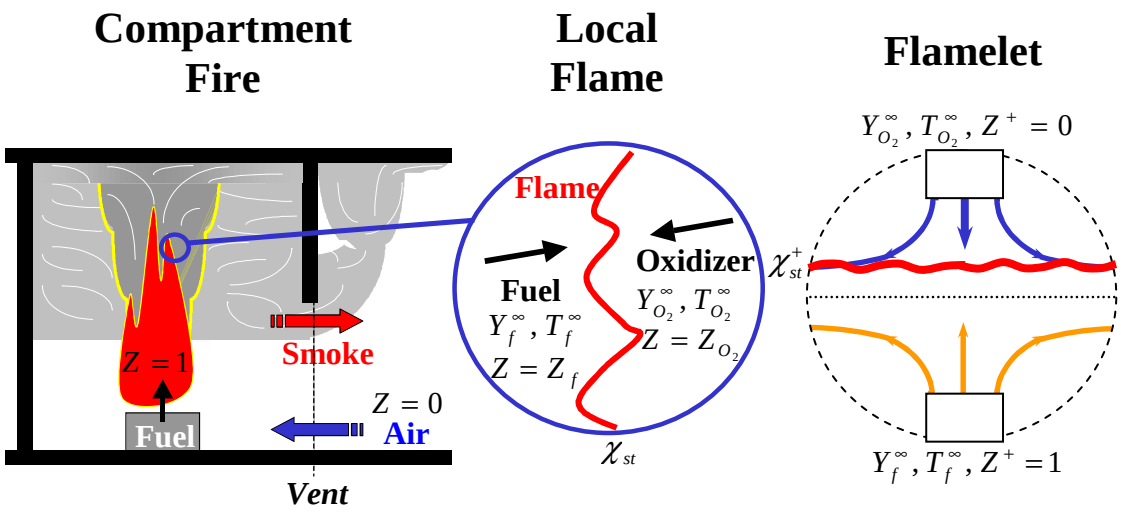

Figure 1: Compartment fire with air vitiation effects and the association between 1-D flamelet studies and local flame behavior. Local reactants are affected by dilution ($Y_{O_2}^{\infty} \leq Y_{O_2}^{amb}$) and preheating ($T_{O_2}^{\infty} \geq T_{O_2}^{amb}$).

combustion before reaching the reaction zone, and it is a reasonable assumption that this oxidizer will turbulently mix with the smoke and become vitiated. Fuel stream vitiation and mixed vitiation are also possibilities. Fuel stream vitiation can occur when a compartment fire becomes severely under-ventilated and the reaction zone moves to the vent as seen in Figure 2, or it can occur in a ceiling fire configuration inside a compartment. In either of these scenarios, fuel must transport through products of combustion before reaching the reaction zone, thus vitiating the fuel. Mixed vitiation, or the simultaneous occurrence of oxidizer and fuel vitiation, can occur because neither oxidizer vitiation nor fuel vitiation are mutually exclusive events.

The effects of vitiation can have a significant impact on the overall physical behavior of the fire. The mechanism of reactant dilution will act to reduce the intensity of the fire while the mechanism of reactant pre-heating will act to increase

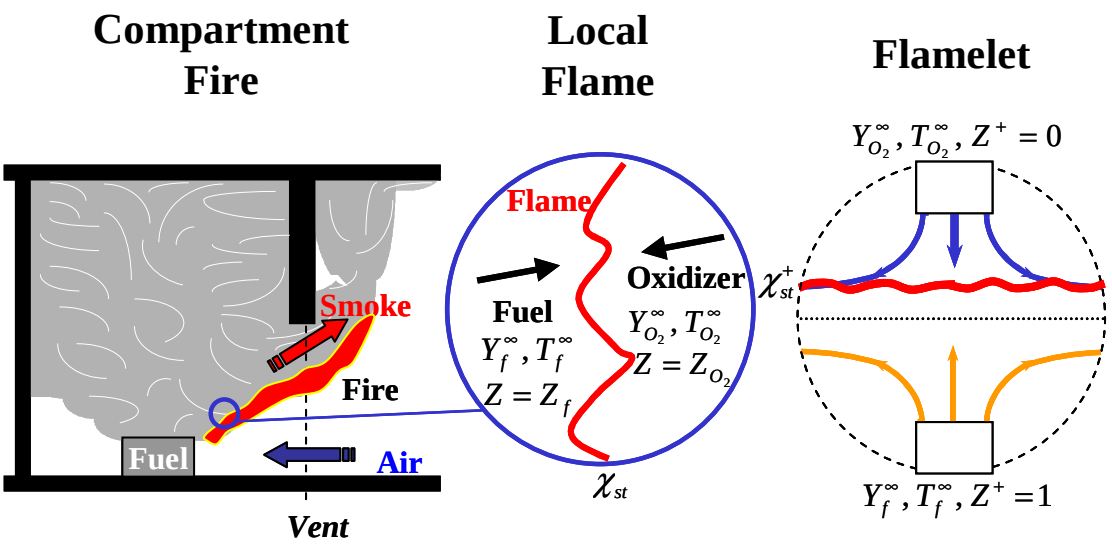

Figure 2: Compartment fire with fuel vitiation effects and the association between 1-D flamelet studies and local flame behavior. Local reactants are affected by dilution ($Y_F^\infty \leq Y_F^{amb}$) and preheating ($T_F^\infty \geq T_F^{amb}$).

the intensity of the fire. The effects of these mechanisms can include; local flame extinction, global flame extinction, modified hazardous species production, modified flame energy release rate, and modified temperatures. Combustion models in CFD codes for fire applications often use infinitely fast chemistry assumptions because of their simplicity, computational efficiency, and fidelity [2]. Unfortunately, these models are incapable of predicting extinction. In under-ventilated fires where vitiated combustion occurs, extinction must be considered to accurately predict the production of heat and the transport of unburned reactants. There is a need for extinction models suitable for integration with infinitely fast chemistry based combustion models, particularly as they apply to vitiated flame applications. Such extinction model could be used to determine critical vitiated conditions where the chemistry is sufficiently slow, which would correct the infinitely fast chemistry model where it breaks down.

It is also worth noting that fire hazard analysis is often performed to establish requirements for fire suppression or extinguishment. Physical understanding and modeling of vitiated extinction will also be useful for fire suppression applications utilizing reactant dilution and cooling. The purpose of this work is to develop a simple model to predict local flame extinction from measurable vitiation conditions and provide guidance on the application of this model to infinitely fast combustion.

In order to study the effects of vitiation, it is important to identify the composition of the product gases that will be mixing with the reactants. Examination of the chemical expression for stoichiometric burning of methane in air:

$$CH_4 + 2(O_2 + 3.76N_2) \rightarrow CO_2 + 2H_2O + 7.52N_2$$

demonstrates that product gases are produced in the ratios of 9.5% CO_2, 19% H_2O and 71.5% N_2 by volume. In fact, N_2 will always be the dominant species by mass in product gases for methane burning in air up to equivalence ratios of 4. The other major species, CO_2 and H_2O, are smaller diluent contributors than N_2; however, there are other minor species that exist in real product gases that deserve notice. These secondary product gases include but are not limited to CO, C (soot), and UHC. These species are not chemically stable, and they can all react exothermically with O_2 or they can contribute to slower secondary reactions away from the flame [7-9]. The reactive nature of these minor species can prove challenging when studying the primary impacts of dilution. This coupled with the fact that it is impossible to determine the ratios with which these species will occur in real fires makes control of a system with real vitiation virtually impossible. This study examines vitiation using N_2 dilution based on the fact that it is the dominant diluent species for methane

combustion. The chemical contributions from other species present in smoke are not considered. The radiative emission of CO_2, H_2O, and soot present challenges to the analysis of the system since these species are historically the largest contributors to radiative losses from the flame, especially soot. However, radiation losses are addressed in this study in a more canonical manner. First, N_2 vitiated flames are studied to evaluate non-radiative extinction. The effects of radiation losses are then studied by evaluating extinction behavior with canonically imposed radiation losses.

1.1.3 Flame Extinction

Williams first introduced the concept of flamelet theory as a means to study local combustion phenomena [10]. Flamelet theory states that a diffusion flame can be decomposed into a series of interconnected laminar flames called flamelets. This concept is illustrated in Figure 1 and Figure 2. Local flame extinction in this study is defined as the dynamic transition from a fuel-air reacting flamelet to a local fuel-air mixing system. In the limit of infinitely fast combustion, this transition occurs instantaneously; therefore the timescale of the event can be ignored. Some basic characteristics of an extinction event include: the production of product gases stops; the production of energy stops; reduction in temperature; reactant gases escaping the reaction zone; and soot and other products of fuel decomposition escaping the reaction zone. Each of these characteristics is a direct result of the combustion reaction abruptly stopping while the mixing of reactants remains. There may be secondary characteristics associated with flame extinction as well. One secondary characteristic is that unburned reactants may contribute to secondary reactions such as backdraft or premixed combustion. Other secondary characteristics that can occur are,

unburned reactants may contribute to additional vitiation, and increase the concentration of toxic gases through recirculation. These characteristics of extinction events have major implications in determining the hazards associated with an accidental fire, and therefore predicting flame extinction is necessary in order to accurately determine these hazards. The reaction rate of the fire and the gas temperature are significantly altered by extinction and play an important role in determining thermal hazards. Flame extinction is similarly important in determining the hazard from toxic gases, because the presence of CO_2, H_2O, and C allow for slow chemical reactions to become significant in the smoke layer, which will play an important role in the production of CO [7-9]. The primary goal of this study is to determine the precise effect vitiation has on flame extinction locally. This will help predict conditions in which extinction will occur and facilitate the modeling of secondary reactions by predicting the release of unburned reactants, and the temperature of these reactants.

Another important aspect of flame extinction is its relationship to fire suppression systems. Fire suppression systems can greatly reduce the energy released by a fire and even completely extinguish the fire. Many of these fire suppression systems use vitiation to control fires. These systems can cool the reactants, or they can displace and dilute the reactants. Each of these mechanisms will reduce the energy released by the fire, and may induce local or global flame extinction. Suppression systems that use mechanisms of vitiation include: water sprinklers, water mist, water with surfactant additives, water based fire extinguishers, CO_2 fire extinguishers, CO_2 flooding systems, and dry chemical fire extinguishers. Developing

an extinction model that can account for vitiation will greatly enhance the ability of simulation tools to predict the influence of fire suppression systems on any fire.

Some methods already exist to account for flame extinction. The first and most obvious method is to model the chemistry of the system directly [11]. This is a costly computational endeavor because even the simplest of fuels can result in hundreds of reactions and intermediate species, all of which would have to be included in transport equations. Detailed chemistry is typically left only for simulations of greatly simplified geometries where the transport equations can be reduced analytically. Another method for determining extinction comes from simplified finite rate chemistry approximations with high order closure of the energy generation term [12]. This method eliminates some of the weaknesses of the detailed chemistry model, but it still requires significant research in order to be applicable to various fuel types. Another method to account for flame extinction can be found in flamelet models that use state relationships to solve the chemistry [13]. These models require that a library of all the possible reactant configurations be created prior to simulation, and the products of combustion and energy release rate are determined by cross-referencing the library to the local conditions. Again, this method produces promising results, but the combustion behavior in the simulation is limited to the parameter space built into the library. Its weakness lies in the fact that it is prohibitive to develop a library for every fuel that incorporates every possible variable that can impact combustion and extinction. An underlying issue associated with all of the above models is the necessity to resolve the flame in the computational grid. Given the small length scale and dynamic nature of the flame, the computational costs can

be prohibitively high when implementing these models. Flamelet studies have led to theoretical developments in combustion modeling that are the basis of the current state-of-the-art with the intention of reducing the computational costs of flame simulation [10]. This study will provide a simple extinction model based on existing combustion theories to produce an accurate prediction of flame extinction without requiring dramatically increased computational costs that are associated with modeling finite rate chemistry.

1.2 Literature Review

To gain a comprehensive understanding of extinction in diffusion flames, one must explore some of the many areas of research where flame extinction has been observed. One scenario that is of particular importance to the fire community is the compartment fire configuration. This area has received a great deal of attention from researchers, and many have observed global and/or partial extinction in this configuration. A second and less obvious fire scenario that may produce extinction events is the unconfined accidental fire, or the classical pool fire. It has been widely observed that increasing the fuel source area results in increased production of soot and other products of incomplete combustion. These fires are known to entrain more than enough air to support the complete combustion of fuel; however, the combustion is still incomplete as indicated by the presence of copious amounts of soot. This soot suggests that some level of local flame extinction is occurring in these fires, resulting in products of incomplete combustion. A third configuration where extinction has been extensively studied is in counterflow geometry. These counterflow experiments and numerical simulation allow for specifically controlled boundary conditions and

provide a greatly simplified algorithm for characterizing extinction. A key area of research, outside of fire, where extinction has been found to be significant is in combustion systems, including internal combustion engines, high Reynolds number jets, and many others. Numerical fire simulation tools have also been developed to account for local extinction events. A review of these areas provides insight into the understanding of flame extinction and will demonstrate a clear path for developing a physically sound extinction model from existing extinction theories.

1.2.1 Extinction in Compartment Fires

Under-ventilated compartment fires are common classical fire problems that have been the focus of considerable attention by researchers. Earlier studies focused on the behavior of severely under-ventilated fires [6,14]. These studies have provided insight into the global fire phenomena that can occur when the oxygen supply to the fire is limited. Most recently, Utiskul classified the fire dynamics in scale model experiments into three burning modes, which include steady well-ventilated burning, steady under-ventilated burning, and unsteady under-ventilated burning [15]. Fundamental differences in the combustion process associated with these different burning modes must be quantified for accurate prediction of the associated fire dynamics. Some of these differences have already been explored through steady state experiments. In these experiments, turbulent diffusion flames were placed within an extended exhaust hood while ventilation was carefully adjusted until the experimental flame was partially or completely enveloped by its own exhaust [16-18]. Measurements in these 'hood' experiments were performed to assess changes to exhaust gas composition and temperature under various ventilation conditions. The

CO concentration in the exhaust gases and its relationship with the degree of ventilation were of particular interest in Beyler's experiments [16,17]. Beyler found that CO and UHC concentrations in the exhaust gases increased sharply for under-ventilated conditions with a global equivalence ratio, $\Phi > 1$. On the other hand, Morehart et al. focused on fire behavior very close to extinction in completely enveloped fires [14]. They found that no soot was produced in flames very close to extinction in this basic configuration. This result is similar to observations made in Takeda [18] and Utiskul's [15] severely under-ventilated fires. Furthermore, Morehart et al. found that limiting oxygen concentrations and temperatures at extinction for their large-scale fires compared favorably with laminar flame experiments. This result provided some evidence, albeit not yet with explanation, that extinction experiments using laminar flames may be suitable for studying large-scale fire phenomena [14].

The production of CO in compartment fires is of particular interest to the fire community for the evaluation of smoke toxicity. Under-ventilated fires have been found to enhance the global production of CO and soot [7-9,19]. The presence of these species is a preliminary indicator of local flame extinction events within the fire, even without the presence of global extinction. Furthermore, research by Tuovinen suggests local reactant properties have a significant impact on the local reaction physics [20]. Reactants at elevated temperature and reduced mass concentration when compared to their ambient conditions are defined as vitiated. Tuovinen has developed a scheme for determining local vitiation and he suggests that the reactant properties surrounding the flame sheet can be probed and used as inputs

for a combustion model [20]. This is a useful tool for sampling local vitiation, as it will impact the combustion process. Several studies have been performed that illustrate the importance of local vitiation with a focus on species production in the upper layer of compartment fires [21,22]. These studies suggest that chemistry of UHC in the upper layer may be needed to fully resolve the production of CO in compartment fires. While these studies focus on post-flame reaction behavior, development of an extinction model will provide a method for predicting and tracking the UHC in a compartment configuration. Extinction modeling is at least a preliminary tool to predict the overall production of CO and other toxic species in compartment fires.

1.2.2 Extinction in Unconfined Fires

The classical unconfined pool fire is another scenario that may result in local extinction events. For large fires it is common to observe soot, CO and even UHC in the post-flame region such that the production of these species increases with fire size [24,25]. The presence of these species suggests that local extinction may occur in large fires. These fires have been studied extensively resulting in scaling laws for burning rates [26], plume dynamics [27], and flame height [3]. The turbulent mixing in this fire configuration is of particular interest in understanding local extinction events. Extinction is known to occur when the time scales of turbulent mixing become comparable to the time scales associated with the chemical reaction of the fire. This time scale comparison forms the basis of a critical Damköhler number argument that will be discussed in further detail. In order to determine the relative importance of turbulent mixing, researchers have studied the turbulent behavior of

fires [28-30] and also non-reacting plumes [31]. These studies have established that turbulent velocity fluctuation intensities are similar for many fires and non-reacting plumes. In particular, the local RMS velocity fluctuation is approximately 25 - 35 % of the local mean velocity in the vicinity of the flame height along the centerline for fires ranging from 0.3 m to 1.0 m diameters. A measurement of these turbulence characteristics in larger fires is problematic due to the interference of soot particles with experimental diagnostics. This result will provide a useful relationship for scaling the turbulent mixing in large open pool fires. Some very useful reviews also provide guidance on the validity of the scaling equations and turbulent behavior of these fires [32,33].

1.2.3 Extinction in Counterflow Flames

The counterflow configuration has also received a great deal of attention. The counterflow flame configuration has been employed extensively to generate laminar flames, providing the capability to control the flow condition, reactant composition, and reactant temperature. Liñán sparked this field of research when he analytically characterized the structure of the counterflow flame along with providing theoretical guidance on key parameters of flame extinction [34]. The understanding of the structure of laminar flames paved the way for Williams to introduce the laminar flamelet concept. The flamelet theory provides a theoretical basis for the application of experiments and analysis of laminar flames to characterize turbulent flame behavior locally [10]. This approach requires the flame thickness to be much smaller than turbulent eddies in the flow, which is easily satisfied in typical accidental fires. This approach is known as the large Activation Energy Asymptotics (AEA). Peters,

Williams, Law and co-workers primarily have expanded the flamelet theory to produce a very comprehensive theory of flame extinction [35-39]. The AEA theory expands the understanding of the key parameters of extinction and provides guidance for correlating extinction conditions based on multiple variables. Some parameters that can be included analytically in AEA are reactant temperature, reactant concentration, fuel activation energy, and mixing rate. The effect of radiation losses and non-uniform species diffusion can also be accounted for analytically, although with considerably more complex analysis [36,39-41]. The theoretical work developed by Liñán, Williams, Peters, Law and their colleagues provides detailed analysis of experimental and numerical simulation of counterflow flames using AEA, particularly near extinction. Williams has written a comprehensive review paper describing the recent advancements in the field of AEA and counterflow flame studies [42]. Recently, AEA theory has been expanded to include the combined effects of kinetic losses, radiation losses, and general Lewis numbers [43]. Clearly, the theoretical work in AEA has demonstrated its fidelity and applicability over a wide range of conditions.

Motivated by the AEA theory, numerous experiments and analysis have been conducted to evaluate extinction criteria and near extinction behavior in counterflow flames [44-65]. The experimental work by Puri and Seshadri is particularly noteworthy, as they examined extinction at various strain rates and levels of reactant dilution. Puri and Seshadri have developed an AEA-based extinction model that accounts for variable reactant concentration, reactant temperature, and strain rate [44]. Other experimental studies have focused on the low strain rate extinction of

counterflow flames with various suppressants [45-47]. These studies illustrate the importance of chemical and thermal properties of various diluents. More recently, spherical diffusion flame experimental studies have been conducted as an alternative to studying the counterflow flame configuration [48-63]. These studies typically utilize micro-gravity [48-62] or reduced buoyancy conditions [63] in order to accurately produce a spherical diffusion flame. The spherical flames produced in these studies are typically transient in nature and frequently experience extinction due to radiative heat losses. The occurrence of extinction was an unintended consequence of microgravity combustion due to the reduction in strain, and it has therefore driven interest in characterizing the radiative losses from these flames [48-50,52,54-56,59,60]. Diluents have also been characterized to have a combination of chemical, thermal capacity, and radiative effects [59,61]. Recently, a novel burner design by Bai et al. demonstrates the ability to produce low stretch flames in normal gravity [64]. This type of design will ease in characterizing radiation losses from flames by eliminating the need for drop towers as well as the transient effects associated with spherical diffusion flames.

It is also worth noting that the counterflow flame configuration has been characterized with simplified one-dimensional partial differential equations amenable to numerical simulation with detailed chemistry [11]. The emergence of numerical simulation tools has prompted research using both experimental and numerical methods to study counterflow flames over a wide range of parameter space [66-76]. Among the parameters studied are dilution, pressure and flow field effects [72]; oscillations with radiation losses [73]; kinetic extinction compared with radiative

extinction [74-76]; and the complications caused by higher order fuels [74]. These studies have revealed that the scalar dissipation rate, as opposed to strain rate, should be used as the fundamental parameter for evaluating extinction in diffusion flames. The scalar dissipation rate is a fundamental measure of the rate of mixing combined with the effects of strain. Since both mixing and strain affect diffusion flames, the scalar dissipation rate is a more appropriate measure of flame behavior than strain alone. These studies also highlight the importance of radiation losses from the flame. Numerical studies with detailed chemistry provide substantial information about the species, temperature, and velocity fields in counterflow flames that far surpass the capacity of experimental diagnostics. Williams has examined the effect of various models used to simulate mass diffusion as a possible source of error in numerical simulation tools [70]. These errors are small in comparison to the added fidelity that numerical simulations provide over experiments.

1.2.4 Extinction in Combustion Systems

Many combustion systems designed to simulate very specific parameters that affect extinction have been developed. Some researchers have constructed simplified burners that are recognized historically as valid and repeatable. Examples include the Wolfhard-Parker burner [77,78], the Tsuji burner [79], and the Burke-Schumann burner [80]. Each of these burners is intended to create reproducible extinction of low strain flames in a manner that is well suited for experiments. These early experiments provide the basis for some simple extinction models used in infinitely fast chemistry combustion. Other researchers have examined turbulent jet combustion. These studies focus on possible finite-rate chemistry effects by characterizing the local scalar

dissipation rate and its fluctuations. Such studies illustrate the advancements in experimental diagnostics required to measure local scalar dissipation rate in fires, as well as the significance of this rate in determining local extinction events [81-83]. Others have researched the effects of conduction [84] and radiation [85] losses on combustion. These thermal loss effects can be a significant source of local extinction that cannot be ignored in a comprehensive fire model. These works provide insight into the various ways that researchers characterize and model extinction events in a wide array of configurations.

1.2.5 Numerical Simulation of Extinction

Recently, some efforts have been made to capture fire extinction in numerical fire simulations. The methods of predicting extinction vary widely with the numerical tools to which they are applied. Direct Numerical Simulation (DNS) provides a tool with which the most detailed causes and effects of local extinction can be examined. The computational cost of a DNS is prohibitive; therefore these studies are currently limited to simple geometries and small domains. Some DNS studies have been performed to specifically examine the effect of extinction. These studies have examined a variety of combustion problems, including the temporally-evolving mixing layer by Givi et al. [86], turbulent flamelets with detailed chemistry by Bastiaans et al. [13], and cold wall interactions by Yi and Trouvé [87] among many others. DNS simulation of extinction highlights the importance of thermal loss effects caused by increased strain as well as heat transfer mechanisms. Pitsch and colleagues have employed Large Eddy Simulation (LES) to examine local extinction events [12, 88-91]. These simulations employ high order moment closure turbulence modeling of

the energy equation in order to numerically simulate local extinction events. These tools are quite powerful, and much work has been done to study the capacity of these models to predict both extinction and ignition events. However, moment closure turbulence modeling requires an additional model for the source term in the energy equation, which is ill-defined in the infinitely fast chemistry framework. LES tools such as the Fire Dynamics Simulator (FDS) developed by the National Institute of Standards and Technology (NIST) utilize infinitely fast chemistry to avoid direct solution of the energy balance equation entirely [2]. This framework requires a different formulation for modeling extinction events. The development of a simple extinction model, applicable to the infinitely fast chemistry formulation is the motivation for the current work.

There has also been an attempt recently to predict partial extinction in the global context as motivated by the work of Utiskul [15]. Some zone models have been modified to account for mixing between the upper layer smoke and lower layer reactants, resulting in vitiated oxidizer [92,93]. These models produce a reduction in burning rate following a reduced oxidizer concentration, although the oxidizer temperature can increase the burning rate. These reduced fidelity zone models have computational cost orders of magnitude lower than that of DNS or LES, allowing for fast predictions of the global fire behavior.

1.3 Objectives

1.3.1 Identify Physical Parameters that Govern Extinction

The first objective of this study is to determine the basic physical parameters that govern extinction. Following the guidance of previous research suggests that extinction occurs as a result of a critical reduction in flame temperature, and therefore any variable that impacts the flame temperature should be considered. The mechanisms of vitiation have a direct impact on flame temperature and are present in a compartment fire as illustrated by Figure 1 and Figure 2. Other parameters that should be considered include any factor that causes enthalpy losses from the reaction zone, including incomplete chemistry, conduction and radiation.

1.3.2 Determine the Most Significant Parameters Governing Extinction

The second objective of this study is to demonstrate which of the physical parameters that affect flame extinction are significant in accidental fires. While it is important to capture as many physical parameters as possible, it is more important to ensure that the most significant physical parameters are captured. It is clear that the effects of vitiation will be present in any compartment fire configuration, therefore the significance of reactant concentration and temperature are undoubted. The effects that remain in question are those of kinetics, conduction and radiation. Kinetic and radiation losses can impact any portion of the flame, while conduction losses can only impact portions of the flame experiencing cold wall interactions. The effect of conduction losses from the flame can be a complex, multi-variable problem in itself,

and is the topic of ongoing research [87]. Therefore, conduction losses from the flame will be ignored in this study as a first order approximation for large accidental fires.

1.3.3 Develop an Approach to Identify Extinction Conditions

The third objective of this study is to develop an experimental and numerical approach to determine extinction conditions based on the most significant physical parameters. This will provide sufficient data to validate, invalidate, or limit the validity of any extinction model. An extinction model is only useful if it is able to reproduce the behavior of real flames. A counterflow burner capable of producing a wide range of vitiation and kinetic loss parameters was implemented in this study. Radiation losses from flames with the current experimental setup have proven insignificant compared to the effects of vitiation and reactant leakage due to kinetic effects. A numerical study of counterflow flames was also performed to observe extinction over a larger range of parameter space. The numerical study provided greater flexibility in varying vitiation, kinetic losses, and radiation losses. Moreover, the numerical tools used have proven accurate in comparison with real flames, while providing much greater detail about the flame structure, which will prove useful for diagnostic purposes. The compilation of extinction conditions determined from experiments and numerical simulations demonstrates the fidelity of the extinction model with several orders of magnitude of variation in parameter space.

1.3.4 Formulate an Extinction Model

The fourth and most significant objective of this study is to formulate a simple, physically accurate and theoretically based model to predict flame extinction

conditions. An exhaustive review of flame extinction theory was performed to compile an effective extinction model. Theoretical research regarding flame extinction has existed in the combustion community for thirty years, and it is well received and validated [34]. The existence of this robust theory for three decades without being widely used by the fire safety community is due largely to the fact that the theory is not written in a context that the fire safety community understands. This work will serve as a translation of the works performed by the combustion community into terms that are useful for the fire safety community. The model includes all of the major contributing parameters for extinction such that it can capture variations in any of these parameters simultaneously, as validated by experimental and numerical data. This model will be well suited for integration into CFD applications used by the fire safety community.

Chapter 2: Approach

2.1 Flame Theory

2.1.1 Vitiation

As discussed in Section 1.3, vitiation is a critical characteristic in determining the propensity of local flame extinction. In order to determine the impact that vitiation has on combustion, it is useful to examine the basic single step Arrhenius equation for the rate of consumption of methane reacting with oxygen:

$$\frac{d[\mathrm{CH_4}]}{dt} = -A[\mathrm{CH_4}]^b[\mathrm{O_2}]^c \exp\left(-\frac{E}{RT}\right), \quad (1)$$

where $[CH_4]$ and $[O_2]$ are the concentrations of methane and oxygen, t is time, A is the pre-exponential factor, b and c are reaction order constants, E is the activation energy, R is the universal gas constant, and T is the temperature. This expression highlights a few important effects of vitiation on the rate of consumption of methane. First, the rate of consumption of fuel is proportional to the concentration of the reactants, depending on the values of b and c, which typically are between -1 and 1. The second and most significant effect that the Arrhenius expression highlights is the effect of temperature. This reaction temperature can be somewhat challenging to predict, but the laws of thermodynamic mixing dictate that increasing the temperature of the reactants will cause an increase in the temperature of the reaction. It is also the case that decreasing reactant concentrations will reduce the reaction temperature by reducing the chemical enthalpy in the system. The exponential term from

Equation (1) illustrates the property of increasing monotonically with increasing temperature. Therefore, any increase in reactant temperature will increase the reaction rate, while any decrease in reactant concentration will decrease the reaction rate. In fact, the exponential term will dominate the magnitude of the Arrhenius expression. This highlights the importance of monitoring the local values of $Y_{O_2}^{\infty}$, Y_F^{∞}, $T_{O_2}^{\infty}$, and T_F^{∞} for every portion of the reaction.

The superscript ∞ denotes that the reactant property is sampled infinitely far away from the flame. The term infinitely far away from the flame is simply meant to ensure that these parameters are sampled sufficiently far away from the reaction zone, but not so far away that they are physically meaningless. Since the reaction zone for a typical flame is approximately of the order of 1 mm thick or less, "infinitely far away from the flame" should be defined as an order of magnitude larger than the reaction zone or of the order of 1 cm. Therefore, parameters that are sampled infinitely far away from the flame should be sampled approximately 1 cm or more away from the reaction zone.

The challenge lies in predicting the reaction temperature based on $Y_{O_2}^{\infty}$, Y_F^{∞}, $T_{O_2}^{\infty}$, and T_F^{∞}. In the framework of infinitely fast chemistry, the flame is typically characterized by the mixture fraction:

$$Z = \frac{r_s Y_F - (Y_{O_2} - Y_{O_2}^{amb})}{Y_{O_2}^{amb} + r_s Y_F^{amb}}, \tag{2}$$

which is a measure of the quantity of the local fuel concentration that originated from the source, denoted by the superscript *amb*. The stoichiometric mixture fraction is

defined as the value of Z where fuel and oxidizer are present in stoichiometric ratios defined as:

$$Z_{st} = \frac{Y_{O_2}^{amb}}{Y_{O_2}^{amb} + r_s Y_F^{amb}}, \tag{3}$$

which defines the location of the flame. In this framework, the Burke-Schumann flame temperature relationship is widely used:

$$T_{st,BS} = T_F^{\infty} \frac{(Y_{O_2}^{\infty}/r_s)}{Y_F^{\infty} + (Y_{O_2}^{\infty}/r_s)} + T_{O_2}^{\infty} \frac{Y_F^{\infty}}{Y_F^{\infty} + (Y_{O_2}^{\infty}/r_s)} + \frac{\Delta h_c}{c_p} \frac{Y_F^{\infty}(Y_{O_2}^{\infty}/r_s)}{Y_F^{\infty} + (Y_{O_2}^{\infty}/r_s)}, \tag{4}$$

where $T_{st,BS}$ is the adiabatic temperature of the flame at $Z = Z_{st}$, r_s is the stoichiometric oxygen to fuel mass ratio and $\Delta h_c / c_p$ is the ratio of heat of combustion to constant pressure specific heat. This expression captures the essence of vitiation such that preheating reactants will result in a linear increase in the stoichiometric flame temperature, while diluting the reactants will result in a linear decrease. This also highlights another connection to the Arrhenius equation in that both reactant concentrations affect the reaction temperature.

The Burke-Schumann flame temperature expression has some notable limitations. One of these limitations is that the expression requires the assumption of a constant and equal specific heat for both fuel and oxidizer, which is frequently not the case. The specific heat of the oxidizer and the fuel are typically different and both depend on temperature. As a result, in the Burke-Schumann expression, both fuel and oxidizer heating contribute equally to the temperature increase of the system. Another limitation is the assumption that the temperature profile across the flame follows a piecewise linear relationship with the mixture fraction, which is also frequently not

the case. This caveat is somewhat inconsequential because the temperature at the stoichiometric interface is of much more importance than the temperatures at intermediate values of *Z*. Furthermore, some care must be taken such that the Burke-Schumann adiabatic flame temperature for the pure air reacting with pure fuel condition matches more precise predictions of the real adiabatic flame temperature determined from chemical equilibrium solutions. This condition is defined as the reference condition ($Y_{O_2}^{\infty} = 0.23$, $Y_F^{\infty} = 1$, $T_{O_2}^{\infty} = T_F^{\infty} = 300$ K, and $T_{st,BS}^{ref} = 2230$ K) as determined from chemical equilibrium calculations with a stoichiometric mixture of air with Methane. In order to obtain this result with the Burke-Schumann expression, $\Delta h_c / c_p = 3.55 \times 10^5$ K is required for matching the real adiabatic flame temperature. Despite the weaknesses of the Burke-Schumann expression, it is still widely used in flamelet studies [35-44]. It is worth noting that the Burke-Schumann flame temperature expression was designed to predict adiabatic conditions. In reality, flames always experience losses and these temperatures are challenging to achieve, but it is possible to account for these losses. Some of these effects occur in oxygen enriched environments, which allow for substantial kinetic losses in the form of free radicals. Thus, the application of the Burke-Schumann flame temperature expression should be limited to oxidizer mass fraction 0.25 or less.

2.1.2 Incomplete Chemistry

One source of thermal losses from the flame that must be accounted for is that caused by incomplete chemical kinetics, resulting in reactant leakage. In this study, kinetic losses from the flame are caused by increased reactant velocity and leakage;

therefore, the local velocity of reactants $U_{O_2}^{\infty}$, and U_F^{∞} supplied to the flame are significant. More importantly, there are more appropriate measures of the impact of velocity in a diffusion flame such as the strain rate or scalar dissipation rate. The scalar dissipation rate in particular is a fundamental parameter used to define the rate of mixing in a diffusion flame, and therefore it is the most appropriate parameter for characterizing kinetic losses in this analysis.

In the context of the diffusion flame, conservation of mass requires that reactants must have a relative velocity toward the reaction zone, balanced by the flow of products away from the reaction zone and thermal expansion. This flow condition results in a velocity gradient at the flame, which is typically called a strain rate. The velocity gradient drives the mixing of fuel and oxidizer, which is the defining characteristic of the diffusion flame. The scalar dissipation rate at the stoichiometric interface,

$$\chi_{st} = 2D_{th}(\nabla Z)^2, \tag{5}$$

is a fundamental measure of the mixing rate between fuel and oxidizer reactants. When the chemistry is infinitely fast, this mixing rate limits the reaction rate, and consequently the energy release rate. This fundamental relationship becomes evident by the definition of the volumetric energy release rate from oxygen consumption for infinitely fast chemistry:

$$\dot{q}''' = \frac{\Delta h_{O_2} \rho}{2} \frac{\partial^2 Y_{O_2}}{\partial Z^2} \chi_{st}, \tag{6}$$

evaluated at the stoichiometric mixture fraction [97]. However, Equations (5 and 6) do not illustrate how the scalar dissipation rate can characterize kinetic losses from

the flame. Upon closer examination of Equation (6), it is apparent that increasing the scalar dissipation rate will increase the volumetric production of energy by the flame. This is in contrast to the claim that scalar dissipation rate corresponds to kinetic losses. In order to understand the mechanism in which scalar dissipation rate is a measure of kinetic losses, one must examine conservation of mass again. While the scalar dissipation rate is a measure of the rate of mixing between reactants, it is also related to the flow of products away from the flame. These products transport energy away from the flame, which is a source of enthalpy losses from the flame. More importantly, kinetic losses arise from the increasing temperature gradient in the flame caused by increasing the scalar dissipation rate. As this temperature gradient increases, there is a corresponding increase in the transfer of energy away from the flame. Flame extinction resulting from this enthalpy loss is typically referred to as kinetic extinction.

Examining the ratio of energy production by the flame and kinetic losses from the flame is a powerful tool for characterizing extinction of diffusion flames. The Damköhler number, $Da = t_{mix} / t_{chem}$, is introduced to describe finite rate chemistry effects on flame extinction. Extinction occurs at sub critical *Da,* where diffusive losses result in mixing times, t_{mix}, less than the characteristic reaction time, t_{chem}. The mixing time is inversely proportional to the scalar dissipation rate, and the chemical time is inversely proportional to the first order Arrhenius rate. In other words, the rate of chemistry losses can start to compete with the rate of energy production at high scalar dissipation rates. A classical assumption is that the critical Damköhler number, Da_{crit}, is a constant for all diffusion flames with a given fuel [35-44].

It is of interest to estimate scalar dissipation rates in actual fires for comparison with critical values to determine if extinction will occur. The physical meaning of the scalar dissipation rate is a measure of the rate of local mixing. The inverse of this rate provides a characteristic mixing time scale in the reaction zone. Recently, the scalar dissipation rate was measured in high strain diffusion flames [82,83]. However, the spatial and temporal requirements for measurement of χ are extremely demanding. Measurement of this quantity is even more challenging in configurations relevant to large-scale accidental fires because of the harsh fire environment and copious levels of soot. Although the scalar dissipation rate has been estimated to be small in fires [94], measurements of χ are not yet available in the fire environment. In lieu of these measurements, it is useful to estimate the magnitude of χ through scaling arguments. Characteristic velocities, turbulence, strain rates and ultimately scalar dissipation rates will be determined from fundamental scaling analysis for pool fires. This analysis will highlight the order of magnitude of kinetic effects in pool fires of various diameters.

Scaling arguments are provided below to estimate the scalar dissipation rate using a pool fire as a classical representation of an accidental fire. Reference values are provided in parentheses corresponding to a 1 m diameter heptane pool fire. The reference configuration represents a typical large accidental fire size based on energy release rate. The large-scale fire behavior is described by the energy release rate,

$$\dot{Q} = \Delta h_c \frac{\pi D^2}{4} \dot{m}''_\infty (1 - e^{-kBD}) \ (= 2.4 \text{ MW}), \qquad (7)$$

where the known fuel dependant parameters, Δh_c = 44,600 kJ/kg is the heat of combustion of the fuel, $\dot{m}''_\infty$ = 0.101 kg/m^2-s is the mass flux for an infinite diameter pool, and kB = 1.1 m^{-1} is the product of the extinction absorption coefficient of the flame (k) and the mean beam length corrector (B) as described by Babrauskas [26]. The mean centerline velocity at the flame tip can be approximated by

$$u_{0,\max} = 0.54\left(\Delta T_0 \frac{\dot{Q}}{1000}\right)^{1/5} \quad (= 9.3 \text{ m/s}), \tag{8}$$

where ΔT_0 = 650 K is the increase in bulk flow temperature at the flame height [3]. Equations (7 and 8) are considered accurate for fires up to diameters O(10^2 to 10^3 m) based on measurements made by Koseki et al. [24,25] and Heskestad [32]. The turbulent integral length scale is assumed to be directly proportional to the pool diameter so that

$$l_t = 0.5D \quad (= 0.5 \text{ m}). \tag{9}$$

The flame height is another possible length scale; however, in a pool fire these length scales are closely related and of the same order. The pool diameter is chosen in this analysis for simplicity. In fires, the root mean square (RMS) velocity fluctuation has been found to be proportional to the mean centerline velocity

$$u' = 0.3u_{0,\max} \quad (= 2.8 \text{ m/s}), \tag{10}$$

which is used as the integral turbulent velocity scale [27-33]. These integral quantities are useful for determining the Kolmogorov scales describing turbulent diffusion. Because diffusion flames are defined by the rate of diffuse mixing, these Kolmogorov quantities are appropriate for describing interactions with the flame. The Kolmogorov scales are given by:

$$\mathrm{Re}_t = \frac{u' l_t}{\nu} \ (= 1700), \tag{11}$$

$$\eta_k = l_t \, \mathrm{Re}_t^{-3/4} \ (= 1.8 \text{ mm}), \tag{12}$$

$$\text{and } V_k = u' \mathrm{Re}_t^{-1/4} \ (= 0.43 \text{ m/s}), \tag{13}$$

where the viscosity is given by,

$$\nu(T_{amb} + \Delta T_0) = \nu_{amb}(1 + \Delta T_0 / T_{amb})^{1.7} \ (= 7.9 \times 10^{-4} \text{ m}^2/\text{s}), \tag{14}$$

where ν_{amb} is the kinematic viscosity of air at standard temperature and pressure. This expression accounts for the significant change in viscosity due to the high bulk temperature at the flame tip. A turbulent strain rate can now be approximated from the Kolmogorov scales following Yeung et al. [95],

$$a_t = 0.28 \frac{V_k}{\eta_k} \ (= 63 \text{ s}^{-1}). \tag{15}$$

This strain rate estimated for the 1m-diameter heptane pool fire is non-negligible.

The scalar dissipation rate can be determined from the strain rate and stoichiometric mixture fraction using an expression obtained from asymptotic analysis [10,34,35,37] combined with a correction factor, φ, to account for variations in reaction density [42] yielding,

$$\chi_{st} = \frac{a_t}{\pi} \varphi \exp[-2(\mathrm{erfc}^{-1}(2Z_{st}))^2] \ (= 2.86 \text{ s}^{-1}), \tag{16}$$

where erfc^{-1} is the inverse complimentary error function and

$$\varphi = \frac{3((\rho_{O_2}^{\infty} / \rho_{st})^{1/2} + 1)}{4(2(\rho_{O_2}^{\infty} / \rho_{st})^{1/2} + 1)} \ (= 1.56). \tag{17}$$

Ideal gas densities are used for air where $\rho_{O_2}^{\infty} / \rho_{st} = T_{st} / T_{O_2}^{\infty}$, with $T_{O_2}^{\infty}$ =300 K and T_{st} = 2000 K assumed as characteristic temperatures. It is important to note that the oxidizer density could be evaluated at either ambient temperature or the bulk temperature at the flame tip. The ambient temperature was selected to capture the extreme scalar dissipation events.

This scaling argument provides an estimate for characteristic values of the local scalar dissipation rate at the flame tip. In this analysis, the scalar dissipation rate at the flame tip is completely specified by the pool diameter and fuel properties. Figure 3 illustrates the effect of pool diameter on χ_{st} at the flame tip using heptane as the fuel. It is apparent from Figure 3 that for large diameter pool fires, the characteristic scalar dissipation rate at the flame tip remains small compared to non-vitiated extinction scalar dissipation rates having a density corrected value of $\chi_{st}^{ref} = 11.2 \mathrm{s}^{-1}$, determined from similar analysis of opposed flow diffusion flame simulations. However, the scalar dissipation rates indicated by the scale analysis are significant in the presence of vitiation, or other heat losses. Comparing a diffusive time scale to a reaction time scale is necessary in order to strictly determine the local extinction propensity of the flame in the presence of vitiation or other enthalpy losses.

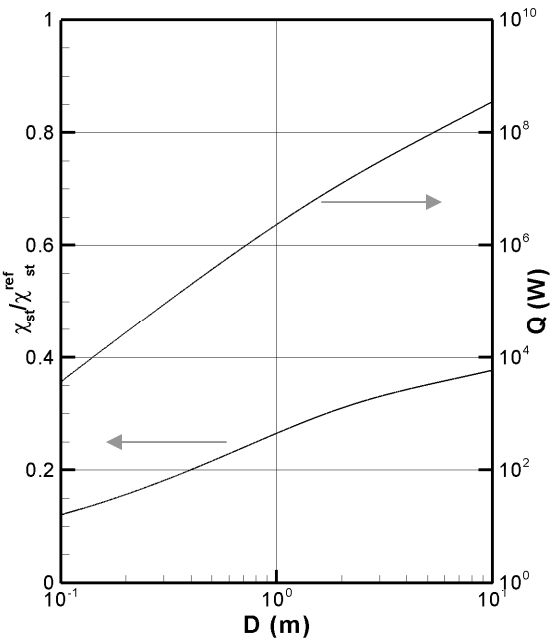

Figure 3: The mean scalar dissipation rate at the flame tip for heptane pool fires as a function of pool diameter from the scaling analysis. The flame energy release rate is provided for reference.

2.1.3 Radiation Losses

Radiation losses should also be considered because of the nature of flames to emit light energy. There is some debate regarding the method in which to model radiation losses from flames; however, this work does not attempt to recommend radiation models. Instead, this work will provide a method to account for radiation losses for any generalized radiation model by using a fundamental measure of the radiation losses from the flame. This will ensure that the method used in this study to account for radiation losses will be applicable to radiation models that may be used in CFD codes. The radiation model used in this study is not intended to be a representation of real flame radiation, but more specifically a canonical method to produce variable radiation losses from flames.

In real flames, radiation losses are highly complex and dependent upon several variables. One component of flame radiation is caused by the presence of gases and particles with radiatively emitting properties. These species include CH_4, CO_2, H_2O, CO, and C (soot), which are all significant species present in the Methane-Air combustion. These species are known to emit radiation based on their local concentration and temperature, and in the case of soot the particle size and the number density of the particles are also contributing parameters. One model that is frequently used to account for radiation from flames is the optically thin radiation model used in many fundamental combustion simulations [36,75,76,99]. The optically thin radiation model is desirable because of the simplicity of its implementation given that the model ignores the possibility of radiative absorption at the scale of the flame. This is typically considered good when examining a single flamelet because the thin nature of the reaction zone does not provide sufficient optical path length for radiation to be absorbed. This assumption breaks down if there are substantial amounts of soot, if the flame thickness increases dramatically, or if nearby flamelets emit enough radiative energy to interact with each other. Any of these scenarios may result in substantial absorption at the flame level. Away from the flame, radiative absorption can occur because product gases can exist in high concentration and the optical path length is substantially larger. The absorption that occurs away from the flame will result in pre-heating of reactant gases supplied to the flame, which will be captured by the variables defining vitiation as a flame strengthening factor. Another important characteristic to consider is that, in the vitiated environment, these product gases will be re-circulated back to the flame,

increasing their local concentrations in the flame zone while also increasing reactant temperatures. This in turn will increase the propensity of the flame to lose energy from radiation by increasing the radiative properties of the gases (temperature and emissivity), while decreasing the propensity of extinction due to the increased reactant temperature. Any CFD codes that include radiation losses from the flame must be able to account for the re-circulation of these species and the various associated effects.

The optically thin radiation model is used in this study as a canonical means of producing radiation losses from the flame. More complex models will only serve to complicate the analysis of radiation losses in the context of a singular local flamelet where the net energy lost is the only important feature of radiation losses. The optically thin radiation model is represented by:

$$\dot{q}'''_{rad} = 4\sigma\kappa(T^4 - T_{amb}^4), \tag{18}$$

where $\dot{q}'''_{rad}$ is the local rate of energy lost by radiation per unit volume, σ is the Steffan-Boltzmann Constant, κ is the Planck mean absorption coefficient, and T is the local temperature. The total energy loss per unit area of the flame can then be written:

$$\dot{q}''_{rad} = \int_{-\infty}^{\infty} \dot{q}'''_{rad}\, dx, \tag{19}$$

where x is the relative position normal to the flame sheet with the bounds of integration, $-\infty$ to ∞, defined as infinitely far away from the flame. It is also convenient to define the rate of production of energy by the flame:

$$\dot{q}''_{gen} = \int_{-\infty}^{\infty} \dot{q}'''_{gen}\, dx, \tag{20}$$

where $\dot{q}''_{gen}$ is the total energy production per unit area of the flame, and $\dot{q}'''_{gen}$ is the local energy production per unit volume of the flame as defined by the heat of production and rate of consumption of species in the flame. This generation term can also be defined based on the integral of Equation (6) following asymptotic expansions resulting in:

$$\dot{q}''_{gen} = \int_{-\infty}^{\infty} \frac{\Delta h_c \rho}{2} \frac{\partial^2 Y_F}{\partial Z^2} \chi_{st} dx \propto \frac{Y_F}{(1-Z_{st})} \chi_{st}^{1/2} \tag{21}$$

which will be a useful model for quantifying the radiation losses analytically [97]. The definition of these variables allows for the specification of a fundamental measure of the radiation losses from the flame, the radiative fraction:

$$\Gamma = \frac{\dot{q}''_{rad}}{\dot{q}''_{gen}}, \tag{22}$$

which defines the relative magnitude of radiation losses to the total generation of energy by the flame.

The radiative fraction can be used in a numerical scheme to correct the Burke-Schumann flame temperature for the effects of radiation losses. This scheme was first proposed by Sohrab et al. and is detailed in Appendix A:

$$T_{st,BS}^{rad} = T_{st,BS} - \frac{Y_F^{\infty} Y_{O_2}^{\infty} / r_s \left(Y_{O_2}^{\infty} / r_s + T_{O_2}^{\infty} c_p / \Delta h_c - T_F^{\infty} c_p / \Delta h_c \right)}{\left(Y_F^{\infty} + Y_{O_2}^{\infty} / r_s \right)\left(Y_F^{\infty} - Y_{O_2}^{\infty} / r_s \right)} \times \frac{\Delta h_c}{c_p} \left\{ \left[1 + \frac{2 l_f \left(Y_F^{\infty} - Y_{O_2}^{\infty} / r_s \right)}{\left(Y_F^{\infty} + Y_{O_2}^{\infty} / r_s \right)\left(Y_{O_2}^{\infty} / r_s + T_{O_2}^{\infty} c_p / \Delta h_c - T_F^{\infty} c_p / \Delta h_c \right)^2} \right]^{1/2} - 1 \right\}, \tag{23}$$

where $T_{st,BS}^{rad}$ is the Burke-Schumann flame temperature corrected for radiation losses, $\Delta h_c / c_p = 3.55 \times 10^5$ K, and l_f is an Arrhenius modeled radiant loss parameter:

$$l_f = F\left(\frac{T_{st,BS} c_p Y_F^{\infty}}{\gamma \Delta h_c}\right) \exp\left[-\gamma\left(1-\frac{T_{st,BS}^{rad}}{T_{st,BS}^{ref}}\right)\right], \tag{24}$$

where $T_{st,BS}^{ref}$ = 2230 K is the adiabatic flame temperature at the reference condition, γ = 5 is the radiant loss sensitivity to the flame temperature, and F is a radiant loss term defined:

$$F = \frac{4\sigma\kappa T_{st,BS}^4}{2\rho_{st}\Delta h_c \chi_{st}}. \tag{25}$$

Sohrab et al. state that Equation (25) is defined as a local parameter solely based on the fact that evaluation of an integral value presented ill-posed numerical behavior, and therefore they modeled the radiant losses assuming a maximum loss at the stoichiometric interface [36]. Following integral scale analysis, F can effectively be written in terms of the integral radiant fraction in a first assumption:

$$F = \frac{\Gamma \dot{q}''_{gen}}{2\rho_{st}\Delta h_c \delta_{gen} \chi_{st}}, \tag{26}$$

where

$$\dot{q}''_{gen} = \dot{q}''_{gen,1} \frac{(1-Z_{st,1})}{(1-Z_{st})}\left(\frac{\chi_{st}}{\chi_{st,1}}\right)^{1/2} \tag{27}$$

is a model for the generation of energy per unit volume of the flame where $\dot{q}''_{gen,1} = 2.06\times10^5$ W/m^2 is the generation of energy per unit area and for a Methane-Air flame at $\chi_{st,1}$ = 1 s^{-1}, $Y_{O_2,1} = 0.23$, and $Y_{F,1} = 1.0$. The relationship of $\chi_{st}^{1/2}$ is attributable to the integration of Equation (6) following the advice of Poinsot and Veynante [97]. While Equation (26) is a desirable definition of F for any radiation model, it is difficult to justify a general model for δ_{gen} for small values of χ_{st}, where

the flame thickness is observed to be constant. Until an appropriate justification for δ_{gen} is developed, Equation (25) will be used directly to account for radiation losses. This radiative correction scheme requires iterative numerical methods to solve Equation (23) for $T_{st,BS}^{rad}$ based on the dependence of Equation (24) on $T_{st,BS}^{rad}$, any simple iteration scheme should be sufficient. This scheme is a non-trivial correction for the flame temperature, which depends upon the radiative fraction, the scalar dissipation rate, and the flame temperature itself. Dependence on the scalar dissipation rate makes sense because the high temperature region is thicker at low scalar dissipation rates and thinner at high scalar dissipation rates; therefore flames at low scalar dissipation rates should be affected more by radiation losses than flames with high scalar dissipation rates. This dependence further emphasizes the importance of the scalar dissipation rate on predicting flame extinction.

2.1.4 Extinction Physics

Three scalar dissipation rate-based extinction models were evaluated in this research. These models may differ in the methods used to predict flame temperature, scalar dissipation rate, and/or scaling equations. The models provide a tool to predict critical scalar dissipation rates as a function of flame temperature and reactant composition: $\chi_{st,crit} = f[T_{st}(T_{O_2}^{\infty}, Y_{O_2}^{\infty}, T_{F_2}^{\infty}, Y_F^{\infty}, \kappa), Z_{st}(Y_{O_2}^{\infty}, Y_F^{\infty})]$. This critical scalar dissipation rate is determined from local reactant properties and radiation losses, and then compared to the local scalar dissipation rate. When the local scalar dissipation rate is greater than the critical value, the local flame element will experience

extinction. Acquiring a local scalar dissipation rate may prove challenging, but these models require that it is known in order to predict local extinction.

In addition to these critical scalar dissipation rate models, a simplified critical flame temperature model will also be evaluated. A critical flame temperature model provides a computational simplification because it does not require the determination of a local scalar dissipation rate. Due to the possible computational cost associated with determining a local scalar dissipation rate, this simplification may be desirable in CFD applications. The inherent assumptions, and deficiencies associated with the critical flame temperature extinction model will become apparent upon further analysis. It is the duty of the CFD publisher and the end user to determine if the cost versus benefit of any of these extinction models is appropriate for their specific application.

It is important to realize that the mixture fraction definition used to analyze a typical compartment fire configuration is different from that used in a flamelet calculation as illustrated in Figure 1 and Figure 2 [69]. At the global level, mixture fraction is a parameter that describes mixing between pure fuel and pure air. At the flamelet level, mixture fraction is a local parameter that describes fuel-air mixing near a particular flame element under conditions that may be affected by air and fuel vitiation. In the following analysis, Z designates the global mixture fraction and Z^+ designates its local flamelet equivalent. Following the classical definition of mixture fraction from Equation (2), $Z = 0$ in ambient air and $Z = 1$ in ambient fuel conditions. In typical fire scenarios, the ambient condition is pure air and pure gaseous fuel, as is the case for both the unconfined pool fire and the compartment fire configurations. In

contrast, in the flamelet analysis illustrated in Figure 1 and Figure 2, $Z^+ = 0$ corresponds to the vitiated oxidizer inlet and $Z^+ = 1$ corresponds to the vitiated fuel inlet. The relationship between the local and global definitions of mixture fraction can be derived from the definition of the global mixture fraction as:

$$Z^+ = \frac{Z - Z_{O_2}}{Z_F - Z_{O_2}}, \tag{28}$$

where Z_F and Z_{O_2} denote the values of global mixture fraction in the vitiated fuel and oxidizer supply streams respectively. This renormalization is necessary to properly compare results from local flamelet space to global space. The local and global definitions of scalar dissipation rate have the following relationship:

$$\chi_{st} = \chi_{st}^{+}\left(Z_F - Z_{O_2}\right)^2. \tag{29}$$

In the following discussion and analysis, this expression will be used to map the local flamelet results back to global space unless otherwise noted. This applies to both experimental and numerical counterflow flame extinction results where either of the reactant streams can be diluted.

2.1.4.1 Detailed Chemistry

The first extinction model under evaluation is simply an observation of behavior within the context of detailed finite-rate chemistry and detailed spatial resolution of the flow field. This model is essentially a DNS of the counterflow diffusion flame and it is used as a proof of concept. Extinction in the context of detailed finite-rate chemistry is an observation of the detailed flame behavior at extinction, where the generation and loss of energy are modeled exactly. The detailed

chemistry and high resolution allow for very precise determination of the temperature at the stoichiometric interface, as well as the scalar dissipation rate from its definition:

$$\chi_{st} = 2D_{th}(\nabla Z)^2 \left(Z_F - Z_{O_2}\right)^2 : \quad Z = Z_{st}\,, \tag{30}$$

which accounts for the mixture fraction normalization from Equation (29). This allows for an evaluation of real extinction behavior without modeled inputs. The extinction conditions will be evaluated following the critical Damköhler number theory. This evaluation will indicate the physical validity of the assumption that there is a constant critical Damköhler number at extinction. The critical *Da* concept provides an expression relating the critical scalar dissipation rate to the flame temperature given by:

$$\chi_{st,crit} = Da_{crit}^{-1} \exp\left(-\frac{T_a}{T_{st}}\right), \tag{31}$$

where $T_a = E/R$ is the fuel specific activation temperature, and T_{st} is the temperature at the stoichiometric interface [37]. It is convenient to normalize Equation (31) by a known reference extinction condition to eliminate the need to determine the magnitude of Da_{crit}. The reference condition is simply the kinetic extinction limit for the pure air and pure fuel flame. The scaled equation for the detailed chemistry extinction is written:

$$\frac{\chi_{st}}{\chi_{st}^{ref}} = \exp\left[-T_a\left(\frac{1}{T_{st}} - \frac{1}{-T_{st}^{ref}}\right)\right]. \tag{32}$$

Furthermore, it is convenient to define a Zel'dovich number:

$$\beta = T_a \frac{T_{st}^{ref} - T^{amb}}{\left(T_{st}^{ref}\right)^2}, \tag{33}$$

and an enthalpy deficit term:

$$H_{st} = \frac{T_{st} - T_{st}^{ref}}{T_{st}^{ref} - T^{amb}}, \tag{34}$$

which is a measure of temperature deviation from the reference condition. In a word of caution about this enthalpy deficit term, it is not defined in the same manner as AEA defines enthalpy deficit. In AEA, enthalpy deficit is defined as the loss of enthalpy due to kinetic losses or reactant leakage across the flame, as it is frequently observed at conditions near flame extinction [39,42,85]. The enthalpy deficit term in Equation (34) is defined as the difference in enthalpy due to temperature differences between the observed extinction condition, and the reference extinction condition. Thus Equation (32) can be written in an enthalpy deficit formulation:

$$\frac{\chi_{st}}{\chi_{st}^{ref}} = \exp\left[\frac{\beta H_{st}}{1 + H_{st}\left(1 - T^{amb}/T_{st}^{ref}\right)}\right], \tag{35}$$

which cannot be simplified by order of magnitude arguments. This expression can be used to correlate all known extinction conditions in a proof of concept of the critical Damköhler number theory for extinction. Given the ability of such a detailed model to produce flame temperature based on the enthalpy of the reaction, there is no requirement to correct temperature for radiation. The effect of radiation losses will be accounted for directly in the temperature profile, given that the radiation sub-model is appropriately coupled to the energy balance equation. It is also important to remember that all extinction conditions in the detailed chemistry framework must be normalized into global mixture fraction space following Equation (29).

2.1.4.2 Activation Energy Asymptotics

The second extinction model under evaluation is that produced from AEA analytic solutions. A similar critical Damköhler number expression has been developed from AEA, where the simplified partial differential equations have been solved analytically to produce:

$$\frac{f(Z_{st})\chi_{st}}{\chi^5_{st,BS}} = \exp\left(-\frac{T_a}{T_{st,BS}}\right) + K, \tag{36}$$

where K is a constant defined by various fuel properties, $T_{st,BS}$ is the Burke-Schumann flame temperature from Equation (4). The scalar dissipation rate has the form:

$$\chi_{st} = \frac{a_g}{\pi}\exp\left[-2\left(\text{erfc}^{-1}(2Z_{st})\right)^2\right], \tag{37}$$

where the global strain rate is defined as:

$$a_g = \left(\frac{U^{\infty}_{O_2}}{d}\right)\left[1+\left(\frac{U^{\infty}_{F}}{U^{\infty}_{O_2}}\right)\left(\frac{\rho^{\infty}_{F}}{\rho^{\infty}_{O_2}}\right)^{1/2}\right]. \tag{38}$$

The term $f(Z_{st})$ is defined in a way that captures the mixture fraction normalization, eliminating the need to use Equation (29):

$$f(Z_{st}) = \frac{Z_{st}\left[1+a(1-Z_{st})\right]}{(1-Z_{st})^2}\left(Y^{\infty}_{F}\right)^3, \tag{39}$$

$$a = \frac{T^{\infty}_{O_2} - T^{\infty}_{F}}{T_{st,BS} - T_u}, \tag{40}$$

$$\text{and } T_u = T^{\infty}_{O_2} + Z_{st}\left(T^{\infty}_{F} - T^{\infty}_{O_2}\right), \tag{41}$$

following the guidance of Peters [37]. Equation (36) can be normalized by a known reference extinction condition to simplify the expression by eliminating the *K* term resulting in:

$$\frac{\chi_{st}}{\chi_{st}^{ref}}\frac{f(Z_{st})}{f(Z_{st}^{ref})}=\left(\frac{T_{st,BS}}{T_{st,BS}^{ref}}\right)^{5}\exp\left[-T_a\left(\frac{1}{T_{st,BS}}-\frac{1}{-T_{st,BS}^{ref}}\right)\right], \tag{42}$$

with the $f(Z_{st})$ terms on the LHS to capture the mixture fraction normalization. This normalization gives the expression a more convenient form for analysis. The only parameters that remain to be determined for this model to work are χ_{st}^{ref}, $T_{st,BS}^{ref}$, and T_a. The reference scalar dissipation rate can be determined from analysis of the classical S-shaped curve pathway to extinction using Equation (37) as the model for the scalar dissipation rate. The reference flame temperature is simply the adiabatic flame temperature for pure fuel reacting with pure air stoichiometrically. The activation temperature can be easily determined from extinction conditions following the guidance of Puri and Seshadri, which will be discussed in more detail in Section 3.3.3 [44]. Equation (42) can again be rewritten in terms of a dimensionless, enthalpy deficit term defined based on Burke-Schumann temperatures:

$$H_{st,BS}=\frac{T_{st,BS}-T_{st,BS}^{ref}}{T_{st,BS}^{ref}-T^{amb}}, \tag{43}$$

and the Zel'dovich number also defined based on Burke-Schumann temperatures:

$$\beta_{BS}=T_a\frac{T_{st,BS}^{ref}-T^{amb}}{\left(T_{st,BS}^{ref}\right)^2}, \tag{44}$$

resulting in the enthalpy deficit formulation:

$$\frac{\chi_{st}}{\chi_{st}^{ref}}\frac{f(Z_{st})}{f(Z_{st}^{ref})}=\left(\frac{T_{st,BS}}{T_{st,BS}^{ref}}\right)^{5}\exp\left[\frac{\beta_{BS}H_{st,BS}}{1+H_{st,BS}\left(1-T^{amb}/T_{st,BS}^{ref}\right)}\right], \tag{45}$$

following the guidance of Yi and Trouvé [87]. Radiation heat losses can be applied to this model through the correction of the Burke-Schumann flame temperature following Equation (23). This results in a new definition of the Burke-Schumann enthalpy deficit:

$$H_{st,BS}^{rad}=\frac{T_{st,BS}^{rad}-T_{st,BS}^{ref}}{T_{st,BS}^{ref}-T^{amb}}, \tag{46}$$

therefore, Equations (42) and (45) can be written:

$$\frac{\chi_{st}}{\chi_{st}^{ref}}\frac{f(Z_{st})}{f(Z_{st}^{ref})}=\left(\frac{T_{st,BS}^{rad}}{T_{st,BS}^{ref}}\right)^{5}\exp\left[-T_{a}\left(\frac{1}{T_{st,BS}^{rad}}-\frac{1}{-T_{st,BS}^{ref}}\right)\right], \tag{47}$$

$$\text{and }\frac{\chi_{st}}{\chi_{st}^{ref}}\frac{f(Z_{st})}{f(Z_{st}^{ref})}=\left(\frac{T_{st,BS}^{rad}}{T_{st,BS}^{ref}}\right)^{5}\exp\left[\frac{\beta_{BS}H_{st,BS}^{rad}}{1+H_{st,BS}^{rad}\left(1-T^{amb}/T_{st,BS}^{ref}\right)}\right], \tag{48}$$

which can fully account for vitiation, kinetic losses, and radiation losses from the flame. It is also critical to recall that the term $f(Z_{st})$ captures the mixture fraction normalization in the AEA analysis, thus eliminating the need to use Equation (29).

2.1.4.3 Simplified Critical Damköhler Number

The third extinction model under evaluation is a Simplified Critical Damköhler Number (SCDN) methodology. The SCDN methodology is the theoretical extinction model that is being developed in this study as a possible alternative to AEA. It is based on a critical timescale argument that defines extinction events as a ratio between mixing time and chemical generation time, the Damköhler Number. The SCDN approach is very similar to AEA, in that they use similar expressions for

flame temperature and scalar dissipation rate. However, the simplified model is based entirely on the critical Damköhler time scale argument, while AEA solves the governing equations analytically. SCDN utilizes the expression for scalar dissipation rate from AEA, while increasing the fidelity of the expression based on a non-constant density correction [42] from Equation (17) resulting in:

$$\chi_{st} = \frac{a_g}{\pi}\varphi \exp\left[-2\left(\text{erfc}^{-1}\left(2Z_{st}\right)\right)^2\right]\left(Z_F - Z_{O_2}\right)^2, \tag{49}$$

which accounts for the mixture fraction normalization from Equation (29). The simplified model also utilizes a Burke-Schumann flame temperature prediction following Equation (4). The SCDN formulation provides an expression that relates extinction conditions from Equation (31). A similar normalization has been performed on this expression in order to eliminate the need to determine Da_{crit}:

$$\frac{\chi_{st}}{\chi_{st}^{ref}} = \exp\left[-T_a\left(\frac{1}{T_{st,BS}} - \frac{1}{-T_{st,BS}^{ref}}\right)\right]. \tag{50}$$

This expression can also be re-written in terms of the enthalpy deficit and the Zel'dovich number from Equations (43) and (44) resulting in:

$$\frac{\chi_{st}}{\chi_{st}^{ref}} = \exp\left[\frac{\beta_{BS} H_{st,BS}}{1 + H_{st,BS}\left(1 - T^{amb}/T_{st,BS}^{ref}\right)}\right]. \tag{51}$$

The SCDN model provides some advantages over the AEA model. First, the mathematical expressions are slightly simpler without the additional dependence of $T_{st,BS}^5$ and $f(Z_{st})$. Secondly, the addition of the non-constant density correction factor should improve the accuracy of the analytic expression for scalar dissipation rate in comparison to real values. It is worth noting that the activation temperature must be determined based on an evaluation of extinction conditions using Equation

(31), which will be discussed in more detail in a later section. Also similar to AEA is the method for accounting for radiation losses in Equations (50) and (51) using Equations (23) and (46), resulting in:

$$\frac{\chi_{st}}{\chi_{st}^{ref}} = \exp\left[-T_a\left(\frac{1}{T_{st,BS}^{rad}} - \frac{1}{-T_{st,BS}^{ref}}\right)\right], \tag{52}$$

$$\text{and } \frac{\chi_{st}}{\chi_{st}^{ref}} = \exp\left[\frac{\beta_{BS} H_{st,BS}^{rad}}{1 + H_{st,BS}^{rad}\left(1 - T^{amb}/T_{st,BS}^{ref}\right)}\right], \tag{53}$$

which can fully account for vitiation, kinetic losses, and radiation losses from the flame. These simplifications over AEA may seem trivial, but they provide an accurate and simple physical explanation of extinction physics. It is also critical to recall that all extinction conditions must be normalized into global mixture fraction space following Equation (29).

2.1.4.4 Critical Flame Temperature

The fourth extinction model under evaluation is a critical flame temperature criterion. The critical flame temperature concept (used in FDS) is equivalent to a constant scalar dissipation rate extinction model based on Equation (31) [2]. The Burke-Schumann flame temperature model from Equation (4) illustrates that extinction conditions are parameterized by reactant temperature and reactant concentration. Equation (4) can be rewritten in terms of a constant critical flame temperature:

$$T_c = T_F^{\infty}\frac{\left(Y_{O_2}^{\infty}/r_s\right)}{Y_F^{\infty} + \left(Y_{O_2}^{\infty}/r_s\right)} + T_{O_2}^{\infty}\frac{Y_F^{\infty}}{Y_F^{\infty} + \left(Y_{O_2}^{\infty}/r_s\right)} + \frac{\Delta h_c}{c_p}\frac{Y_F^{\infty}\left(Y_{O_2}^{\infty}/r_s\right)}{Y_F^{\infty} + \left(Y_{O_2}^{\infty}/r_s\right)}, \tag{54}$$

where the reactant temperatures and concentrations correspond to extinction conditions. Equation (54) can be formulated into a model for extinction:

$$\left(T_{st,BS}-T_c\right)=T_F^{\infty}Z_{st}+T_{O_2}^{\infty}\left(1-Z_{st}\right)+Y_F^{\infty}\left(\frac{Z_{st}}{Z_{st}^{ref}}\right)\left(T_{st,BS}^{ref}-T_u\right)-T_c\le 0\,, \qquad (55)$$

where any local flamelet that satisfies this condition will experience extinction. This model is desirable for its simplicity, and because extinction can be modeled with a single input parameter in the critical flame temperature. Selection of this critical flame temperature can be somewhat challenging, but many researchers have indicated that a critical flame temperature of approximately 1700 K is appropriate for low strain flames [79,94]. It is also worth noting that the Burke-Schumann flame temperature equation is well suited for adding other non-adiabatic effects such as radiation losses and conduction losses to a cold wall [87]. The effects of radiation specifically can be added to this formulation following Equation (23), resulting in:

$$T_c=T_{st,BS}-\frac{Y_F^{\infty}\,Y_{O_2}^{\infty}/r_s\left(Y_{O_2}^{\infty}/r_s+T_{O_2}^{\infty}c_p/\Delta h_c-T_F^{\infty}c_p/\Delta h_c\right)}{\left(Y_F^{\infty}+Y_{O_2}^{\infty}/r_s\right)\left(Y_F^{\infty}-Y_{O_2}^{\infty}/r_s\right)}$$
$$\times\frac{\Delta h_c}{c_p}\left\{\left[1+\frac{2l_f\left(Y_F^{\infty}-Y_{O_2}^{\infty}/r_s\right)}{\left(Y_F^{\infty}+Y_{O_2}^{\infty}/r_s\right)\left(Y_{O_2}^{\infty}/r_s+T_{O_2}^{\infty}c_p/\Delta h_c-T_F^{\infty}c_p/\Delta h_c\right)^2}\right]^{1/2}-1\right\}, \qquad (56)$$

and the corresponding model:

$$\left(T_{st,BS}^{rad}-T_c\right)=T_{O_2}^{\infty}Z_{st}+T_F^{\infty}\left(1-Z_{st}\right)+T_F^{\infty}\left(\frac{Z_{st}}{Z_{st}^{ref}}\right)\left(T_{st,BS}^{ref}-T_u\right)$$
$$-\frac{Y_F^{\infty}\,Y_{O_2}^{\infty}/r_s\left(Y_{O_2}^{\infty}/r_s+T_{O_2}^{\infty}c_p/\Delta h_c-T_F^{\infty}c_p/\Delta h_c\right)}{\left(Y_F^{\infty}+Y_{O_2}^{\infty}/r_s\right)\left(Y_F^{\infty}-Y_{O_2}^{\infty}/r_s\right)} \qquad (57)$$
$$\times\frac{\Delta h_c}{c_p}\left\{\left[1+\frac{2l_f\left(Y_F^{\infty}-Y_{O_2}^{\infty}/r_s\right)}{\left(Y_F^{\infty}+Y_{O_2}^{\infty}/r_s\right)\left(Y_{O_2}^{\infty}/r_s+T_{O_2}^{\infty}c_p/\Delta h_c-T_F^{\infty}c_p/\Delta h_c\right)^2}\right]^{1/2}-1\right\}$$

where l_f must be defined at the scalar dissipation rate that corresponds to T_c without radiation losses. This method can produce extinction accounting for vitiation and

radiation losses; however, it assumes that the scalar dissipation rate affecting the flame is constant for all fires and at all flame locations. The scaling analysis results illustrated in Figure 3 suggests that the mean scalar dissipation rate is not constant with increasing fire size, and fluctuations in the scalar dissipation rate caused by instantaneous turbulent fluctuations in the flow field are not accounted for. CFD publishers and end users should be aware of these assumptions in order to properly evaluate the cost versus benefit of such a simplified model.

2.2 Experimental Methodology

2.2.1 Counterflow Burner Design

A counterflow slot burner was developed for this study as shown in Figure 4. This burner was designed with the intended functionalities of achieving low flow rates, heated reactants and reactant concentration variability along the slot. The final design of this burner, while simple and elegant, was produced through systematic design and fabrication testing performed in conjunction with Sigfried Dobrotka [96].

The counter flow nozzle assembly is constructed almost entirely out of 316 Stainless Steel (SS) materials for high temperature resistance. English units are presented below for simplicity given that many of the components used in the burner construction are standardized in inches. Both the fuel and oxidizer nozzle assemblies consist of eleven individually fed nozzles, three of which

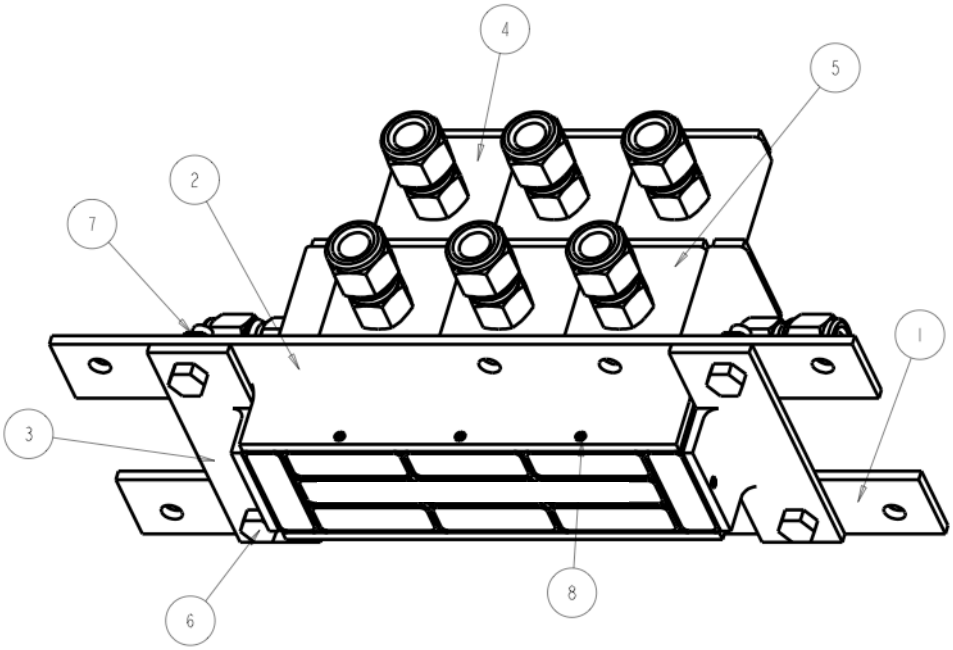

Figure 4: Top injector of the Opposed Flow Slot burner. Oxidizer is injected along the central axis surrounded by N_2 co-flow. An identical injector assembly is used for fuel.

are welded together to create a continuous slot dedicated to reactant streams, and the remaining eight are dedicated to N_2 co-flow. Each of the individual nozzles is fabricated from 316 SS 1-½" by ½" OD and 0.062" thickness rectangular tubing. The tube is cut to lengths of 5" for reactant nozzles and 3" for co-flow, nozzles, and precision-milled at the ends to produce a consistent end surface. One end of the tube is sealed and the other end of the tube is conditioned to produce a top-hat velocity injection profile. Each nozzle is supplied its respective gas through a welded 3/16" compression fitting and tubing in excess of 100 diameters in total length to ensure thorough mixing. On the heated oxidizer side, the tubing connected to the nozzle is 316 SS tubing 6" in length to reduce the risk of tube melting by thermal conduction from the heated nozzle assembly. All additional tubing is color-coded vinyl, with red corresponding to fuel, white to oxidizer, and blue to Nitrogen.

The three reactant nozzles for each assembly are welded together to create a continuous slot injector. The internal tube walls are milled away to 0.5” depth, and the inside of the tube is precision milled with 1/8” diameter end mill to ensure consistent and reproducible interior tube dimensions. The oxidizer side is fitted with a nickel alloy sintered (porous) metal insert 12-micron grade and 0.24” thickness. To further reduce the propensity of leakage pathways, a continuous bead of JB Weld® metal epoxy was applied to the outer edge of the sintered nickel. On the fuel side, the sintered nickel insert is replaced by filling the injectors with glass beads of nominal diameter 0.06” to achieve flow distribution without the risk of leakage pathways associated with the sintered metal insert. The eight co-flow dedicated nozzles are fitted with a bronze sintered metal insert 12-micron grade and 0.24” thickness. The inside of the tube is precision milled with 1/8” diameter end mill to ensure consistent and reproducible interior tube dimensions. The bronze or nickel sintered material is cut with an Electron Discharge Machine to +0.001” tolerance of the milled interior tube dimensions. The sintered metal insert is then friction-fit into the SS tube with a press. This method of fabrication produced the most consistent and reproducible plug flow velocity profile for each nozzle. The tube thickness on the ½” wall side is milled to reduce the separation distance between the nozzles to 0.05” total. The fuel and oxidizer nozzle assemblies are held in place by 1” by 1” by 1/8” thickness 90 º angle bars, which allow for application of compression force to the nozzles further reducing any possible variations from plug flow. The entire burner is mounted by an aluminum framing system that allows for alignment of both nozzle assemblies in a counterflow configuration with a separation distance of precisely 15mm.

2.2.2 Controls

Because this study is focused on extinction in accidental fires and the reactants in accidental fires are often vitiated, it is critical to identify extinction criteria for various reactant compositions and temperatures. Following the laminar flamelet concept, the extinction of opposed flow diffusion flames is studied to characterize extinction behavior in accidental fires. In this study, experimental conditions are controlled to achieve extinction while maintaining a constant scalar dissipation rate. A constant value for χ_{st} is maintained based on the expression from asymptotic theory provided in Equations (38) and (49) at a fixed $T_{O_2}^{\infty}$ and T_F^{∞}, while reducing $Y_{O_2}^{\infty}$ and Y_F^{∞} in the reactant streams. Other prescribed inlet quantities include the nozzle separation distance, the nozzle injection area, and the velocity ratio. Gas densities are modeled based on the Ideal Gas Law, and known gas densities at room temperature. The flame temperature is approximated by the Burke-Schumann expression to determine the density at the reaction zone required in Equation (17). This approach provides the ability to create extinction maps in terms of oxidizer temperatures and oxygen concentrations at fixed scalar dissipation rates.

The mass flow rates of fuel and oxidizer are controlled by mass flow controllers with a maximum error of 1% of their full-scale reading. Inlet conditions are pre-determined based on the Williams analytical expression for scalar dissipation rate from Equation (38), accounting for the temperature dependence of inlet densities and velocities. In this method, a scalar dissipation rate and an oxidizer temperature are selected, and then the required flow conditions are determined for variable reactant mass fractions. Dilution of reactants is achieved by combining a reactant

stream with a diluent stream, and the corresponding mass fraction of the reactant is determined from the mass flow rates of each stream. The mass flow system can be operated in either oxidizer dilution mode or fuel dilution mode, and each mode is capable of achieving mass fractions ranging from pure reactant to pure diluent. Nitrogen co-flow is operated by a simple rotameter, with the only flow requirements being that the co-flow must isolate the reaction to the region between the nozzles. Insufficient co-flow velocities will result in trailing diffusion flames of unburned reactants that may damage the nozzle assembly after long-term exposure.

High temperature flexible heaters capable of operating up to 1000 K control the oxidizer temperature. The heaters are wrapped around the oxidizer nozzle assembly and heated to a steady state temperature as monitored by surface mounted thermocouples. A 120V 24A Variac allowed for manual control of the steady state nozzle temperature by metering the power applied to the heaters. During high temperature operation, the exit gas temperature is measured to be within 10 K of the measured surface temperature of the nozzles. If the surface temperature of the nozzle deviated from the desired operating condition by more than 5 K, then testing was stopped and the temperature of the burner was allowed to equilibrate back to the operating condition before further testing. The high thermal inertia of the nozzle assembly assured that temperature changes occurred very slowly and there was always opportunity to adjust the heating power as needed. Based on the temperature limitations of the bronze sintered metal material, heating of the burner is limited to 600 K to avoid thermal degradation of the sintered insert or metal epoxy. This combination of variable reactant dilution, reactant heating, and scalar dissipation rate

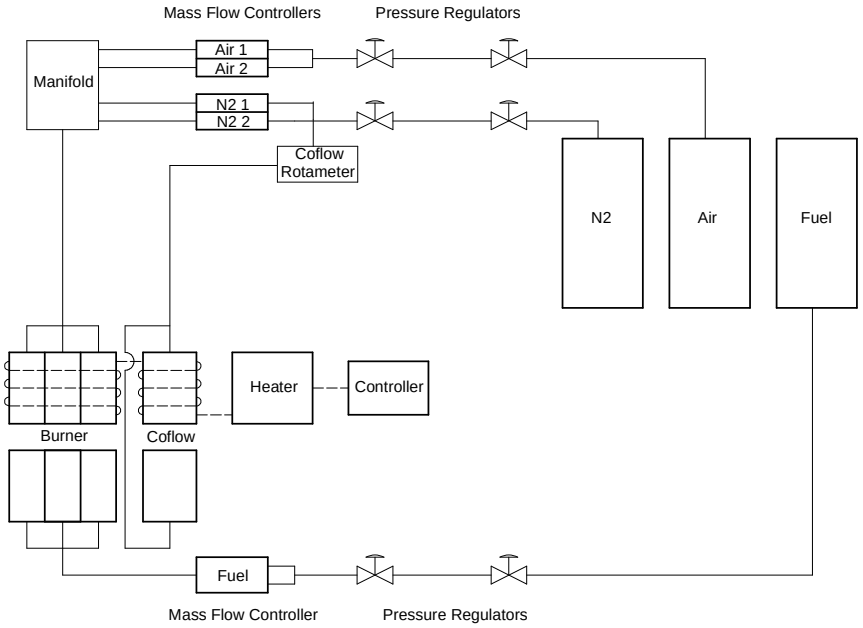

Figure 5: Diagram of experimental flow control and reactant heating system for oxidizer vitiation.

is thought to be unique for a counterflow burner. A diagram of the flow control and heater system is illustrated in Figure 5 in the oxidizer vitiation configuration. Converting the system to a fuel vitiation system requires minor plumbing modifications.

Operation of the burner must be approached with some caution. Due to the delay between initiation of fuel flow, ignition of the flame, and initiation of the co-flow system, there is the risk of creating a cloud of flammable mixture around the burner, or a large diffusion flame. A cloud of flammable mixture presents a risk of operator injury caused by thermal exposure to a fireball that is created when the burner is ignited. The large diffusion flame presents a risk of thermal damage to the burner itself or initiation of an accidental fire in the laboratory. In order to mitigate these risks, the operator of the burner must follow the steps listed in Table 1. These

steps are designed to minimize the release of fuel until the co-flow system is capable of isolating the reaction, thus minimizing the risk of thermal exposure to the operator, the burner and the laboratory.

In addition to the vitiated operating conditions discussed above, an attempt was made to artificially enhance the radiation losses from the experimental counterflow flames. It was the original intention that independent radiation losses can be applied to an opposed flow flame via a $TiCl_4$ delivery system. This is following a flow visualization technique used in combustion systems. The fuel stream is mixed with $TiCl_4$ vapor (concentration in the 1-10 ppm range), and at the flame, TiO_2 particles are produced when the $TiCl_4$ vapor reacts with water from the combustion. The reaction is $TiCl_4$ (g) + $2H_2O$ (g) → TiO_2 (s) + 4HCl (g). Since the concentration of $TiCl_4$ is low, it will not contribute a significant energy release rate compared to that of the combustion of fuel. The TiO_2 particles will radiate energy away from the flame in a manner similar to soot particle radiation, thus increasing the radiative losses from the flame. This radiative energy would have been measured with a heat flux gage near the flame in order to determine the experimental radiative fraction. Preliminary tests were conducted to test the overall impact of the radiatively enhanced flame. These tests demonstrated that flames with enhanced radiation losses had extinction conditions that were nearly identical to flames without enhanced radiation losses. Since there was no substantial difference between the two types of flames, it was concluded that $TiCl_4$ produced an insignificant radiative fraction at the scalar dissipation rate operating range of the burner. This, combined with other operational issues, led to the discontinuation of $TiCl_4$ doped flame experiments. In a hope to find

an alternative to $TiCl_4$, some OPPDIF simulations were performed with optically thin radiation models included with the software [11]. In these preliminary tests, the radiative fraction was determined for methane reacting with oxygen diluted with carbon dioxide. It was the hope that such elevated levels of carbon dioxide would produce a sufficient radiant fraction for the scalar dissipation rate range appropriate to the burner. The radiant fraction for a flame at χ_{st} = 0.5 s^{-1}, $T_{O_2}^{\infty} = T_F^{\infty}$ = 300 K, Y_F^{∞} = 1, $Y_{O_2}^{\infty}$ = 0.1791, $Y_{CO_2}^{\infty}$ = 0.8209 produced a radiant fraction of Γ = 0.0457, which would coincide with the maximum achievable radiative fraction for the burner. Due to the many possible complications that may arise with CO_2 dilution, primarily chemical interactions, highlighted by Chernovsky et al. and through personal communication with M. Chernovsky, this method was abandoned based on the low magnitude of Γ [59,61]. These discouraging results ultimately led to the discontinuation of experimentally enhancing radiation losses in favor of canonical numerical methods.

Step 1	Create a printout of the desired operating conditions for a set of tests.
Step 2	Turn on the oxidizer stream flow to the desired final operation level.
Step 3	Turn on the diluent nitrogen stream flow to a setting less than the desired final operation level.
Step 4	Turn on the fuel stream flow to less than 2 std. L/min of methane and ignite the fuel with a utility lighter if needed.
Step 5	Turn on the nitrogen co-flow to isolate the flame.
Step 6	Adjust the diluent nitrogen stream flow to the desired final operation level.
Step 7	Adjust the fuel stream flow to the desired operation level.
Step 8	Monitor the flame for several seconds. Determine if the co-flow or velocity ratio needs adjustment to maintain proper flame isolation and location.
Step 9	Observe the steady condition of the flame for several seconds and record if the condition produces a steady flame or extinction.
Step 10	Monitor the temperature of the burner to ensure it is within the range of the desired operating condition.
Step 11	If the operating condition produces a steady flame, repeat steps 2-10 while decreasing the reactant concentration.
Step 12	If the operating condition results in extinction, immediately stop the flow of methane followed by the flow of nitrogen co-flow, diluent, and air.
Step 13	Allow the burner to equilibrate to the desired operating temperature if necessary.
Step 14	Repeat steps 2-10 starting at a reactant concentration below that which was determined in step 12.
Step 15	If the operating condition results in extinction, repeat steps 2-10 while increasing the reactant concentration.
Step 16	If the operating condition produces a steady flame, immediately stop the flow of methane followed by the flow of nitrogen co-flow, diluent, and air.
Step 17	Compare the extinction conditions determined by decreasing and increasing reactant concentration to ensure accuracy and repeatability.
Step 18	Record the reactant concentration and burner temperature associated with the minimum reactant concentration capable of sustaining a flame.
Step 19	Repeat steps 1-16 for all desired reactant temperatures and vitiation modes.
Step 20	When testing is discontinued for an extended period, the operator must always ensure that all reactant and diluent supply vessels are closed.

Table 1: Operation procedure for conducting extinction experiments with the counterflow burner.

2.2.3 Diagnostics

The experimental diagnostics used in this study were simple visual observations of the flame behavior, and recording surface temperature readings. Images of the flame for $\chi_{st} = 0.49\ s^{-1}$ and decreasing oxidizer concentration are provided in Figure 6 along with a summary of the operating capabilities of the burner. It is clear from Figure 6 that the flame is initially luminous orange when burning in pure air, but as the operating conditions approach extinction, the flame changes to a weakly luminous blue. During steady operation of the burner, the operator must visually observe a few key features of the flame. The first key feature is the general location of the flame relative to the nozzle injectors. In order to minimize the possibility of conduction losses from the flame to the nozzle itself, the operator must ensure that the luminous reaction zone of the flame is near the center of the two nozzles. This will minimize temperature gradients at the nozzle surface, which would result in unwanted conductive heat transfer away from the flame. Visual observations in combination with preliminary OPPDIF testing indicate that reactant velocity ratios, $U_r = U_{O_2}^{\infty} / U_F^{\infty}$ between 2.0 and 3.0 are sufficient to ensure zero temperature gradient at the nozzle. The second key observation of the flame is the existence of the flame itself. In a typical testing scenario, the operator will search for an extinction condition by starting with a flammable condition, and slowly decrease the reactant concentration by factors as small as 0.001 in mass fraction, until the flame no longer exists at the steady state operating condition. It is the duty of the operator to observe the existence of the flame in said conditions, and record the extinction condition as the lowest concentration of reactants capable of sustaining a flame. The operator is

Burner Features

- Low strain flames: (12 s^{-1} – 75 s^{-1})
- Vitiated and heated reactant inlet.
  - 300 K < $T_{O_2}^{\infty}$ < 600 K
  - 0.0 < $Y_{O_2}^{\infty}$ < 0.23
  - 0.0 < Y_F^{∞} < 1.0
- Nitrogen co-flow flame isolation
- Constant scalar dissipation rate control algorithm: (0.3 s^{-1} – 1.5 s^{-1})

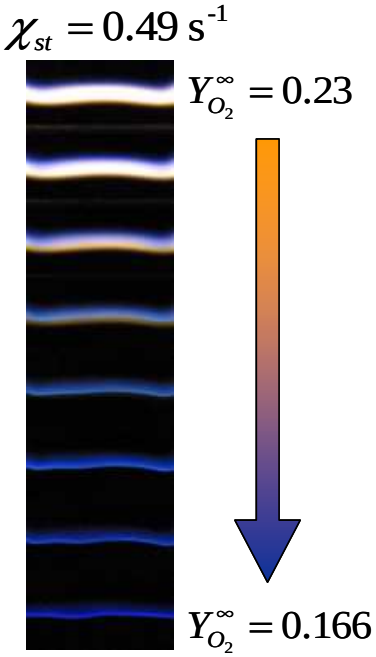

Figure 6: Summary of burner operating capabilities and sample flame images for oxidizer vitiation between pure air and extinction at $\chi_{st} = 0.49\ s^{-1}$.

required to record the surface temperature reading of the nozzle at the extinction condition. If the surface temperature deviates from the pre-selected operating temperature by less than 5 K, the extinction condition will be permanently recorded. If the surface temperature deviates more than 5 K, the operator must allow the burner to return to the desired operating temperature before attempting another experiment or recording the extinction condition. Should a second round of testing be required, the operator will have a good approximation of the extinction condition, expediting the ability to find the actual extinction condition. The experiment is then repeated at various oxidizer temperatures and scalar dissipation rates to produce a wide range of extinction conditions.

2.2.4 Error Analysis

Error analysis is critical when performing flame extinction analysis. The asymptotic behavior of flames near extinction implies that small errors in the control of the system will result in large errors in analysis of the results. The uncertainties in the control system are assumed to be random in nature, and the error in critical calculated quantities is derived from the method of addition of variances. Furthermore, the error analysis will assume that any covariance is negligible, i.e. any calculated quantity can be expressed as a system of independent variables. Following this assumption, a quantity Q is expressed as a function of independent variables, w_i:

$$Q = Q(w_1, w_2, ..., w_n), \tag{58}$$

and the overall uncertainty, ΔQ, is expressed as a function of uncertainties, Δw_i, resulting in:

$$\Delta Q = \sqrt{\sum_{i=1}^{n} \left(\frac{\partial Q}{\partial w_i} \Delta w_i \right)^2}. \tag{59}$$

While some quantities can be expressed solely based on control errors, other quantities must be expressed based on errors in calculated quantities. The most critical examples of this are $\chi_{st} = \chi_{st}(a_g, \varphi, Z_{st})$ and $T_{st,BS} = T_{st,BS}(Y_{O_2}^{\infty}, Y_F^{\infty}, T_{O_2}^{\infty}, T_F^{\infty})$. Fortunately, uncertainties can be determined for each of these quantities separately based on the fact that each of these variables has an associated analytic expression. The partial differentiation of quantities has been performed numerically for the sake of simplicity. Furthermore, the derivatives are evaluated at two characteristic experimental extinction conditions corresponding to χ_{st} = 0.49 s^{-1}, χ_{st} = 0.5 s^{-1}, $T_{O_2}^{\infty}$

= T_F^∞ = 300 K, Y_F^∞ = 1, $Y_{O_2}^\infty$ = 0.166 for oxidizer vitiation, and χ_{st} = 0.49 s^{-1}, χ_{st} = 0.5 s^{-1}, $T_{O_2}^\infty$ = T_F^∞ = 300 K, $Y_{O_2}^\infty$ = 0.23, and Y_F^∞ = 0.127 for fuel vitiation. The error is calculated separately for oxidizer and fuel vitiation because, experimentally, these modes were performed separately and never combined, and from the observation that some errors were dramatically different between these two modes. The results of the error analysis are illustrated in Table 2 for some key parameters.

Characteristic Control Quantities				
w_i (units)	Range	Δw_i	$\Delta w_i / w_i$ (%)	Notes
$T_{O_2}^\infty$ (K)	300 – 500	10	2.0 – 3.3	Oxidizer temperature
T_F^∞ (K)	300	10	3.3	Fuel temperature
U_{air}^∞ (m/s)	0.069 – 0.242	0.0013	0.6 – 1.9	Air flow rate
U_F^∞ (m/s)	0.025 – 0.162	0.0020	1.2 – 8.1	Fuel flow rate
$U_{N_2}^\infty$ (m/s)	0.029 – 0.072	0.0013	1.9 – 4.7	Diluent flow rate
Calculated Quantities, Oxidizer Vitiation				
Q (units)	Range	ΔQ	$\Delta Q/Q$ (%)	Notes
$Y_{O_2}^\infty$	0.151 – 0.193	0.0040	2.1 – 2.7	Oxidizer mass fraction
Y_F^∞	1.0	0.0	0.0	Fuel mass fraction, fixed
$T_{st,BS}$ (K)	1640 – 1935	34	1.8 – 2.1	Equation (4)
χ_{st} (s^{-1})	0.4 – 2	0.0074	0.4 – 1.8	Equation (49)
Calculated Quantities, Fuel Vitiation				
Q (units)	Range	ΔQ	$\Delta Q/Q$ (%)	Notes
$Y_{O_2}^\infty$	0.23	0.0	0.0	Oxidizer mass fraction, fixed
Y_F^∞	0.110 – 0.156	0.0097	6.2 – 8.8	Fuel mass fraction
$T_{st,BS}$ (K)	1640 – 1800	35	1.9 – 2.1	Equation (4)
χ_{st} (s^{-1})	0.25 – 0.98	0.0400	4.1 – 16.0	Equation (49)

Table 2: Experimental uncertainty of selected quantities calculated for oxidizer and fuel vitiation.

The uncertainty analysis demonstrates the high fidelity of the experimental methods. Only a few quantities have errors exceeding 4 %, with the exceptions affecting fuel vitiation only. One observation of Table 2 is the magnitude of the variation in $T_{st,BS}$, which is 35 K. This value is large with respect to the range of temperatures observed. The magnitude of this error is due to the very strong dependence of Equation (4) to variations in $Y_{O_2}^{\infty}$ and Y_F^{∞}. Fortunately, the error is small with respect to the overall magnitude of $T_{st,BS}$, and results will illustrate that this error is reasonable with respect to the scatter of the data. Another error to address is that associated with the fuel vitiation terms Y_F^{∞} and χ_{st}. The magnitude of the error in these terms is due in large part to the propagation of error from the fuel flow rate. In the fuel vitiation case, extremely small concentrations of fuel are required to cause extinction. This translates to low control operating conditions of the fuel flow rate with respect to those of the diluent. As a result, even a small error in the fuel flow rate will result in a comparatively large error in the fuel concentration and scalar dissipation rate. This error can be mitigated in the future with the purchase of an alternate fuel mass flow controller with a low full-scale flow capacity. In the current study, it is evident that these errors are reasonable with respect to the scatter of the data. Experimental data is published using open symbols, and error bars corresponding to the selected extinction conditions will be shown where significant.

2.3 Computational Methodology

2.3.1 Counterflow Flame Solver

The counterflow flames are evaluated numerically using the OPPDIF code. These numerical simulations are controlled using the same methodology and systematic modification of controlling parameters as the experiment described above. OPPDIF is an opposed flow diffusion flame code included in the detailed chemical kinetics software, Chemkin v4.1. OPPDIF solves the simplified partial differential equations describing opposed flow diffusion flames with detailed chemistry mechanisms provided by GRI mechanism 3.0 [11]. The implementation of the model utilizes mixture averaged diffusion model, but it has the capability to simulate detailed, multi-species diffusion. The solver has a user-modifiable subroutine called QFUN, which simulates optically thin radiation losses from the flame following Equation (18). This subroutine has the capability to define the Planck mean absorption coefficient, κ, based on the local concentration of selected gases, or the flexibility to hold it constant. The first method for determining κ is useful for determining the radiation losses from real flames; however forcing κ to remain constant results in a more canonical method to produce flame radiation losses. Utilizing the OPPDIF code allows for unrestricted prescription of input parameters. This is in contrast to the experimental setup, which limits the producible range of scalar dissipation rates, reactant temperatures and radiation losses. The utilization of a numerical counterflow flame solver allows for the generation of extinction conditions over the largest possible input parameter space of reactant concentration, reactant temperature, scalar dissipation rate, and radiation losses.

2.3.2 Controls

Inputs for the OPPDIF simulations are prescribed following the same method as the experiments. The only notable difference between the experiment and the numerical simulation is that the mass fraction of the reactants is refined to 0.0001 in OPPDIF, while only refined to 0.001 experimentally. Again, it is important to note that the range of applicable input conditions are dramatically increased in OPPDIF compared to that of the experimental setup.

2.3.3 Diagnostics

Due to the level of detail provided by OPPDIF outputs, many more diagnostics are possible. The primary diagnostic used in OPPDIF simulations is the determination of an extinction condition. This diagnostic is performed in a way similar to the experiment in that the operator starts a simulation at a known stable flame condition, and then systematically reduces the reactant concentration maintaining constant scalar dissipation rate. When the simulation output transitions from a reacting solution to a mixing solution, the operator saves the input files for the simulation, and compiles the desired output data for analysis. Again, the extinction condition is defined as the lowest reactant concentration that allows for steady burning. Similarly, increasing the scalar dissipation rate or increasing the radiative fraction can achieve extinction, and these methods will be discussed in Chapter 4.

Other diagnostics can be derived from the detailed OPPDIF output as illustrated in Figure 7 through Figure 16, which illustrate solutions at constant scalar dissipation rate (χ_{st} = 1.0) and reactant temperature while decreasing the oxidizer mass fraction to extinction. Of particular interest to the current study are Figure 8 (b)

for local temperature and Figure 11 (b) for local scalar dissipation rate. The data illustrated in Figure 8 (b) are used to determine the stoichiometric flame temperature following detailed chemistry, by linearly interpolating the data points immediately surrounding $Z = Z_{st}$. An identical method is used for the calculation of χ_{st} from Figure 11. Likewise, $\dot{q}''_{gen}$ is calculated from the numerical integration of Figure 7 (a), which will be useful in determining Γ and $\dot{q}''_{gen,1}$, to be used when radiation losses from the flame are invoked. Figure 7 (a) also illustrates a simple method for determining the integral length scale for energy generation, $\delta_{gen,1}$.

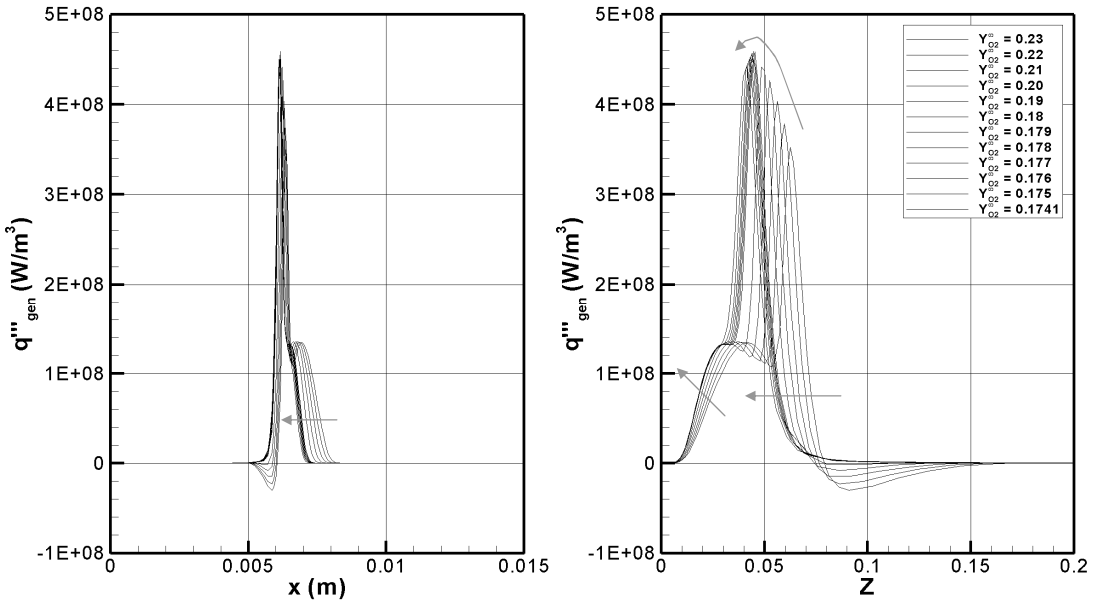

(a) (b)

Figure 7: OPPDIF output of flame energy generation per unit volume versus location (a) and mixture fraction (b). Arrows indicate solutions of decreasing $Y_{O_2}^{\infty}$.

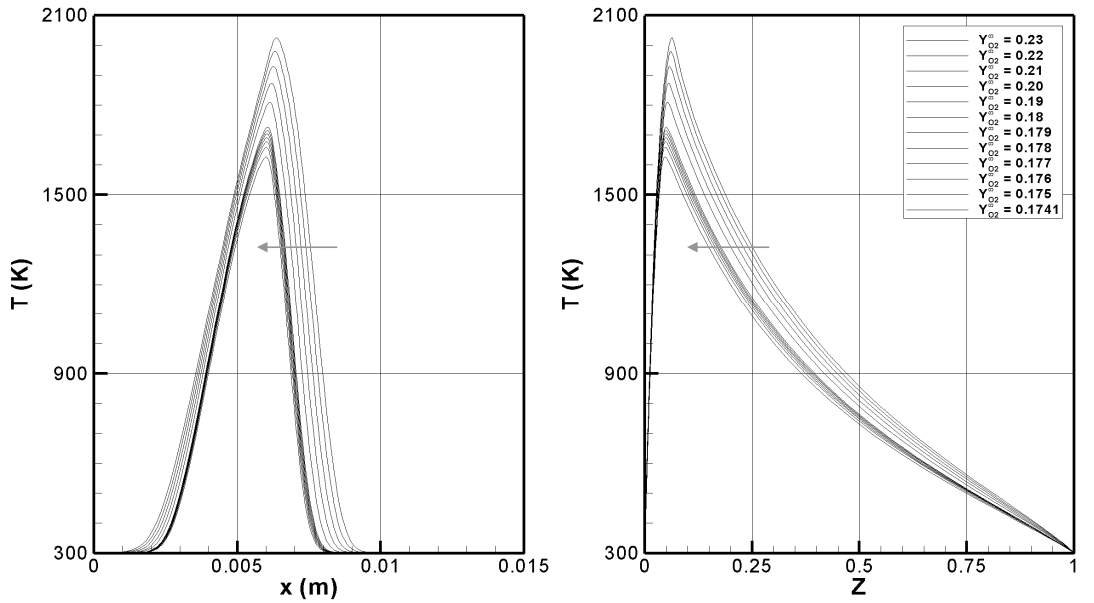

(a) (b)

Figure 8: OPPDIF output of local temperature versus location (a) and mixture fraction (b). Arrows indicate solutions of decreasing $Y_{O_2}^{\infty}$.

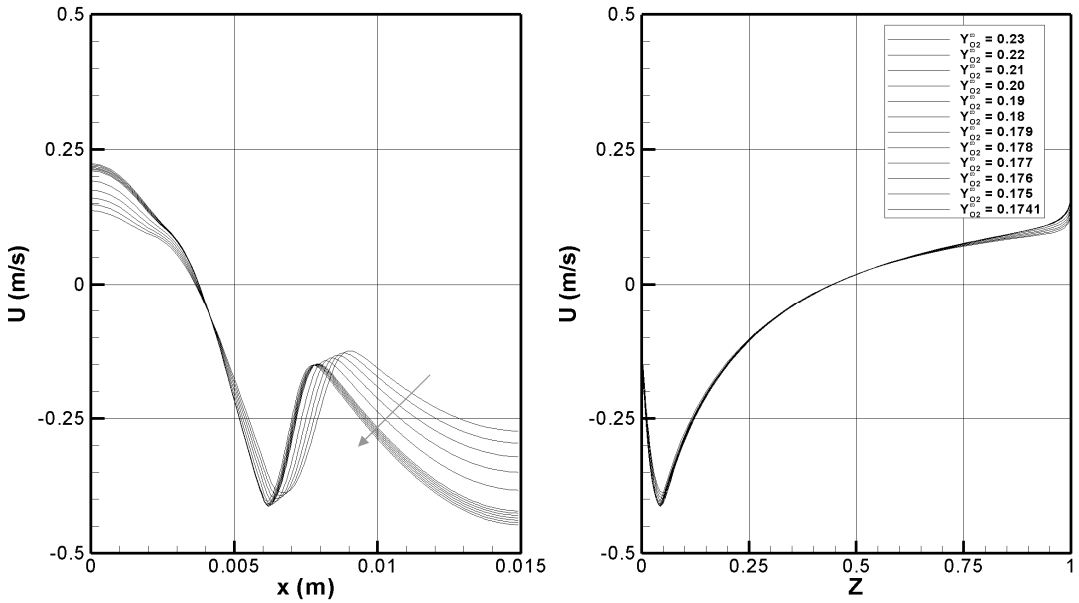

Figure 9: OPPDIF output of local velocity versus location (a) and mixture fraction (b). Arrows indicate solutions of decreasing $Y_{O_2}^{\infty}$.

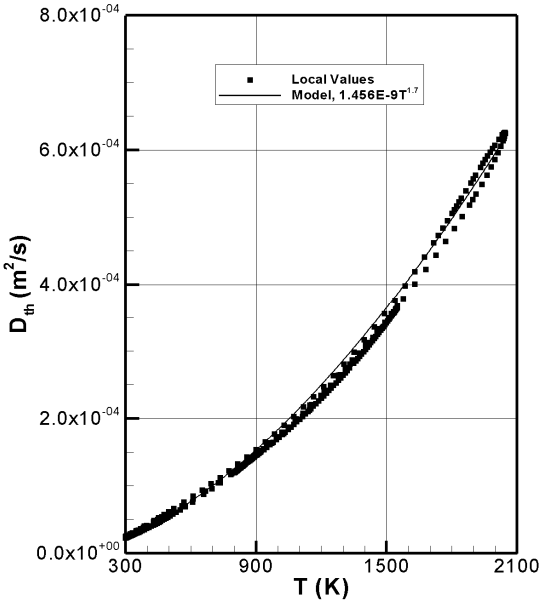

Figure 10: OPPDIF output of local thermal diffusivity versus local temperature for several simulations. Thermal diffusivity is a non-standard output and a commonly used model is illustrated as a simplification.

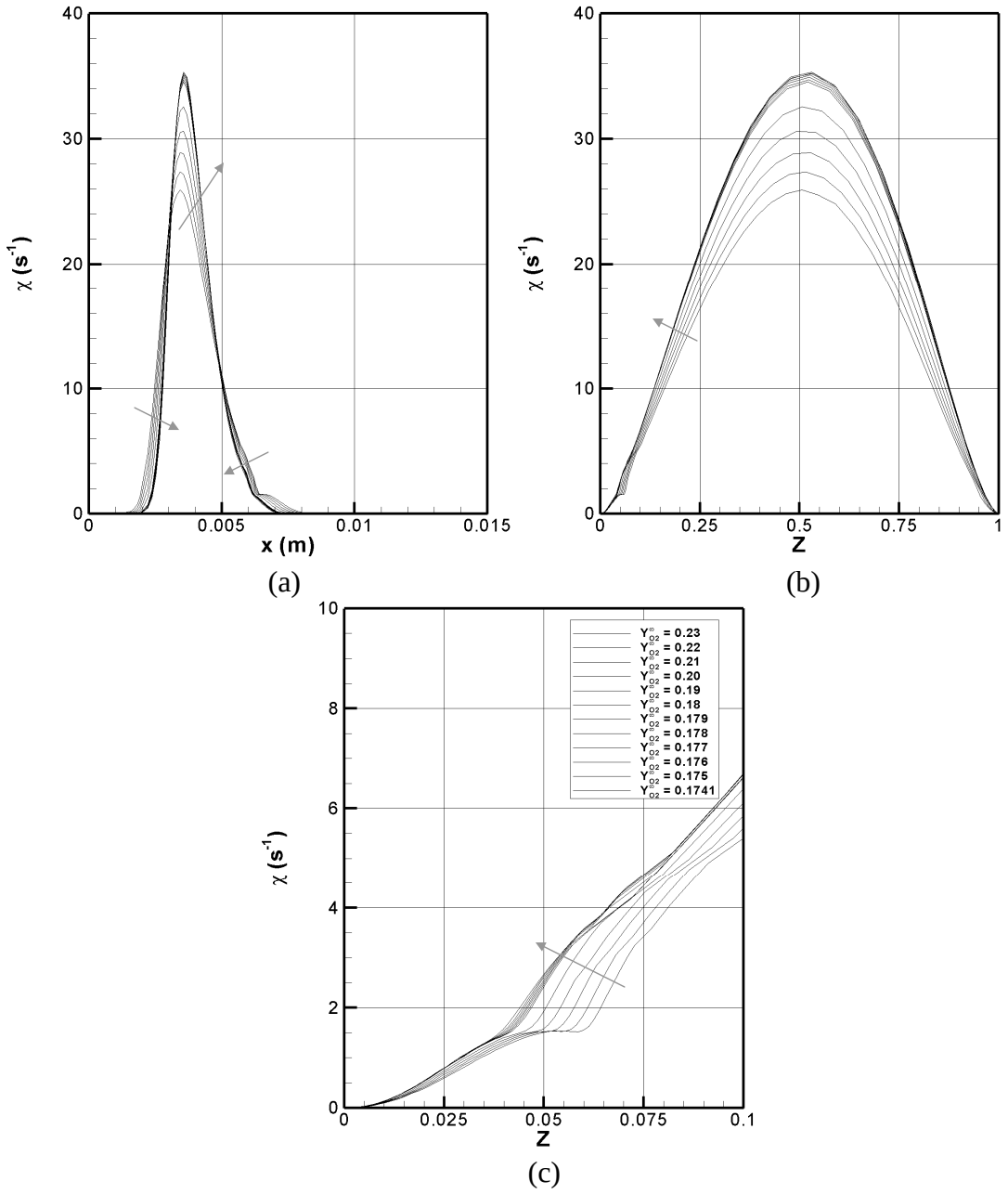

Figure 11: Calculation of scalar dissipation rate from OPPDIF output from Equation (5) versus location (a) and mixture fraction (b) and (c). Arrows indicate solutions of decreasing $Y_{O_2}^{\infty}$.

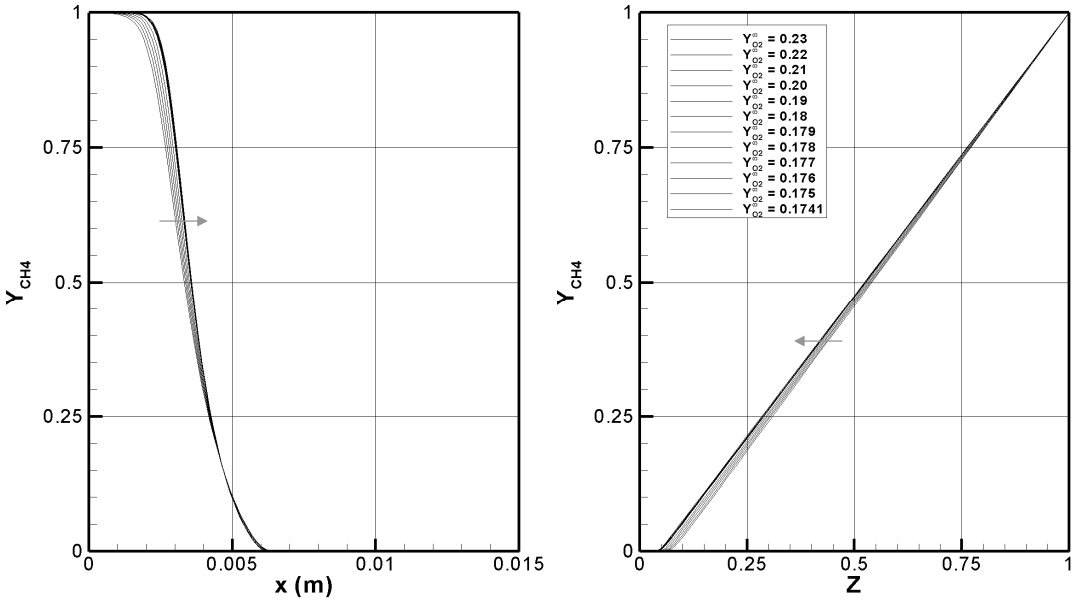

(a) (b)

Figure 12: OPPDIF output of local mass fraction of methane versus location (a) and mixture fraction (b). Arrows indicate solutions of decreasing $Y_{O_2}^{\infty}$.

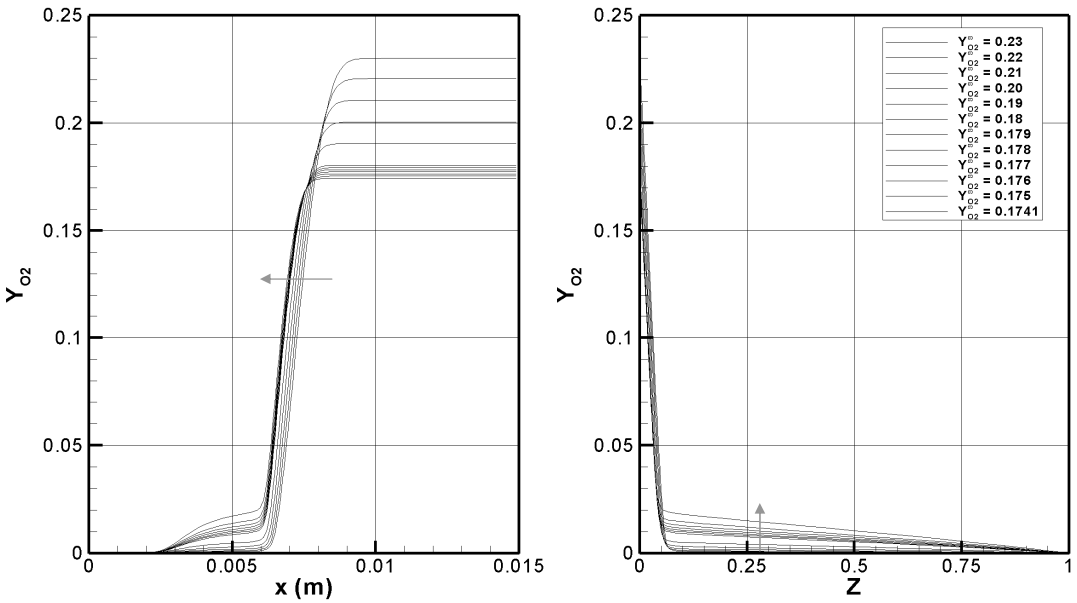

(a) (b)

Figure 13: OPPDIF output of local mass fraction of oxygen versus location (a) and mixture fraction (b). Arrows indicate solutions of decreasing $Y_{O_2}^{\infty}$.

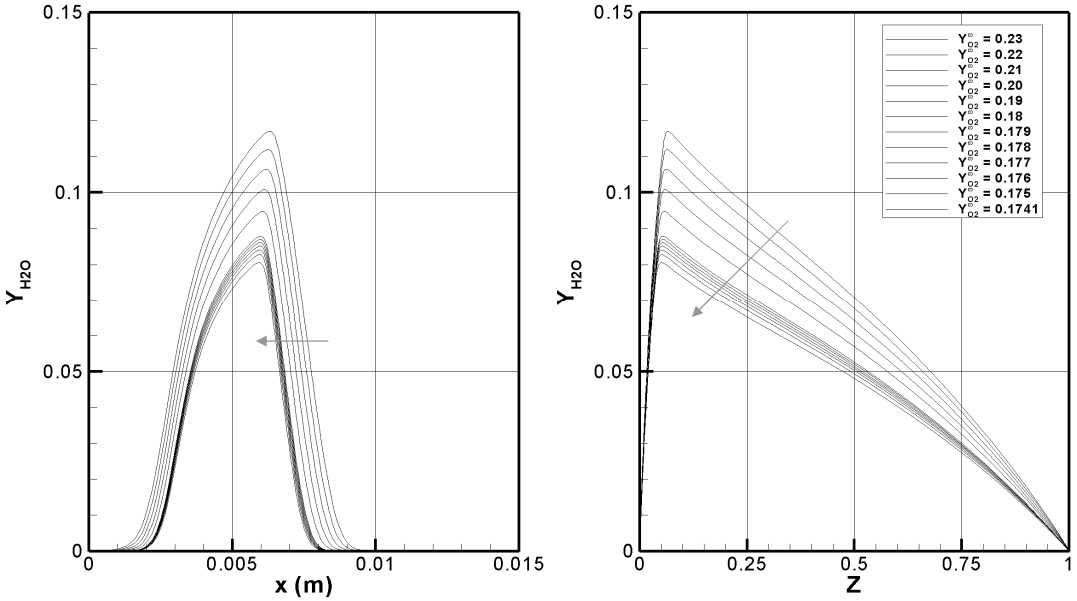

Figure 14: OPPDIF output of local mass fraction of water vapor versus location (a) and mixture fraction (b). Arrows indicate solutions of decreasing $Y^{\infty}_{O_2}$.

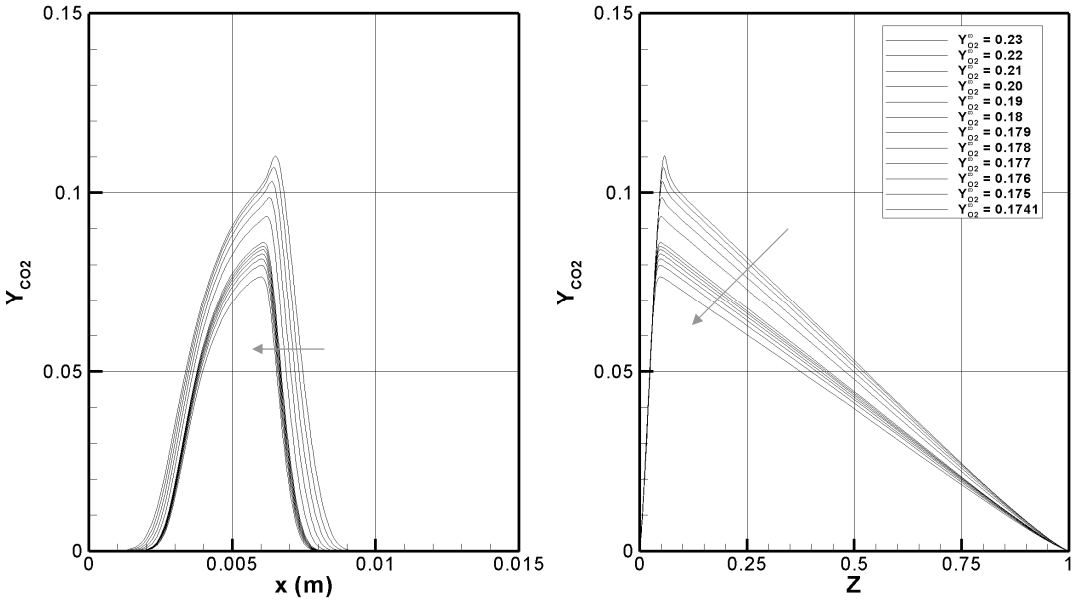

Figure 15: OPPDIF output of local mass fraction of carbon dioxide versus location (a) and mixture fraction (b). Arrows indicate solutions of decreasing $Y^{\infty}_{O_2}$.

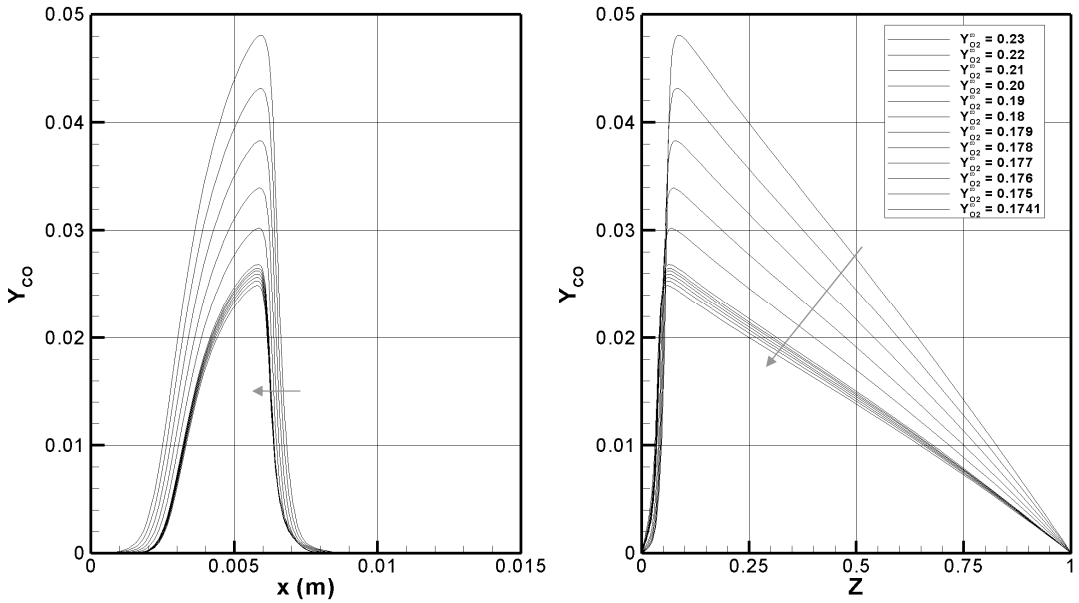

Figure 16: OPPDIF output of local mass fraction of carbon monoxide versus location (a) and mixture fraction (b). Arrows indicate solutions of decreasing $Y_{O_2}^{\infty}$.

2.3.4 Error Analysis

Due to the nature of the OPPDIF solver, errors in output are difficult to quantify. While there may be systematic errors associated with the modeling of the balance equations, and the selection of sub-models used in the OPPDIF solver, these errors will be ignored. Other errors can result from the numerical methods used to analyze the raw data from OPPDIF. These errors will affect the calculation of integrals, derivatives, and linear interpolations that affect the determination of $\dot{q}''_{gen}$, $\dot{q}''_{rad}$, Γ, χ_{st} from Equation (5), and T_{st}. These errors appear to be negated by the fine resolution of the OPPDIF output, and as a result, the magnitude of these errors can be effectively ignored. Future illustration of data and analysis produced by OPPDIF will be published as solid symbols without error bars.

2.4 Summary

The experimental and numerical approach utilized by this study was developed with a thorough review of flamelet theory as the basis. All fundamental parameters affecting flame extinction have been determined based on the most current understanding of flamelet theory. This approach demonstrates the power of flamelet theory to predict extinction conditions over several orders of magnitude of variation in parameter space. Most importantly, the only inputs required for the model presented in this study are local values of $Y_{O_2}^{\infty}$, Y_F^{∞}, $T_{O_2}^{\infty}$, T_F^{∞}, χ_{st} and κ. The ability of any CFD code to model local flame extinction depends entirely on the availability of these 6 parameters. All CFD codes designed to simulate fire already have the capability to determine the properties that define vitiation. The local scalar dissipation rate and radiant fraction present some challenges in the realm of LES, and these values can only be accurately determined from advanced sub-grid models. The goal of the current research is to develop a model that can capture all or most of the applicable physics governing flame extinction and present them in a way that can be applied to CFD codes. The ultimate decision of the implementation of this model must be made by the CFD publisher based on the capabilities of the sub-grid models therein.

Chapter 3: Results

3.1 Extinction of Flames with Pure Air and Pure Fuel

In order to gain the most basic understanding of the causes of flame extinction, it is useful to examine the behavior of flames in pure air and pure fuel conditions. The characterization of flame extinction with pure air and pure fuel demonstrates that extinction can result from any increase in energy losses from the flame while isolating any effects of vitiation. This form of analysis highlights two known regimes of flame extinction. The first is extinction dominated by the increase of convective energy loss from the flame, called the kinetic limit. The kinetic limit is the most commonly recognized and understood mode of flame extinction, as it is historically represented by the classical S-shaped curve [37]. The second regime of flame extinction is dominated by radiation losses from the flame, called the radiative limit. The radiative limit has received increased recognition due to the study of spherical diffusion flames in microgravity [50]. The experimental approach developed in this study is not capable of producing either of these limits; therefore, numerical simulations with OPPDIF are utilized. It is critical to realize that these two mechanisms are not mutually exclusive. While this study only presents two extinction conditions for pure air and pure fuel, there are conceivably infinite combinations of convective and radiative heat losses from flames that will result in extinction.

3.1.1 Kinetic Limit

The kinetic limit of a pure air and pure fuel system is achieved by gradually increasing the reactant leakage losses from the flame until extinction occurs. This regime is also commonly called “blowout,” because it is determined by gradually increasing the velocity of reactants until the flame is extinguished. At the kinetic limit, the reactant leakage loss is orders of magnitude greater than the radiative heat loss from the flame, and it is typical to ignore the effects of radiation losses [36]. The kinetic limit has been reproduced in this study in the context of detailed chemistry solutions from OPPDIF following the classical S-shaped curve pathway to extinction, as illustrated in Figure 17. This pathway to extinction is produced by starting at a stable flame at a moderate scalar dissipation rate, then gradually increasing the scalar dissipation rate until extinction occurs. A unique feature of the kinetic limit is that the generation of energy per unit area of flame increases with increasing scalar dissipation rate per Equation (6) while the flame temperature decreases. This behavior indicates that, despite the increase in energy generation with scalar dissipation rate, kinetic losses increase at a faster rate, resulting in extinction. The kinetic limit as illustrated in Figure 17 will be used as the reference extinction condition for the remainder of the study to aid in the normalization of model expressions. While any extinction condition can be called the reference extinction condition, the kinetic limit provides numerical advantages due to its relatively high scalar dissipation rate and flame temperature at extinction.

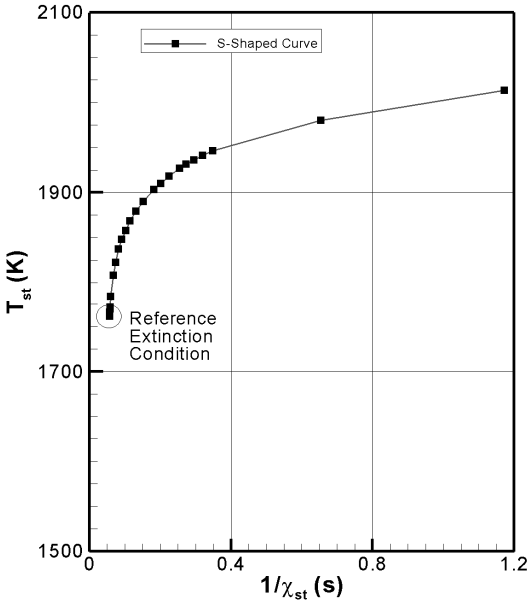

Figure 17: Determination of the reference extinction condition by recreating the classical S-Shaped curve with $T_{O_2}^{\infty} = T_F^{\infty}$ = 300 K, $Y_{O_2}^{\infty}$ = 0.23, Y_F^{∞} = 1 and χ_{st} from Equation (5).

3.1.2 Radiative Limit

The radiative limit is achieved at extremely low scalar dissipation rates where radiation losses become dominant. The radiative limit has been reproduced in this study using detailed chemistry solutions from OPPDIF by gradually reducing the scalar dissipation rate, as illustrated in Figure 18. The numerical solutions of these flames are incredibly stiff, and require approximately one thousand continuation solutions to find the radiative limit. For convenience, only a portion of this data is illustrated below. If one were to reproduce Figure 18 without applying a model for radiation losses, the stoichiometric flame temperature would asymptotically approach the adiabatic flame temperature with decreasing scalar dissipation rate. Instead, while the scalar dissipation rate reduces, the energy production of the flame decreases until it becomes comparable to the radiation losses from the flame, as illustrated in

Figure 19. At the radiative limit, extinction is the direct result of flame temperature reduction due to the relatively large radiative energy losses from the flame. The same is true for the kinetic limit; however, the mechanism for temperature reduction is determined by the reactant leakage losses from the flame. At the kinetic limit, radiation losses are negligible due to the thin nature of the high temperature region of the flame at high strain rates. The radiative limit corresponds to an extremely low value of the scalar dissipation rate, a large value of the radiative fraction due to thickening of the high temperature region, and a relatively low flame temperature at extinction. In the detailed chemistry framework, the kinetic limit has a flame temperature of $T_{st} = 1762$ K, a radiant fraction of $\Gamma = 0.0$, and a scalar dissipation rate of $\chi_{st} = 17.34\ s^{-1}$. At the radiative limit, the flame temperature is $T_{st} = 1359$ K, the radiative fraction is $\Gamma = 0.6139$, and the scalar dissipation rate is $\chi_{st} = 5.167 \times 10^{-3}\ s^{-1}$. These findings are in agreement with the findings of Maruta et al. and Chan et al., with the only differences resulting from selection of radiation model and chemical mechanism [75,76].

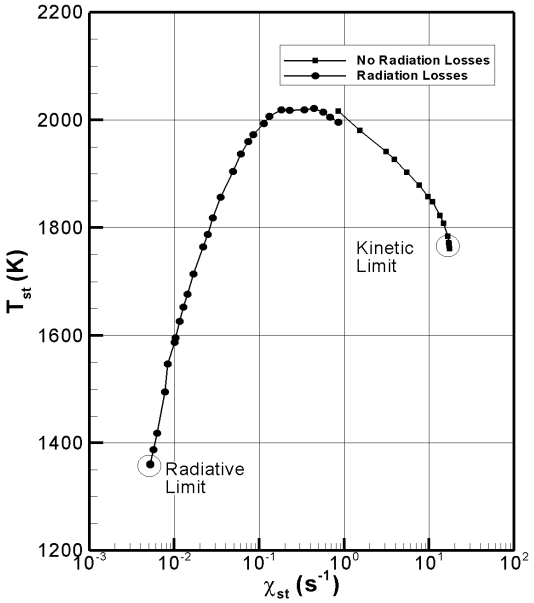

Figure 18: Stoichiometric flame temperature versus scalar dissipation rate for flames between the kinetic extinction limit and the radiative extinction limit with $T_{O_2}^{\infty} = T_F^{\infty}$ = 300 K, $Y_{O_2}^{\infty}$ = 0.23, Y_F^{∞} = 1 and χ_{st} from Equation (5).

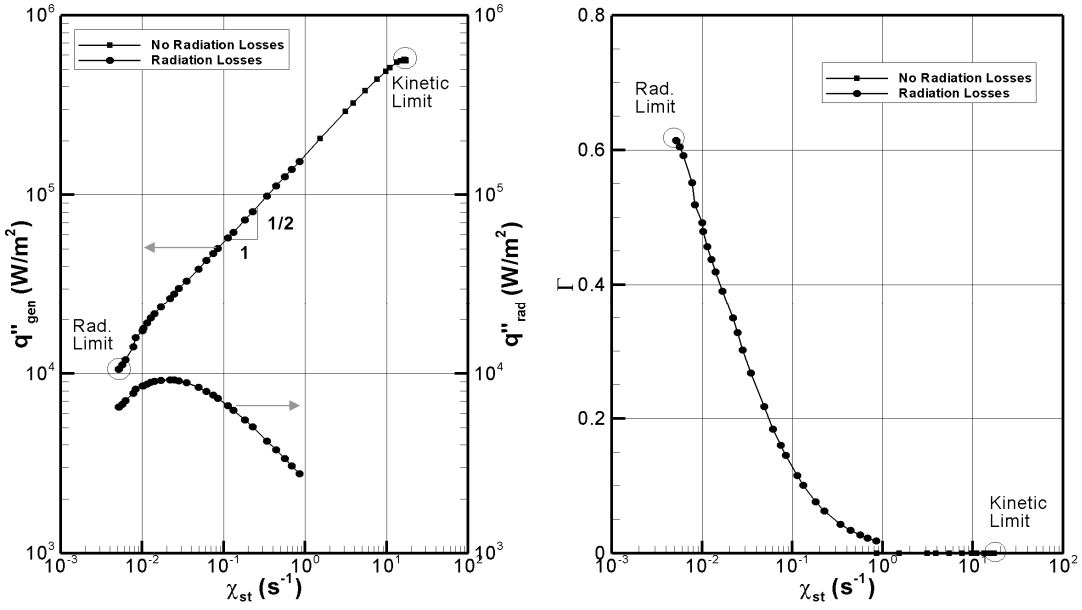

(a) (b)

Figure 19: (a) Flame energy generation and radiation losses per unit area, and (b) integral radiant fraction, versus local scalar dissipation rate between the kinetic and radiative extinction limits with $T_{O_2}^{\infty} = T_F^{\infty}$ = 300 K, $Y_{O_2}^{\infty}$ = 0.23, Y_F^{∞} = 1 and χ_{st} from Equation (5).

The low magnitude of the scalar dissipation rate at the radiative limit is an interesting occurrence, because of its association with a characteristic flow time. The inverse of the scalar dissipation rate is proportional to a characteristic flow time; therefore, the flow timescale associated with the radiative limit is approximately 4 decades larger than the kinetic limit. This timescale may prove to be problematic when applied to CFD simulations of turbulent fires, where instantaneous fluctuations of the scalar dissipation rate may be faster than the timescale required to reach steady state. Moreover, recent DNS studies indicate that regions of low scalar dissipation rate promote soot production, while regions of high scalar dissipation rate force soot to accumulate within the fuel side of the reaction [99]. This combination of effects will increase the radiation losses from the flame, especially in the low scalar dissipation rate regions where the generation of energy is low [101].

3.1.3 Additional Significant Observations

While the primary focus of this work is to examine flame extinction behavior, some other important observations can frequently be made from the data obtained for stable flame conditions. One significant observation can be made from the comparison of the exact determination of the scalar dissipation rate from Equation (5) and the model for scalar dissipation rate from Equation (49), as illustrated in Figure 20. This comparison demonstrates the accuracy of the analytic expression for the scalar dissipation rate over the entire range of flow conditions explored in this study. Another important observation can be made from Figure 19 and Figure 21 regarding the application of the Burke-Schumann flame temperature corrected for radiation

losses from Equation (23) as discussed in Section 2.1.3. Both Figure 19 and Figure 21 demonstrate that $\dot{q}''_{gen}$ can be expressed as a function of $\chi_{st}^{1/2}$, which supports the suggested simplification used in Equation (26). The relationship of $\chi_{st}^{1/2}$ is attributable to the integration of Equation (6) following the advice of Poinsot and Veynante [97]. Also, Figure 21 allows for the determination of $\dot{q}''_{gen,1} = 2.06\times10^{5}$, W/m^2, which is critical for the application of Equation (26) to either the AEA model or the SCDN model.

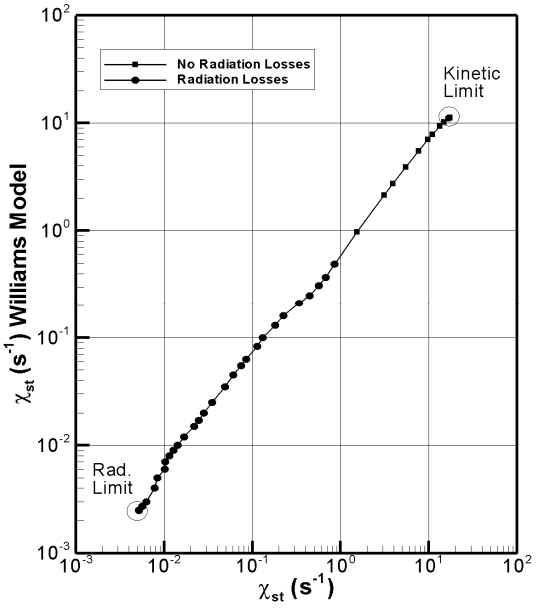

Figure 20: Scalar dissipation rate model from Equation (49) versus the direct calculation of the scalar dissipation rate from Equation (5), illustrating a nearly 1 to 1 relationship.

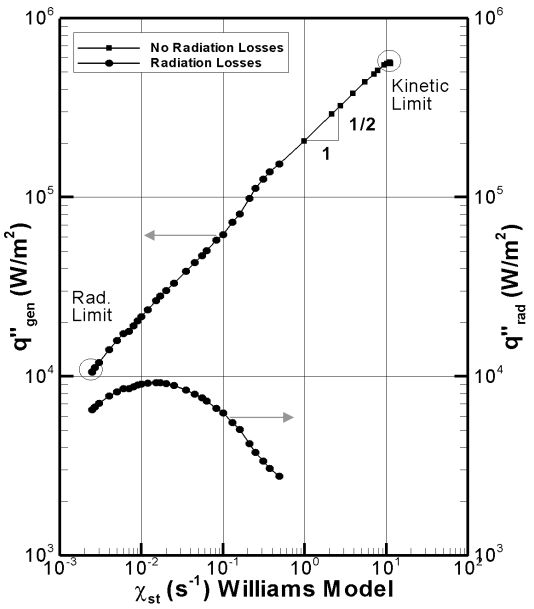

Figure 21: Flame energy generation and radiation losses per unit area versus local scalar dissipation rate between the kinetic and radiative extinction limits with $T_{O_2}^{\infty} = T_F^{\infty}$ = 300 K, $Y_{O_2}^{\infty}$ = 0.23, Y_F^{∞} = 1 and χ_{st} from Equation (49). ($\chi_{st,1} = 1\,\mathrm{s}^{-1}, \dot{q}''_{gen,1} = 2.06\times10^{5}\ \mathrm{W/m}^2$)

3.2 Extinction with Vitiation Effects

In order to properly isolate and study the effects of vitiation on flame extinction, this study has adopted an approach of determining vitiated extinction conditions along a pathway of constant scalar dissipation rate. This is done with the intention of maintaining a constant kinetic loss for each vitiated flame. This approach ensures that the extinction conditions are unaffected by changes in the kinetic loss. Also, in a preliminary step, radiation losses are ignored in order to determine appropriate model parameters prior to exploring the effects of radiation losses. An example of the constant scalar dissipation rate pathway to extinction is illustrated in Figure 22 in the context of detailed chemistry. It is clear from Figure 22 (a) that

vitiated extinction conditions can occur at widely different scalar dissipation rates and flame temperatures. Figure 22 (b) illustrates interesting behavior of the flame energy generation per unit area and temperature as the reactant is diluted. The flame energy generation per unit area appears to remain constant until near extinction where it drops dramatically, like a step function behavior. This behavior can be deduced from Equation (6), which suggests that the energy generation per unit area should be nearly constant with scalar dissipation rate. Another interesting observation from Figure 22 (b) is the nearly linear reduction in flame temperature with oxidizer concentration. This behavior is also to be expected from analysis of the Burke-Schumann flame temperature expression from Equation (4), where, for small values of $Y_{O_2}^{\infty}$, flame temperature is linear with $Y_{O_2}^{\infty}$.

Analysis of Figure 22 indicates that the primary mechanism controlling purely vitiated extinction is the reduction in flame temperature with reducing reactant concentration (increased diluent). This mechanism is not unlike that of the kinetic and radiative limits previously discussed, where the thermal losses primarily result in a reduction in flame temperature and then extinction. The strongest suggestion of this link is based on the fact that a vitiated S-shaped curve can be developed to produce the vitiated extinction condition in Figure 22 (a). This alternative S-shaped pathway to extinction is determined by starting with a stable flame at the desired vitiated conditions and a moderate scalar dissipation rate, then gradually increasing the scalar dissipation rate to extinction. In the conventional pathway to extinction, the temperature is reduced by the relative increase of the kinetic losses compared to generation of energy. In the alternative pathway, these kinetic losses are maintained

constant, and the temperature is reduced by the heat capacity of the added inert diluent. Each of these methods result in the determination of the same vitiated extinction condition. Following a constant scalar dissipation rate pathway has the added benefit of allowing for each input condition to be within the accepted experimental operating conditions, while an S-shaped pathway may require operation outside of the accepted conditions.

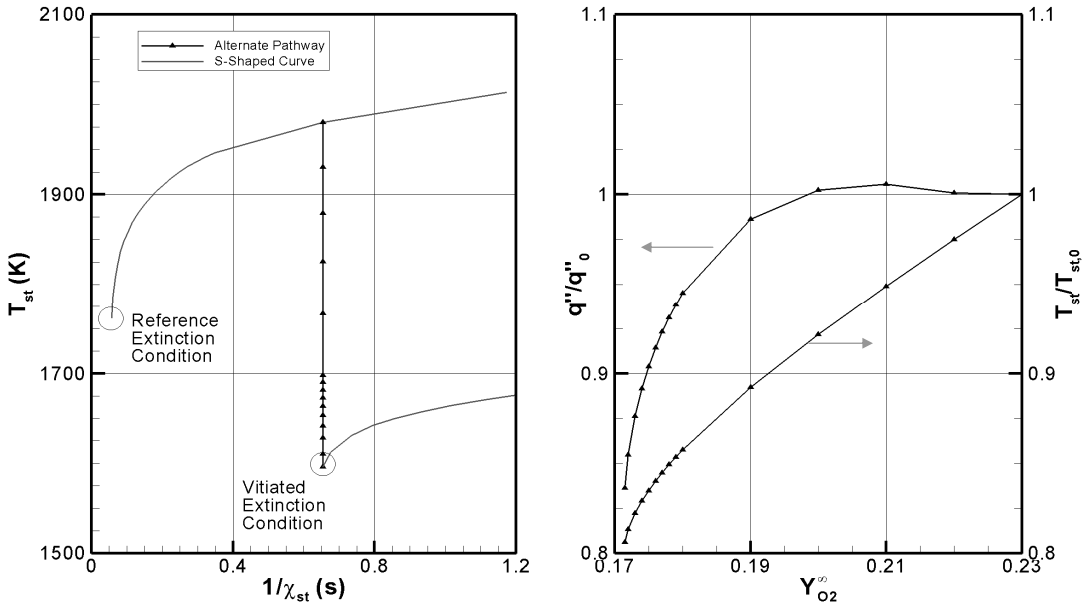

(a) (b)

Figure 22: (a) Illustration of a vitiated constant scalar dissipation rate pathway to extinction. (b) Description of flame energy production per unit area and stoichiometric temperature along the constant scalar dissipation rate pathway where $T^{\infty}_{O_2} = T^{\infty}_{F}$ = 300 K, $Y^{\infty}_{O_2}$ = 0.23, Y^{∞}_{F} = 1 and χ_{st} = 1.53 s^{-1} using Equation (5), $T_{st,0}$ = 1980 K, and q''_0 = 2.06 × 10^5 W/m^2 from OPPDIF.

3.2.1 Oxidizer Vitiation

Oxidizer vitiation is the result of diluting and preheating the oxidizer stream that is supplied to the flame. Dilution of oxidizer will reduce the flame temperature, while preheating of oxidizer will increase the flame temperature. Flame extinction is achieved when the flame temperature is reduced sufficiently by dilution, such that the kinetic losses from the flame become comparable to the generation of energy. In preliminary analysis, the effect of radiation losses will be ignored with only kinetic losses considered. Figure 23 illustrates the critical flame temperatures that are associated with oxidizer vitiation conditions. Figure 23 (a) is the proof of concept from detailed chemistry, and Figure 23 (b) is the application of the Burke-Schumann flame temperature model from Equation (4), with open symbols representing experimentally determined extinction conditions. Each of these models demonstrate that reducing the oxidizer concentration reduces the flame temperature at extinction, while increasing the oxidizer temperature increases the flame temperature at extinction. However, Figure 23 is not an appropriate extinction map, as it is challenging to derive a pathway from flammable mixtures through the critical values to a region where extinction will always occur. Figure 23 is more of a demonstration that the Burke-Schumann model is appropriate for accounting for the effects of vitiation in comparison to the behavior of a flame with detailed chemistry.

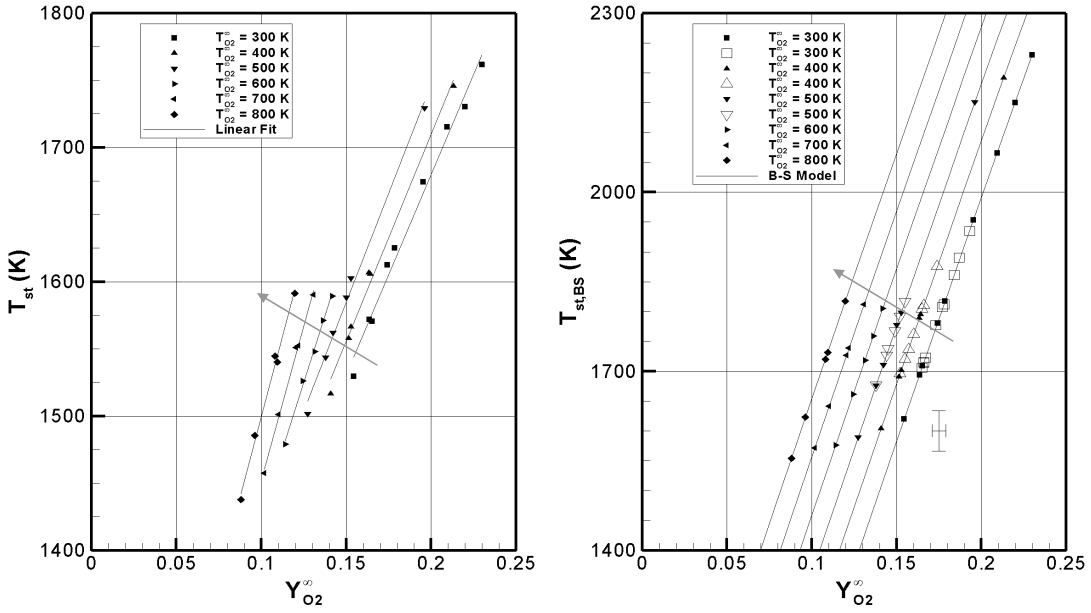

(a) (b)

Figure 23: Illustration of oxidizer vitiation effects on extinction flame temperature for detailed chemistry from OPPDIF (a) and the Burke-Schumann model (b). The linear fit lines in (a) are used to highlight data grouping and the arrows indicate groups of increasing $T^{\infty}_{O_2}$. (T^{∞}_{F} = 300 K, Y^{∞}_{F} = 1)

3.2.2 Fuel Vitiation

Fuel vitiation is the result of diluting and preheating the fuel stream supplied to the flame. Dilution of fuel will reduce the flame temperature, while preheating of fuel will increase the flame temperature. Just as with oxidizer vitiation, extinction is achieved when the flame temperature is reduced sufficiently such that the kinetic losses from the flame become comparable to the generation of energy. In preliminary analysis, the effect of radiation losses will be ignored with only kinetic losses considered, similar to the analysis of oxidizer vitiation. Figure 24 illustrates the critical flame temperatures that are associated with fuel vitiation conditions. Figure 24 (a) is the proof of concept from detailed chemistry, and Figure 24 (b) is the application of the Burke-Schumann flame temperature model from Equation (4), with

open symbols representing experimentally determined extinction conditions. Each of these models demonstrate that reducing fuel concentration reduces the extinction flame temperature, while increasing fuel temperature increases the extinction flame temperature. The non-linear behavior of the flame temperature is due to the form of the Burke-Schumann expression, such that Equation (4) is not linear with Y_F^∞ at large values of Y_F^∞. An identical non-linear behavior can be observed for enriched oxidizer concentrations. The non-linear relationship suggests that fuel dilution plays a weak role in flame extinction at high fuel concentrations, but that role becomes much more significant at low fuel concentrations. It is also important to note that fuel temperature has a much less significant effect on the extinction temperature than that of the oxidizer temperature. Upon examination of Equation (4), the fuel temperature will only become as significant as oxidizer temperature if Z_{st} is near or greater than 0.5, which is rarely the case with combustion in air. Just as with the oxidizer vitiation case, Figure 24 is not an appropriate extinction map, as it is challenging to derive a pathway from flammable mixtures through the critical values to a region where extinction will always occur. Figure 24 is a demonstration that the Burke-Schumann model is appropriate for accounting for the effects of vitiation.

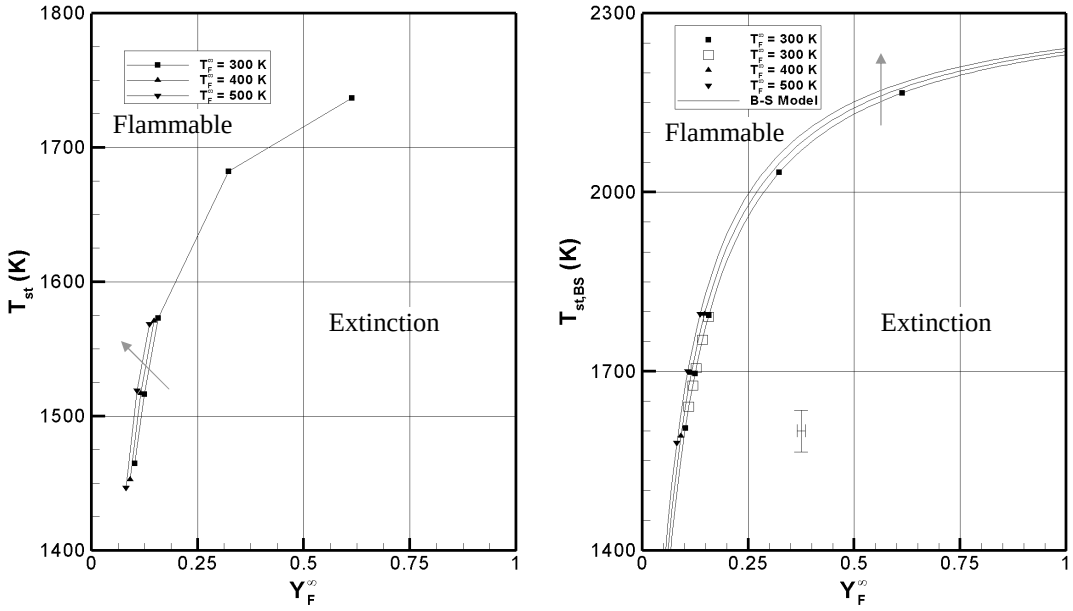

Figure 24: Illustration of fuel vitiation effects on extinction flame temperature for detailed chemistry from OPPDIF (a) and the Burke-Schumann model (b). The lines in (a) are used to highlight data grouping and the arrows indicate groups of increasing T_F^∞. ($T_{O_2}^\infty$ = 300 K, $Y_{O_2}^\infty$ = 0.23)

3.3 Extinction with Scalar Dissipation Rate Effects

The effects of kinetic losses from the flame will be examined through three possible scalar dissipation rate-based extinction models. These models may differ in the methods used to predict flame temperature, scalar dissipation rate, and/or scaling equations; however, the underlying concept is consistent throughout; increasing convective energy losses from the flame increases the likelihood of extinction. These models provide a tool to predict critical scalar dissipation rates as a function of flame temperature and reactant composition,

$\chi_{st,crit} = f[T_{st}(T_{O_2}^\infty, Y_{O_2}^\infty, T_{F_2}^\infty, Y_F^\infty, \kappa), Z_{st}(Y_{O_2}^\infty, Y_F^\infty)]$. The effect of radiation losses is ignored in the preliminary evaluation in order to isolate the effects of kinetic losses.

This critical scalar dissipation rate is determined from local reactant properties, and then compared to the local scalar dissipation rate. When the local scalar dissipation rate is greater than the critical value, the local flame element will experience extinction. It should be noted that determination of a local scalar dissipation rate may prove challenging in the context of LES, a requirement for prediction of local extinction with these models.

3.3.1 Oxidizer Vitiation

The effects of kinetic losses from oxidizer-vitiated flames at extinction are examined in Figure 25, while ignoring radiation losses. Extinction conditions in the framework of detailed chemistry are illustrated in Figure 25 (a) to demonstrate the general behavior of extinction effects, where the scalar dissipation rate is determined from Equation (5). It is clear from Figure 25 (a) that increasing the scalar dissipation rate results in higher critical values of oxidizer concentration and temperature, i.e. flame weakening. Recalling Figure 23, increasing oxidizer concentration and temperature result in an increase in the flame temperature and as such, the rate of energy generation also increases. Therefore, flames with high values of oxidizer concentration and temperature will require high convective energy losses to induce flame extinction. In other words, flames with high oxidizer concentration and temperature are more resistant to blowout. The reverse is also true: flames with low oxidizer concentration and temperature are more susceptible to kinetic extinction. Figure 25 illustrates this behavior exactly for both the detailed chemistry framework in (a), and when the scalar dissipation rate is modeled with Equation (49) in (b). Another convenient feature of Figure 25 is it can be used as an extinction map for

oxidizer vitiation conditions. Any combination of oxidizer concentration and scalar dissipation rate that falls above the line corresponding to the oxidizer temperature is a flammable condition. Likewise, any combination of parameters that falls below the line will result in extinction. However, this map only accounts for the effects of oxidizer vitiation, while ignoring any possible effects of fuel vitiation and radiation losses.

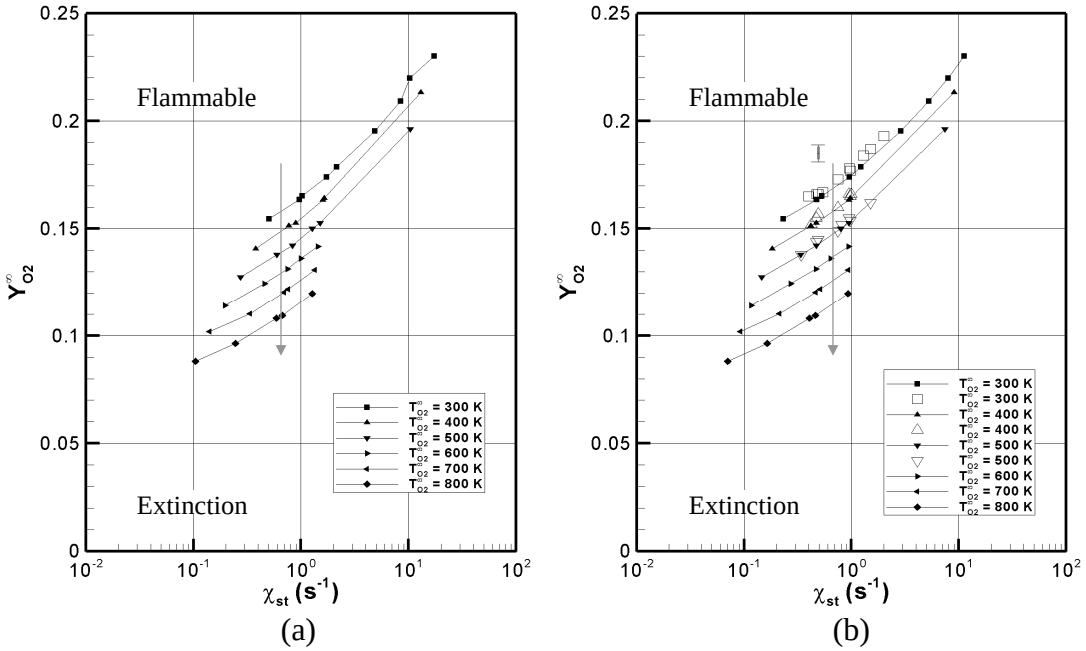

Figure 25: Illustration of scalar dissipation rate effects on critical oxidizer concentrations for detailed chemistry from OPPDIF (a) and the Burke-Schumann model (b). The lines are used to highlight data grouping and the arrows indicate groups of increasing $T^{\infty}_{O_2}$. (T^{∞}_{F} = 300 K, Y^{∞}_{F} = 1)

3.3.2 Fuel Vitiation

The effects of kinetic losses from fuel-vitiated flames at extinction are examined in Figure 26, while ignoring radiation losses. Extinction conditions in the framework of detailed chemistry are illustrated in Figure 26 (a) to demonstrate the general behavior of extinction effects, where the scalar dissipation rate is determined from Equation (5). It is clear from Figure 26 (a) that increasing the scalar dissipation rate results in higher critical values of fuel concentration and temperature. Recalling Figure 24, increasing fuel concentration and temperature results in an increase in the flame temperature and as such, the rate of energy generation also increases. Therefore, just as with oxidizer vitiation, flames with high values of fuel concentration and temperature will require high convective energy losses to induce flame extinction. The reverse is also true: flames with low fuel concentration and temperature are more susceptible to kinetic extinction. Figure 26 illustrates this behavior exactly for both the detailed chemistry framework in (a), and when the scalar dissipation rate is modeled with Equation (49) in (b). Another convenient feature of Figure 26 is it can be used as an extinction map for fuel vitiation conditions. Any combination of fuel concentration and scalar dissipation rate that falls above the line corresponding to the fuel temperature is a flammable condition. Likewise, any combination of parameters that falls below the line will result in extinction. However, this map only accounts for the effects of fuel vitiation, while ignoring any possible effects of oxidizer vitiation and radiation losses. Since fuel and oxidizer vitiation are not mutually exclusive events, Figure 25 and Figure 26 alone cannot produce the full range of possible vitiated extinction conditions.

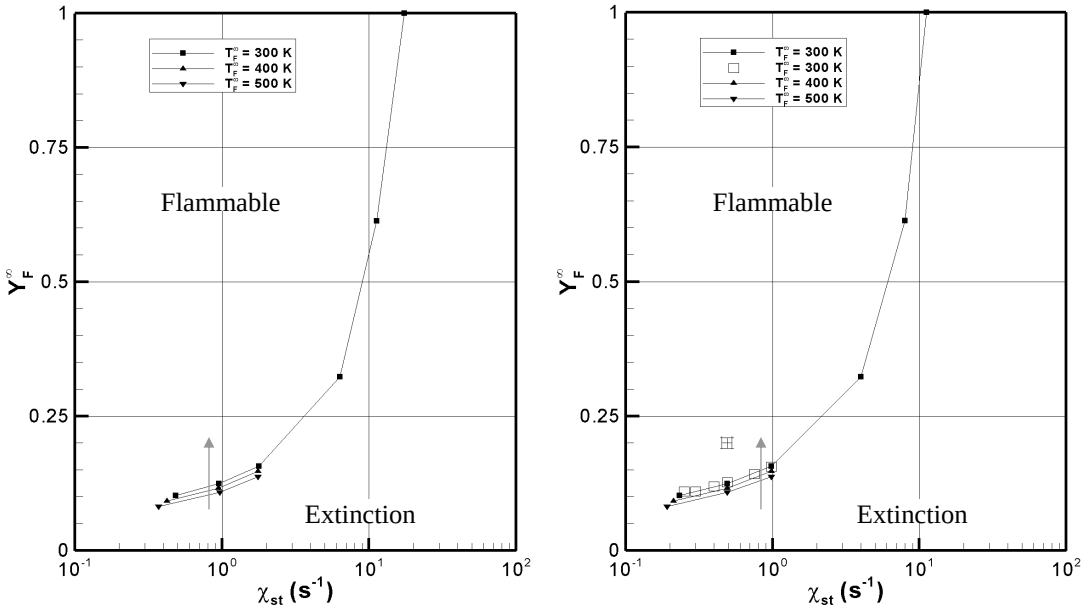

(a) (b)

Figure 26: Illustration of scalar dissipation rate effects on critical fuel concentrations for detailed chemistry from OPPDIF (a) and the Burke-Schumann model (b). The lines are used to highlight data grouping and the arrows indicate groups of increasing T_F^{∞}. ($T_{O_2}^{\infty}$ = 300 K, $Y_{O_2}^{\infty}$ = 0.23)

3.3.3 Activation Temperature

The activation temperature is a measure of the reactivity of the fuel, and it is a primary model parameter for the Arrhenius rate model from Equation (1). Therefore, the activation temperature is a critical parameter to determine in order to accurately balance the rate of generation of energy with the rate of energy losses at extinction. In this study, the activation temperature is determined from the correlation of scalar dissipation rates and flame temperatures for several extinction conditions. Given the different models used to determine the scalar dissipation rate and flame temperature, detailed chemistry, AEA, and SCDN models will each have a different activation temperature. In preliminary analysis, the activation temperature is determined from

extinction conditions without the effect of radiation losses to avoid any possible errors associated with the radiative correction scheme. Due to the exponential dependence of the Arrhenius rate model on activation temperature, it is critical to use the appropriate activation temperature for each model specifically. Selecting a tabulated value of the activation temperature from the literature to apply to these models can result in substantial systematic errors. Great care must be taken to ensure that the tabulated value is appropriate for the model in question.

3.3.3.1 Detailed Chemistry

In the framework of detailed chemistry, the activation temperature can be determined following Equation (31), where the scalar dissipation rate is provided by Equation (5). Figure 27 illustrates extinction conditions plotted in this manner, where the slope of a logarithmic fit determines the activation temperature. Figure 27 demonstrates noticeable differences between the oxidizer and fuel vitiation cases. The activation temperature indicated is for oxidizer vitiation conditions only. The deviation of the fuel vitiation extinction conditions is due to changes in the Lewis number, and reactant leakage associated with fuel vitiation near extinction. The Lewis number of pure methane is approximately 1.06, while that for methane diluted with nitrogen is 0.99, which is a noticeable change. Wang et al. have demonstrated that decreasing the fuel Lewis number without radiation losses results in a corresponding strengthening of the flame (i.e. a lower flame temperature at extinction) [43]. The reactant leakage of O_2 for the oxidizer-vitiated case at χ_{st} = 0.49 s^{-1} is 0.023 mass fraction, while the corresponding leakage for the fuel-vitiated case is 0.031 mass fraction. Increased levels of reactant leakage will likewise correspond to a lower

flame temperature. This trend is consistent with the extinction results in Figure 27, which illustrates a flame strengthening for fuel vitiation in comparison to oxidizer vitiation corresponding to a lower flame temperature at extinction. Nevertheless, the general trend between scalar dissipation rate and flame temperature holds true for both fuel and oxidizer vitiation, and the errors present in the detailed chemistry framework are reduced in analytical models. Figure 27 can also be used as an extinction map, although the need to model extinction is unnecessary in the context of detailed chemistry based on the direct simulation of the reaction kinetics.

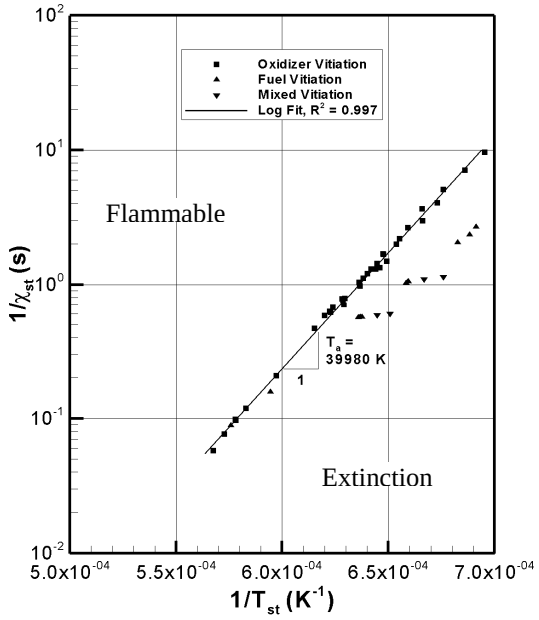

Figure 27: Activation temperature determination for detailed chemistry extinction from OPPDIF. Only oxidizer vitiated extinction conditions are included in the log fit with χ_{st} determined from Equation (5). (T_a = 39980 K)

3.3.3.2 Activation Energy Asymptotics

In the framework of the AEA extinction model, the activation temperature can be determined following Equation (36), where the scalar dissipation rate is provided by Equation (37). Figure 28 illustrates extinction conditions plotted in this manner where the slope of a linear fit determines the activation temperature. It is clear that the application of the AEA model has reduced the effects of the Lewis number and reactant leakage in comparison to the results in Figure 27. In fact, all of the extinction data collapses with reasonable scatter across the full range of parameter space. Data from the current study compares favorably to data from Puri and Seshadri following a minor correction to their scaling equation for $f(Z_{st})$ [44]. Figure 28 can also be used as an extinction map based on vitiated conditions surrounding the flame and the scalar dissipation rate at the flame. In application to CFD, a simple probing scheme can be developed to determine the local levels of vitiation near the flame sheet to predict $T_{st,BS}$ and $f(Z_{st})$ following the advice of Tuovinen [23]. The only remaining term required by the model is a local value of the scalar dissipation rate. If the scalar dissipation rate experienced by the local flamelet element is sufficiently high that it falls above the line in Figure 28, local extinction will occur. Likewise any conditions that fall below the line are flammable. However, Figure 28 does not yet include extinction conditions that are affected by radiation losses in order to reduce any possible complications that can arise from the radiative correction scheme.

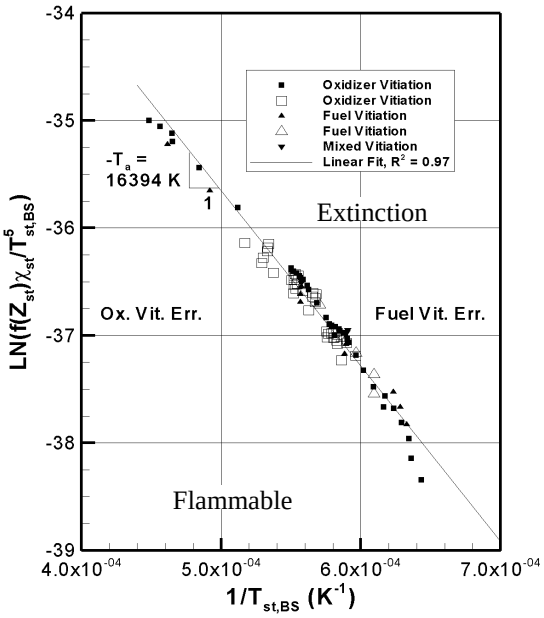

Figure 28: Activation temperature determination for the AEA model from experimentally and numerically determined extinction conditions, with χ_{st} determined from Equation (37). (T_a = 16394 K)

3.3.3.3 Simplified Critical Damköhler Number

In the framework of the SCDN model, the activation temperature can be determined following Equation (31), where the scalar dissipation rate is provided by Equation (49). Figure 29 illustrates extinction conditions plotted in this manner, where the slope of a logarithmic fit determines the activation temperature. It is clear that the application of the SCDN model has reduced the effects of the Lewis number and reactant leakage in comparison to the results in Figure 27. In fact, just as with the AEA model, all of the extinction data collapses with reasonable scatter across the full range of parameter space. Figure 29 can also be used as an extinction map based on vitiated conditions surrounding the flame and the scalar dissipation rate at the flame. A simple probing scheme can be developed to determine the local levels of vitiation

near the flame sheet to determine $T_{st,BS}$. The only remaining term required by the model is a local value of the scalar dissipation rate. If the local scalar dissipation rate experienced by the flamelet element is sufficiently high that it falls below the line in Figure 29, local extinction will occur. Likewise, any conditions that fall above the line are flammable. However, Figure 29 does not yet include extinction conditions that are affected by radiation losses in order to reduce any possible complications that can arise from the radiative correction scheme.

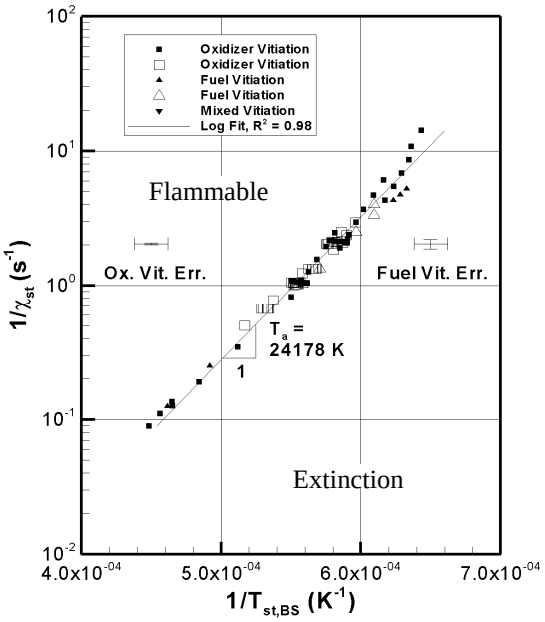

Figure 29: Activation temperature determination for the SCDN model from experimentally and numerically determined extinction conditions, with χ_{st} determined from Equation (49). (T_a = 24178 K)

Comparison of the results from AEA in Figure 28 to the proposed SCDN model in Figure 29 demonstrates that each model provides equivalent performance in predicting extinction conditions. However, the SCDN model provides some interesting advantages over the AEA model. The first advantage stems from the determination of the activation temperature. The SCDN model uses a standardized method for determining the activation temperature, while the AEA model requires a special definition that is dependent on the reaction order constants. The use of a standardized method will ease in the application of the extinction model for various fuels (e.g. propane, ethylene, heptane, wood, etc.) without developing a different set of equations to evaluate the activation temperature and in the extinction model equations. The reaction order constants result in the term $(T_{st,BS})^5$ that is present in the AEA model. The SCDN model avoids this flame temperature dependence by using the classical assumption that a power law function can be expressed as an exponential function. Thus, the reaction order terms are lumped into the activation temperature. This reaction order term is also numerically troubling for the AEA model because any numerical error in predicting $T_{st,BS}$ will be magnified, whereas the SCDN model is less sensitive to such errors. The advantages of the SCDN model will ease in its application to CFD codes by simplifying the process of determining model parameters and reducing the number of inputs required for the model (i.e. the power of the leading reaction order term).

3.4 Extinction with Radiative Loss Effects

As discussed in Section 2.1.3, radiation losses from the flame can be accounted for using an iterative correction scheme for the Burke-Schumann flame temperature expression following Equation (23). This correction scheme is dependent on both the scalar dissipation rate and the corrected flame temperature. Due to the complex nature of the radiative loss, it is not initially clear that the critical flame temperature at extinction is constant with a fixed scalar dissipation rate. Solutions for the critical flame temperature at selected scalar dissipation rates and variable radiative losses are illustrated in Figure 30. The results in Figure 30 demonstrate that the critical flame temperature is always constant with a fixed scalar dissipation rate regardless of the level of radiative loss. This result facilitates the numerical solution of extinction conditions based on $T_{O_2}^{\infty}$, $T_{F_2}^{\infty}$, $Y_{O_2}^{\infty}$, Y_F^{∞}, χ_{st} and κ. Solutions for extinction conditions for oxidizer and fuel vitiation are highlighted in this section to demonstrate some simple physical behavior associated with radiative extinction.

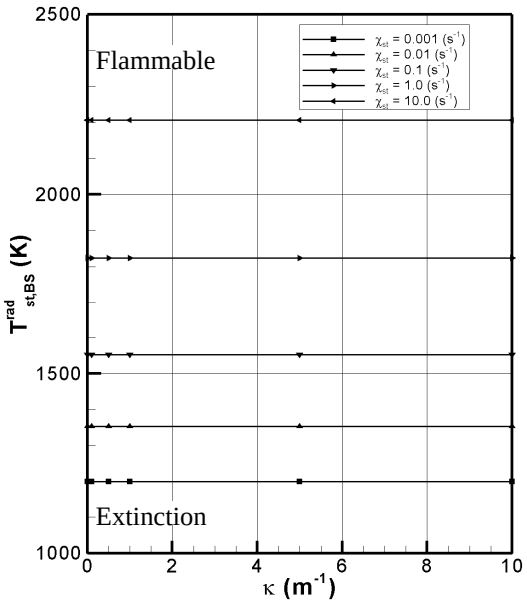

Figure 30: Solutions for the critical flame temperature using the radiation corrected Burke-Schumann model from Equation (23) versus absorption coefficient, demonstrating that the critical flame temperature is always constant for a given scalar dissipation rate. The symbols are used to highlight solution grouping.

3.4.1 Oxidizer Vitiation

The combined effects of oxidizer dilution, scalar dissipation rate and radiative losses on flame extinction are presented in Figure 31. The solutions can only be determined if the value of the activation temperature is known, along with all of the model inputs for Equation (23), and then application of the SCDN extinction model, Equation (53). Numerical and experimental extinction data corresponding to the selected operating conditions are also included to illustrate the fidelity of the model. The solid lines in Figure 31 highlight critical values of oxidizer concentration and scalar dissipation rate for selected absorption coefficients.

Figure 31 demonstrates that radiative loss has a significantly smaller impact on high scalar dissipation rate flames than it does for low scalar dissipation rates. In fact, examination of Figure 31 can determine the transition from kinetically-dominated extinction to radiatively-dominated extinction at the minimum of the solution lines. As is to be expected, the extinction without radiative losses will experience a minimum only at the trivial condition, $Y_{O_2}^{\infty} = 0$ and $\chi_{st} = 0$. As radiation losses are increased, the scalar dissipation rate at the transition point also increases, sometimes suddenly. In fact, for relatively small values of the absorption coefficient, there is almost no appreciable difference in extinction conditions when compared to the case without radiation losses until a critical value is reached. These physical behaviors agree with the conclusions made by Sohrab et al., Wang et al., Maruta et al., Chan et al., and Chao et al. [43,36,75,76,85]. One important feature of the radiatively dominated extinction conditions is that they cannot be determined by following a classical S-shaped pathway to extinction. Extinction on the S-shaped

pathway is produced by increasing the scalar dissipation rate; however, it is impossible to establish a stable flame with a scalar dissipation rate below the critical value in the radiatively dominated limit.

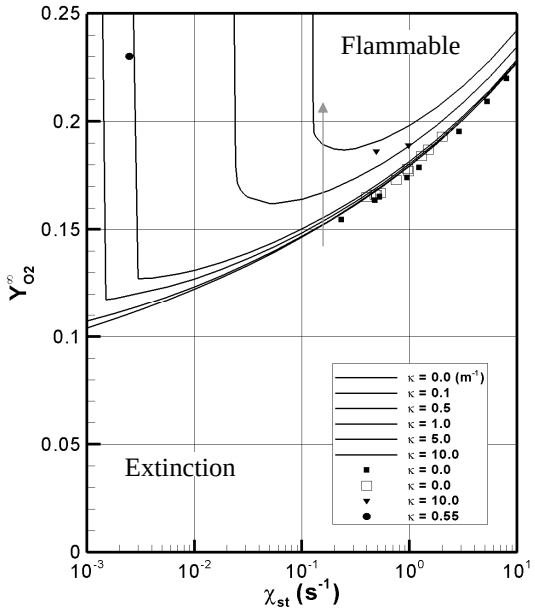

Figure 31: Solutions and data of critical oxidizer concentrations with the combined effects of radiation losses and scalar dissipation rate. The arrow indicates solutions of increasing absorption coefficient. ($T_{O_2}^{\infty} = T_F^{\infty}$ = 300 K, Y_F^{∞} = 1)

3.4.2 Fuel Vitiation

The combined effects of fuel dilution, scalar dissipation rate and radiation losses on flame extinction are highlighted in Figure 32 through the use of Equation (53) and Equation (23). The solid lines in Figure 32 highlight critical values of fuel concentration and scalar dissipation rate for selected absorption coefficients. Numerical and experimental extinction data corresponding to the selected operating conditions are also included to illustrate the fidelity of the model. Figure 32 demonstrates that fuel vitiation is insensitive to small absorption coefficients, but it is much more sensitive at large absorption coefficients. As the absorption coefficient is increased, the scalar dissipation rate at the transition to radiatively dominated extinction also increases, just as with the oxidizer vitiation solutions. This observation serves as a justification for assuming that the experimental extinction results have effectively no radiation losses. Again, these physical behaviors agree with the conclusions made by Sohrab et al., Wang et al., Maruta et al., Chan et al., and Chao et al. [43,36,75,76,85]. All that remains is to apply all extinction conditions, including those with radiation effects, to the extinction models to verify that they are appropriate for determining extinction with radiative losses.

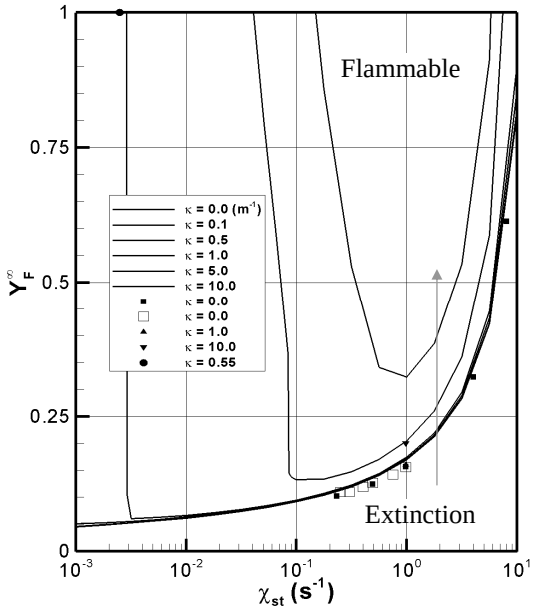

Figure 32: Solutions for the combined effect of radiation losses and scalar dissipation rate on critical fuel concentrations. The arrow in indicates solutions of increasing absorption coefficient. ($T_{O_2}^{\infty} = T_F^{\infty}$ = 300 K, $Y_{O_2}^{\infty} = 0.23$)

3.4.3 Approximating Radiation Losses from Sooty Flames

Due to the optically thick nature of soot particles, it is particularly challenging to approximate the effect of soot concentration on radiation properties [99]. However, it is a useful exercise to approximate the maximum possible radiation loss by ignoring the effects of radiative absorption. This will provide an order of magnitude estimation of the upper limit of soot radiation losses.

Given the result illustrated in Figure 21, it appears that the optically thin gas contribution from CO_2 and H_2O to the radiative loss is approximately constant with scalar dissipation rate. The peak Planck Mean Absorption Coefficients associated with these flames range from 0.1 - 1.0 m^{-1}, regardless of the proximity of the flame to

an extinction condition. The radiative flux from these flames is approximately 1.0×10^{3} W/m^2 at its minimum indicated in Figure 21.

A similar absorption coefficient can be approximated for soot, given a characteristic local concentration. Santoro et al. have performed detailed experiments to determine soot concentrations in the region of the flame for laminar co-flowing flames. The peak value of soot concentration was found to be approximately f_v = 10 ppmv or $Y_{soot} \approx 0.1$, corresponding to the peak flow rate conditions explored [98]. The soot absorption coefficient can then be modeled:

$$\kappa_{soot} = 1864 f_v T \approx 350 Y_{soot} \tag{60}$$

Yielding $\kappa_{soot} \approx 35$ m^{-1}, which is one to two orders of magnitude greater than that of the gas. Ignoring absorption of radiation at this soot concentration will result in a significant over-prediction of the radiation losses; however, it is still valid for an order of magnitude approximation.

Assuming that radiation losses from soot follow a similar structure as gas radiation, while ignoring absorption, results in a linear increase in the radiative power of the flame with increasing absorption coefficient. At 10 ppmv soot, the absorption coefficient of the flame is dominated by soot, and the gas contribution can be ignored. Therefore, a characteristic radiative power flux at 10 ppmv soot is approximately 1.0×10^{5} W/m^2. Following the flame energy generation curve in Figure 21 illustrates that this radiative flux will result in a radiative fraction of $\Gamma = 0.5$ at $\chi_{st} = 1.0$ s^{-1}. According to the solutions for $\kappa = 10$ illustrated in Figure 31 and Figure 32, the flammable domain is substantially reduced. In the event that the soot volume fraction approaches 10 ppmv, the flame can only exist between scalar dissipation rates of 0.1

and 5.0 s-1 without vitiation effects. This is an encouraging result based on the fact that the timescale to reach steady state behavior associated with a flame at $\chi_{st} \approx 1.0\ s^{-1}$ is greatly reduced from that of the radiative limit in Figure 19. While reduced timescales can increase the computational cost, the proposed extinction model may break down if the timescale to reach steady state behavior is greater than the iterative time step of the CFD solver. Therefore, the proposed extinction model is valid for flames that experience significant radiative and kinetic effects, but may be problematic for dynamic radiative flames at with local, ultra-low scalar dissipation rates. Ongoing research by Narayanan and Trouvé indicates that this timescale mismatch is insignificant [101].

3.5 Evaluating the Extinction Models

Given the proposed scheme for characterizing radiation losses from the flame, it is essential to evaluate the performance of the extinction models while including flames that experience radiative losses. In the following sections, radiation losses will be applied to the detailed chemistry, AEA, SCDN and critical flame temperature extinction models. The numerical data with radiation losses in this study range from $\kappa = 1.0\ m^{-1}$ ($\Gamma = 0.01$) to $\kappa = 10.0\ m^{-1}$ ($\Gamma = 0.18$) for both oxidizer- and fuel-vitiated conditions, in addition to the radiative limit at $\kappa \approx 0.55\ m^{-1}$ ($\Gamma = 0.614$) illustrated in Figure 18 through Figure 21.

3.5.1 Detailed Chemistry

Figure 33 illustrates extinction conditions determined from detailed chemistry simulations where the scalar dissipation rate is provided by Equation (5). Figure 33 contains extinction data plotted in an activation temperature context (a) and several model correlation contexts for Equation (35) in log-log (b), full scale linear (c), and reduced scale linear (d) to highlight model performance at various scales. In addition to the noticeable differences between the oxidizer and fuel vitiation cases, Figure 33 illustrates additional deviations for extinction conditions with radiation losses. The deviation of the fuel vitiation extinction conditions can easily be explained by changes in the Lewis number, and the reactant leakage associated with fuel vitiation near extinction following the conclusions of Wang et al. However, the effects of Lewis number variations and reactant leakage are magnified, but not monotonic in the presence of radiation losses [43]. This means that radiation losses can physically result in either flame weakening or strengthening at extinction, with very small deviations in reactant leakage and/or Lewis number. Nevertheless, Figure 33 illustrates that the general trend between scalar dissipation rate and flame temperature holds for all extinction conditions, demonstrating an initial proof of concept. Fortunately, the effects of reactant leakage and Lewis number variations are dramatically reduced in the context of the analytic models.

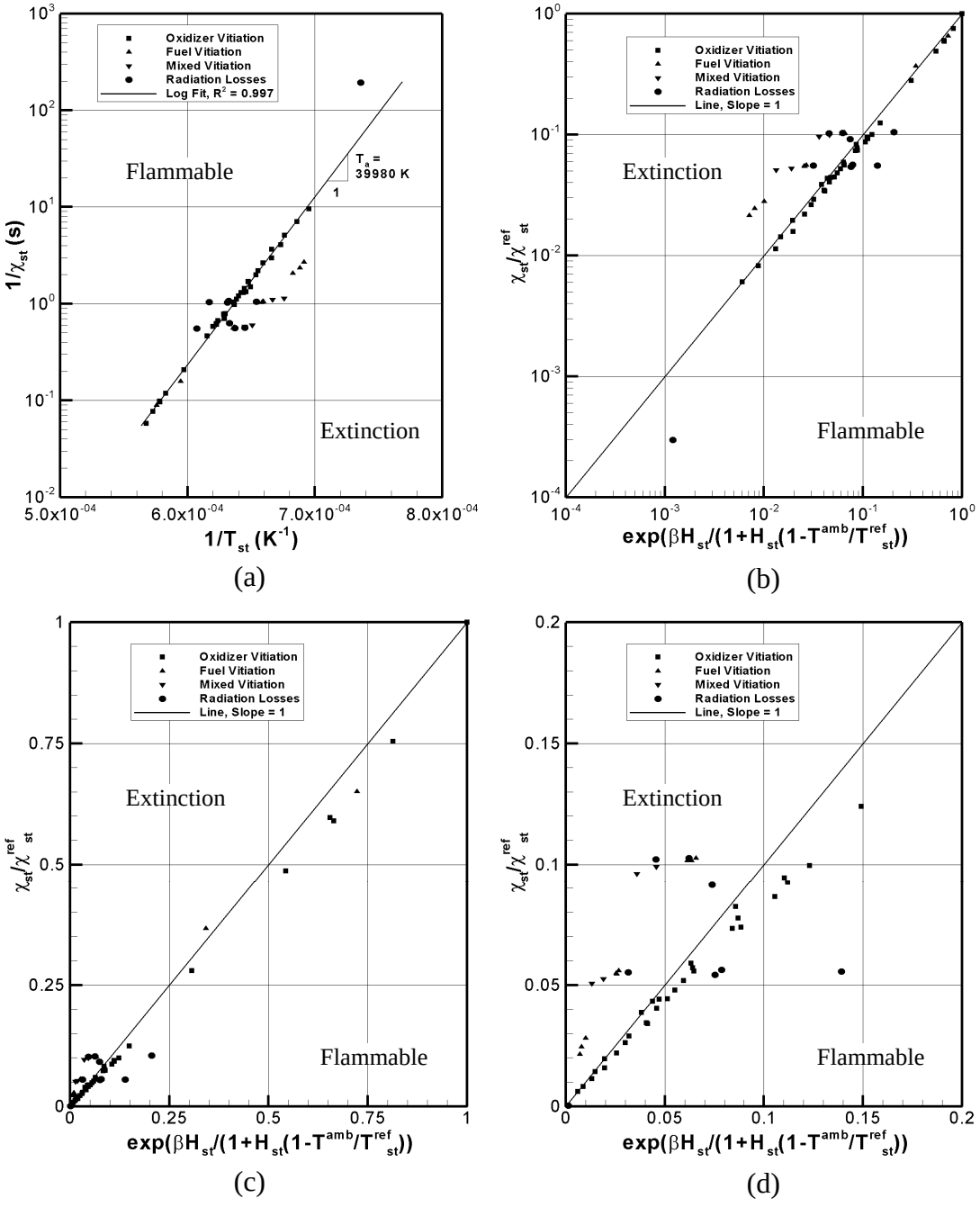

Figure 33: Analysis of all extinction data in the detailed chemistry framework for the activation temperature plot (a), and the full extinction model from Equation (35) in full-scale log-log (b), full-scale linear (c) and reduced scale linear (d). Each plot is designed to highlight the accuracy of the model at different scales of interest.

3.5.2 Activation Energy Asymptotics

Figure 34 illustrates extinction conditions in the context of AEA, where the scalar dissipation rate is provided by Equation (37). Figure 34 contains numerical and experimental extinction data plotted in an activation temperature context (a) and several model correlation contexts for Equation (48) in log-log (b), full scale linear (c), and reduced scale linear (d) to highlight model performance at various scales. Figure 34 illustrates a small deviation for the radiative limit, while all other extinction conditions collapse within a small error range. This is a fortunate result, because reactant leakage and Lewis number effects can be effectively ignored without introducing large systematic errors. AEA is essentially based on a Damköhler number argument, and the terms $f(Z_{st})$ and $(T_{st,BS}^{rad})^5$ represent scalar dissipation rate normalization and reaction order constants respectively. The AEA based extinction model is fully capable of predicting local extinction events based on the parameters $Y_{O_2}^{\infty}$, $T_{O_2}^{\infty}$, Y_F^{∞}, T_F^{∞}, χ_{st}, and κ.

Figure 35 illustrates extinction conditions in the AEA framework from the current study along with those from previous methane-air counterflow flame studies. Previous studies have adopted a wide approach to characterize extinction conditions. Puri and Seshadri examined extinction experimentally for moderate- to high- strain, mixed dilution (constant Z_{st}), and constant reactant temperatures [44]. Maruta et al. studied extinction numerically with OPPDIF (GRI 1.0) for fuel dilution (constant Y_F^{∞}) with radiation losses at moderate- to low- strain [75]. Chan et al. also characterized extinction of pure air and pure fuel with OPPDIF. Their approach was

similar to that used in Section 3.1, although with a slightly different radiation model (RADCAL [100]) and detailed chemistry model (GRI 2.11) were used [76]. Despite the different approaches in these studies, the extinction results from the current study agree well with the previously published results, as illustrated in Figure 35.

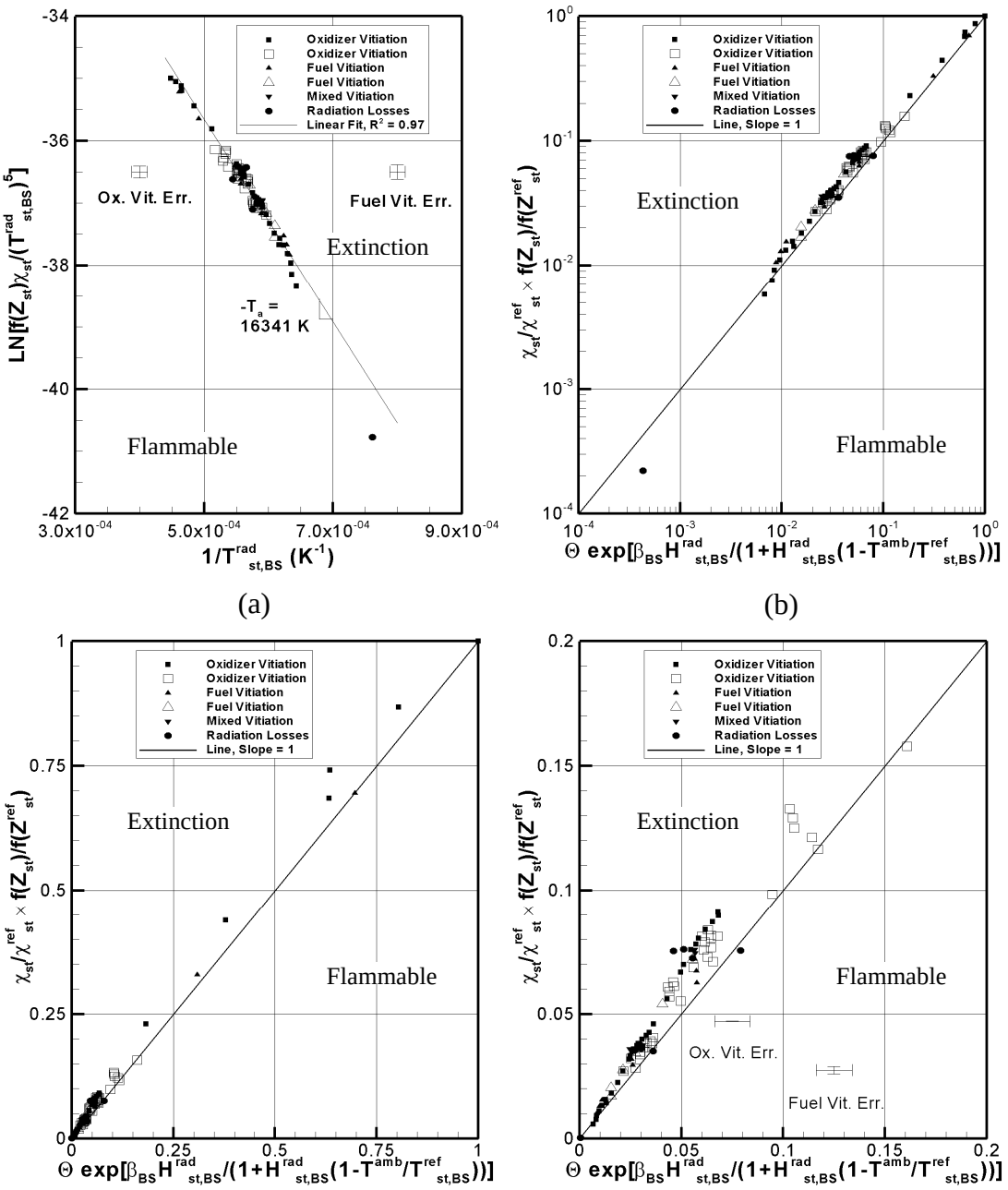

Figure 34: Analysis of all extinction data in the AEA framework for the activation temperature plot (a), and the full extinction model from Equation (48) in full-scale log-log (b), full-scale linear (c) and reduced scale linear (d). Each plot is designed to highlight the accuracy of the model at different scales of interest.

$$\Theta = \left(\frac{T_{st,BS}^{rad}}{T_{st,BS}^{ref}} \right)^5$$

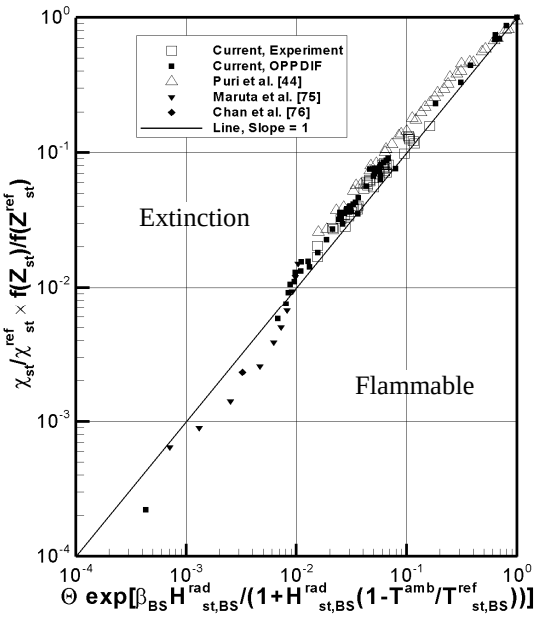

Figure 35: Comparison of extinction results from the current study to those of previous studies in the AEA framework. Open symbols indicate experimental data and solid symbols indicate data from numerical simulations [44,75,76].

3.5.3 Simplified Critical Damköhler Number

Figure 36 illustrates extinction conditions in the context of the SCDN model, where the scalar dissipation rate is provided by Equation (49). Figure 36 contains numerical and experimental extinction data plotted in an activation temperature context (a) and several model correlation contexts for Equation (53) in log-log (b), full scale linear (c), and reduced scale linear (d) to highlight model performance at various scales. Similar to the results of the AEA model, Figure 36 illustrates small deviations for extinction conditions with radiation losses, while all other extinction conditions collapse within a small error range. Again, this is a fortunate result, because reactant leakage and Lewis number effects can be effectively ignored without introducing large systematic errors. The SCDN extinction expression from Equation

(53) provides a useful simplification over the AEA model. Some advantages of using the SCDN model include a simple definition of the Damköhler number, a standard method for determining activation temperature, more realistic predictions of the actual scalar dissipation rate, and mathematical simplification of the extinction expression. The SCDN extinction model is fully capable of predicting local extinction events based on the parameters $Y_{O_2}^{\infty}$, $T_{O_2}^{\infty}$, Y_F^{∞}, T_F^{∞}, χ_{st}, and κ. In this regard, the SCDN extinction model is essentially equivalent to the AEA model in performance, but superior in application.

Figure 37 illustrates extinction conditions in the SCDN framework from the current study along with those from previous studies of methane-air counterflow diffusion flames [44,75,76]. Just as with the results comparison in the AEA framework, the extinction results from the current study agree well with the previously published results. Based on the results illustrated in Figure 37, it is clear that the proposed SCDN extinction model is equivalent in performance to the AEA model.

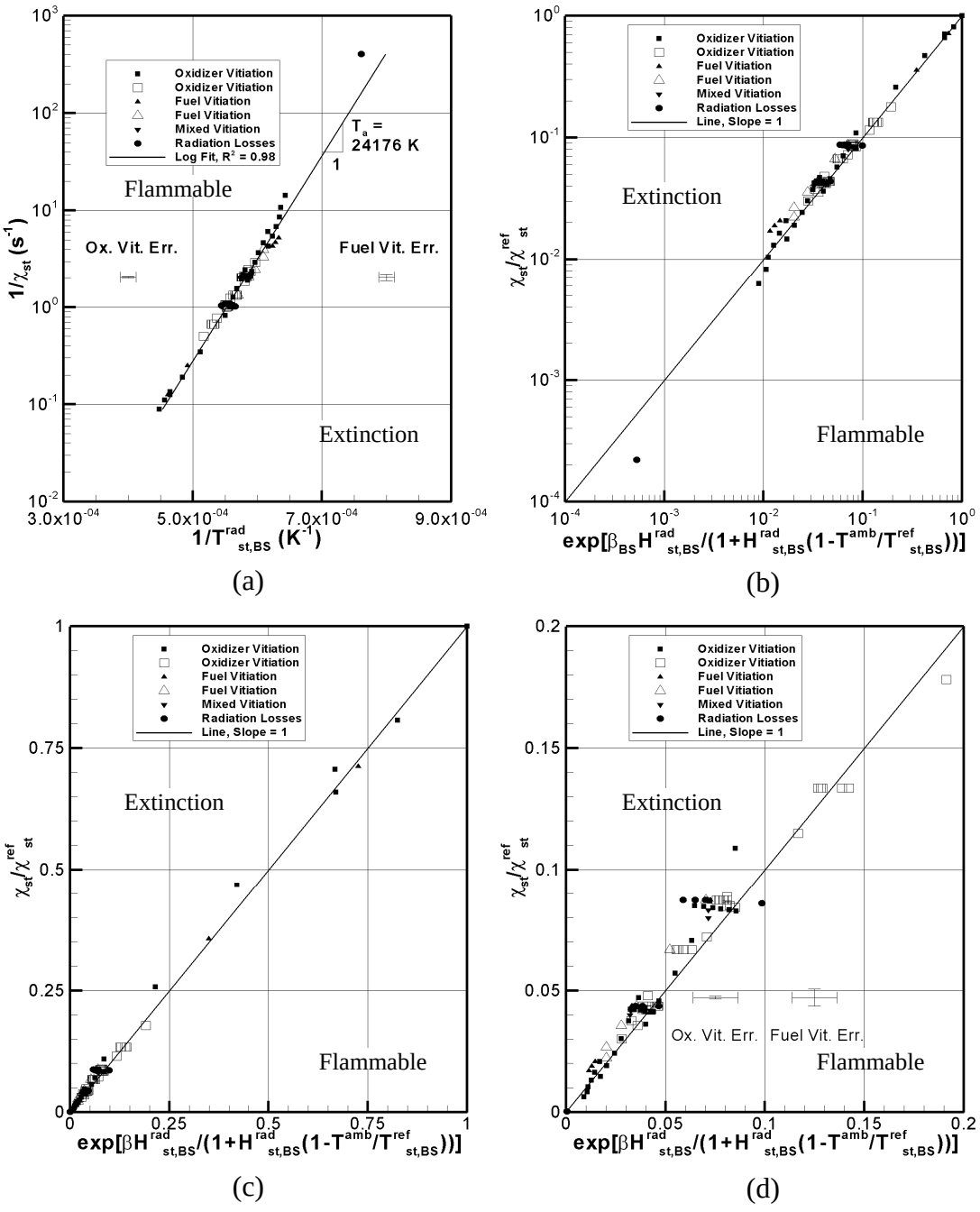

Figure 36: Analysis of all extinction data in the SCDN framework for the activation temperature plot (a), and the full extinction model from Equation (53) in full-scale log-log (b), full-scale linear (c) and reduced scale linear (d). Each plot is designed to highlight the accuracy of the model at different scales of interest.

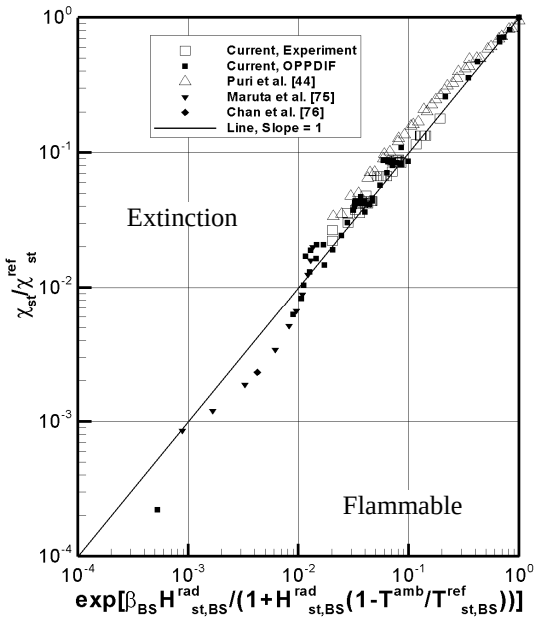

Figure 37: Comparison of extinction results from the current study to previous studies in the SCDN framework. Open symbols indicate experimental data while solid symbols indicate data from numerical simulations [44,75,76].

3.5.4 Critical Flame Temperature

As previously discussed, a critical flame temperature extinction model is currently implemented in popular CFD codes used for accidental fire applications [2]. Theoretically, this model is equivalent to a constant scalar dissipation rate assumption applied to either AEA or the SCDN models. Since the critical flame temperature model is based on a specific solution of the radiation corrected Burke-Schumann equation, the only parameters that can affect extinction are $Y_{O_2}^{\infty}$, $T_{O_2}^{\infty}$, Y_F^{∞}, T_F^{∞}, and κ. The model employed by FDS assumes that $T_c = 1700$ K and only examines oxidizer vitiation without the effects of radiation losses. Equation (57) provides an identical result given $Y_F^{\infty} = 1.0$, $T_F^{\infty} = 300$ K, and $\kappa = 0.0$, while adding the ability to simultaneously explore the effects of changing Y_F^{∞}, T_F^{∞}, and κ. However, in order to

examine the effects of the radiant fraction on extinction in this formulation, it is necessary to determine the flow condition (scalar dissipation rate) associated with $T_c = 1700$ K. Once this scalar dissipation rate is determined, it is possible to quantify the effects of radiation losses. This scalar dissipation rate is determined to be $\chi_{st} = 0.3819$ s^{-1} ($a_g = 9.777$ s^{-1} for a flame with pure air and pure fuel) from a numerical solution of Equation (53) at $T_{st,BS}^{rad} = 1700$ K. This scalar dissipation rate is sufficiently high to ensure that extinction occurs in the kinetically dominated regime unless $\kappa \geq 10$ m^{-1}. Solutions for Equation (57) at selected absorption coefficients are illustrated in Figure 38 for oxidizer vitiation (a) and fuel vitiation (b). The inflection of the critical fuel concentration in Figure 38 (b) suggests that fuel vitiation is particularly sensitive to large radiation losses such that pre-heating of the fuel stream actually increases the likelihood of extinction. The results in Figure 38 highlight the importance of the radiation losses in determining extinction conditions. Figure 38 demonstrates that the current FDS critical temperature model can be easily expanded to account for simultaneous variations in oxidizer vitiation, fuel vitiation and radiation losses.

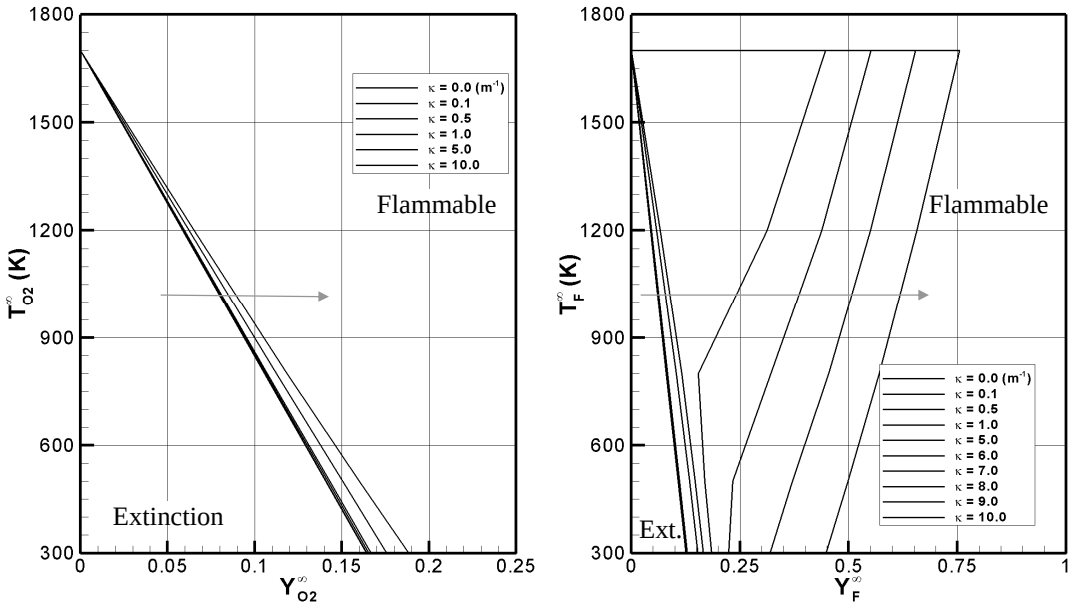

(a) (b)

Figure 38: Solutions of the critical flame temperature extinction model from Equation (57) at selected radiant fractions for oxidizer vitiation (a) and fuel vitiation (b). The arrows indicate model solutions of increasing radiant fraction.
($T_c = 1700$ K, $\chi_{st} = 0.3819$ s^{-1})

3.6 Two-Parameter Extinction Effects

While the extinction models presented in the previous sections are comprehensive and demonstrate accuracy over a wide range of parameter variations, it is useful to break down the model performance into simpler terms. This allows for comparison of the effects of kinetic and radiation losses in the framework of vitiation. It is recognized that the scalar dissipation rate and the radiation losses present a significant challenge to CFD codes in terms of resolution and modeling. Therefore, the following analysis is performed to challenge any possible simplifications that can be applied to the above models.

3.6.1 Oxidizer Vitiation

Figure 39 illustrates the effects of scalar dissipation rate and absorption coefficient on critical oxidizer vitiation conditions. Figure 39 (a) contains solutions for the critical oxidizer vitiation conditions from the SCDN model, along with the corresponding experimental and numerical data at selected scalar dissipation rates. The model solutions demonstrate excellent agreement with the extinction data over the full range of highlighted parameters. Modest changes in the scalar dissipation rate result in a noticeable shift of the critical conditions such that increasing the scalar dissipation rate increases the likelihood of extinction. Figure 39 (b) contains solutions for the critical oxidizer vitiation conditions at selected absorption coefficients. A single numerical data point is illustrated here due to the lack of data at the corresponding absorption coefficients and scalar dissipation rate. Modest changes in absorption coefficient result in significant changes in the critical conditions such that increasing the absorption coefficient increases the likelihood of extinction. The results in Figure 39 suggest that both changes in kinetic and radiation losses play significant roles in determining critical oxidizer vitiation conditions in the range of parameters indicated.

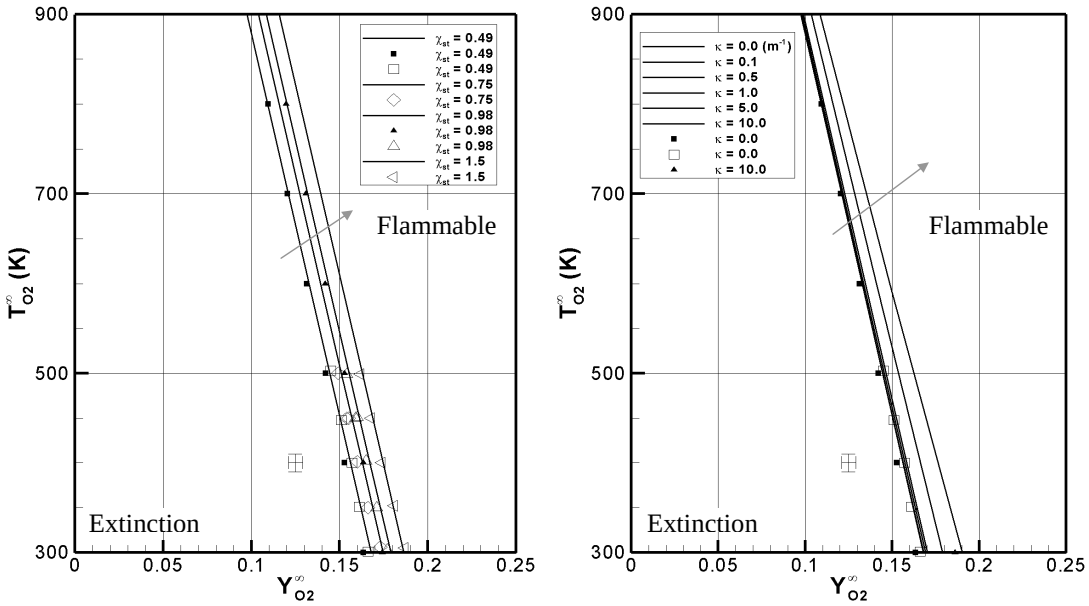

(a) (b)

Figure 39: Oxidizer vitiated extinction conditions for (a) selected scalar dissipation rates and (b) various radiant fractions at χ_{st} = 0.49 s^{-1}. The arrows indicate increasing χ_{st} and κ in (a) and (b) respectively. (T_F^{∞} = 300 K, Y_F^{∞} = 1)

3.6.2 Fuel Vitiation

Figure 40 illustrates the effects of kinetic and radiation losses on critical fuel vitiation conditions. Figure 40 (a) contains solutions for the critical fuel vitiation conditions from the SCDN model, along with the corresponding experimental and numerical data at selected scalar dissipation rates. Similar to the oxidizer vitiation case, the model solutions demonstrate good agreement with the extinction data over the full range of highlighted parameters. The fuel vitiation data demonstrates a slight systematic shift; however, this shift is insignificant considering that the fuel stream must be diluted from $Y_F^{amb} = 1$ to $Y_F^{\infty} \approx 0.1$. Since the experimental and numerical extinction data agree, it can be ascertained that this systematic shift is occurring at the

model level. This shift can be corrected by assuming that fuel vitiation has a slightly reduced activation temperature; however, there is no physical basis for this modification. Modest changes in the scalar dissipation rate result in a noticeable shift of the critical conditions. Figure 40 (b) contains solutions for the critical fuel vitiation conditions at selected absorption coefficients, suggesting that even modest changes in radiation losses results in a significant change in the critical conditions. The fuel-vitiated case appears to be more sensitive to radiation losses than to scalar dissipation rate, but, just as with the oxidizer vitiation case, both are significant.

The results in Figure 39 and Figure 40 suggest that both kinetic (scalar dissipation rate) and radiation losses play significant roles in determining extinction conditions in the range of parameters shown. As scalar dissipation rate increases, the effects of radiation losses will become less significant. However, at the moderate scalar dissipation rates highlighted, radiation losses are still significant. Assuming that most accidental fires experience this moderate- to low- scalar dissipation rate, both of these losses will be significant. This is due to the fact that moderate- to low-scalar dissipation rates are still sufficiently high to be significant in the presence of vitiation while sufficiently low to allow radiation to be important.

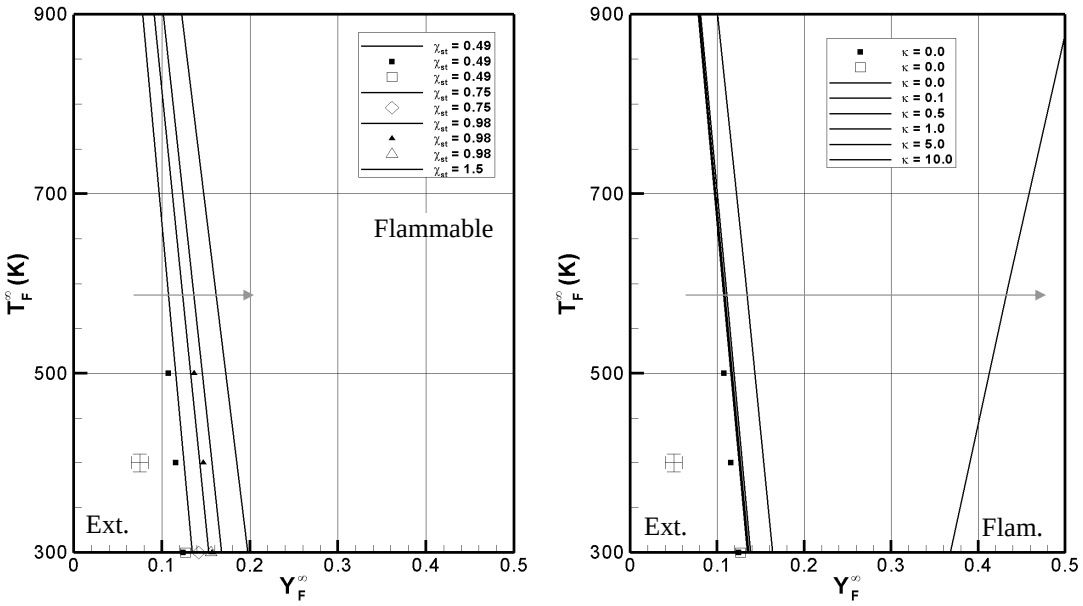

(a) (b)

Figure 40: Fuel vitiated extinction conditions for (a) selected scalar dissipation rates and (b) various radiant fractions at χ_{st} = 0.49 s^{-1}. The arrows indicate increasing χ_{st} and κ in (a) and (b) respectively. ($T_{O_2}^\infty$ = 300 K, $Y_{O_2}^\infty = 0.23$)

Chapter 4: Conclusions

This study has examined the extinction behavior of counterflow diffusion flames experimentally and numerically in order to test the validity of several extinction models. These models are presented in a form that is easily adapted for implementation in an LES code to predict local flame extinction. Improved modeling of local flame extinction will facilitate the prediction of toxicity and thermal hazards associated with accidental fires. A thorough review of the physics of flame extinction has been presented, illustrating the importance of vitiation, kinetic losses and radiation losses.

Both the experimental and numerical approaches utilized in this study have characterized the combined effects of these parameters by systematically isolating each effect and determining the associated extinction conditions. Detailed theories exist that can predict extinction behavior of steady state flamelets based on local parameters $T_{O_2}^{\infty}$, $Y_{O_2}^{\infty}$, T_F^{∞}, Y_F^{∞}, χ_{st}, and κ. The AEA extinction model has been developed by the combustion research community for thirty years, and provides an accurate prediction of extinction over several orders of magnitude variation of these parameters. The SCDN extinction model is presented in the current study, which results in identical performance compared to AEA theory. The SCDN model provides several advantages over the AEA model including; a physical theory based on simple timescales, a model expression with less complexity (independent of fuel specific reaction order constants), a standardized method for determining activation temperature, and reduced potential for numerical error. Recognizing that the scalar

dissipation rate is a difficult parameter to produce in LES simulations, a further simplification to the extinction model is examined. The critical flame temperature extinction model is equivalent to a constant scalar dissipation rate assumption, and it can capture both the effects of vitiation and radiation losses from the flame. However, there is substantial evidence indicating that the critical flame temperature is not constant resulting in substantial differences in critical reactant conditions. Each of these models provides an effective tool for predicting local flame extinction in the context of LES of accidental fires.

Furthermore, this study presents scale analysis of both kinetic and radiation losses from the flame. The order of magnitude prediction of scalar dissipation rate suggests that the characteristic kinetic losses from the flame will increase slightly with increasing fire size. The scalar dissipation rate may also experience significant turbulent fluctuations. Radiation losses from the flame are even more challenging to quantify due to the dependence on scalar dissipation rate, optical properties and flame temperature. Simple order of magnitude analysis suggests that local soot concentration will be the dominant factor in determining local radiation properties. This combination of effects highlights the importance of incorporating sub-grid models for the scalar dissipation rate, soot (production, consumption and transport) and radiation transport in LES with combustion. Each of these sub-grid models will play an important role in predicting local flame extinction.

The following sections summarize the noteworthy conclusions and contributions from this investigation.

General

- This study has identified the major parameters contributing to local flame extinction. These parameters include vitiation ($T_{O_2}^{\infty}$, $Y_{O_2}^{\infty}$, T_F^{∞}, Y_F^{∞}), kinetic losses (χ_{st}), and radiation losses (κ or Γ).
- A comprehensive approach has been developed to examine the effects of these fundamental extinction parameters both experimentally and numerically.
- The current experimental study is unique in examining the combined effects of reactant temperature, reactant concentration and scalar dissipation rate.
- The numerical study expands the range of parameters that can be explored while adding the capacity to induce radiation losses. OPPDIF simulations can produce flame extinction in both the kinetic and the radiative dominated regimes. The parameter space explored in the current numerical study is the largest of any known study.
- A scaling argument is presented to estimate characteristic scalar dissipation rates affecting an accidental fire. This analysis suggests that the scalar dissipation rate increases with increasing fire size. The scalar dissipation rate indicated is also sufficiently large to have a significant impact on vitiated extinction conditions.
- An order of magnitude analysis of radiation losses from sooty flames is presented. This analysis is useful for determining an approximate range of

radiation losses from flames with soot production. This analysis highlights the contribution of soot to the radiation loss from the flame.

Extinction Models

- Both the AEA and SCDN extinction models are equally capable of predicting local flame extinction for steady state flamelets. More importantly, they are written as a function of easily attainable local parameters $T_{O_2}^{\infty}$, $Y_{O_2}^{\infty}$, T_F^{∞}, Y_F^{∞}, χ_{st}, and κ.
- The SCDN model has some advantages over the AEA model including a physical theory based on simple timescales, a model expression with less complexity, a standardized method for determining activation temperature, and less potential for numerical error. This will ease in the understanding and implementation of the model.
- The critical flame temperature model is equivalent to a constant scalar dissipation rate assumption applied to either AEA or SCDN. It is a considerable simplification that can still account for variations in $T_{O_2}^{\infty}$, $Y_{O_2}^{\infty}$, T_F^{∞}, Y_F^{∞}, and κ. However, its physical limitations suggest that it is insufficient to accurately capture extinction in a wide range of accidental fires [102].

Future Work

- The current models are not yet fully comprehensive. While the effects of reactant leakage and non-unity Lewis number are small, the accuracy of these models can be improved by their inclusion. Conduction losses due to

cold wall interactions will also be significant in some applications, warranting further research.

- Further research is necessary to more accurately determine instantaneous scalar dissipation rates and local flame radiation losses in large scale accidental fires. This will be critical to determine the validity of the critical flame temperature model, or provide a more accurate critical flame temperature (scalar dissipation rate).
- The current radiative correction scheme is designed for the counterflow diffusion flame. Some modifications may be necessary in order to successfully apply this model to LES of 3-D turbulent combustion.
- The timescale associated with the ultra-low scalar dissipation rates at the radiative limit may prove problematic in LES of an unsteady flame. Further research is necessary to determine if local extinction at this limit can be predicted by the steady state models detailed above, or by some other means.

Appendix A

The following analysis is a detailed description of the radiative correction term from Equation (23) following the methods of Sohrab et al. [36]. The impact of radiation losses from the flame zone can be determined through analysis of the energy balance equation. This analysis follows the approach used in Activation Energy Asymptotics where the flame is analyzed as two piecewise linear mixing regions (fuel side and oxidizer side) separated by an infinitely thin reaction zone. The energy balance equation can be written in terms of dimensionless parameters:

$$\frac{d^2\theta}{d\zeta^2} = \left(Y_F^{\infty} + \alpha\right)\delta(\zeta) - l_i \exp(-\theta), \tag{A.1}$$

$$\hat{T}_i = \frac{T_i c_p}{\Delta h_c}, \tag{A.2}$$

$$\theta = \gamma \frac{\left(\hat{T}_{st,BS}^{rad} - \hat{T}\right)}{\hat{T}_{st,BS}^{rad}}, \tag{A.3}$$

$$\zeta = \gamma \frac{\left(Z - Z_{st}\right)}{\hat{T}_{st,BS}^{rad}}, \tag{A.4}$$

$$\alpha = \frac{Y_{O_2}^{\infty}}{r_s}, \tag{A.5}$$

$$l_i = \left(\frac{\hat{T}_{st,BS}^{rad}}{\gamma}\right) F \ , \ i = O_2, F \tag{A.6}$$

$$\text{and } \gamma \equiv \frac{d \ln F(\hat{T})}{d \ln \hat{T}} = 5 \tag{A.7}$$

where $\delta(\zeta)$ is a delta function that forces the reaction to occur at $Z = Z_{st}$, and F is defined in Equation (25). The second term in the RHS of Equation (A.1) represents the energy lost due to radiation. Equation (A.1) can be integrated using a jump condition at $\zeta = 0$ ($Z = Z_{st}$) where the temperature profile is assumed to be two piecewise functions of ζ corresponding to the oxidizer side and the fuel side of the domain. The boundary conditions of these piecewise functions are; for the fuel side:

$$\left.\frac{d\theta}{d\zeta}\right|_{\zeta\to+\infty} = \frac{\left(\hat{T}^{rad}_{st,BS} - \hat{T}^{\infty}_{F}\right)}{\left(1 - Z_{st}\right)}, \tag{A.8}$$

$$\left.\frac{d\theta}{d\zeta}\right|_{\zeta=0+} = \left[2l_F + \frac{\left(\hat{T}^{rad}_{st,BS} - \hat{T}^{\infty}_{F}\right)^2}{\left(1 - Z_{st}\right)^2}\right]^{1/2}, \tag{A.9}$$

and for the oxidizer side:

$$\left.\frac{d\theta}{d\zeta}\right|_{\zeta\to-\infty} = \frac{\left(\hat{T}^{rad}_{st,BS} - \hat{T}^{\infty}_{O_2}\right)}{Z_{st}}, \tag{A.10}$$

$$\left.\frac{d\theta}{d\zeta}\right|_{\zeta=0-} = \left[2l_{O_2} + \frac{\left(\hat{T}^{rad}_{st,BS} - \hat{T}^{\infty}_{O_2}\right)^2}{Z^2_{st}}\right]^{1/2}, \tag{A.11}$$

which are temperature gradients at the inlet conditions and on both sides of the reaction zone. Integration of Equation (A.1) analytically through application of the boundary conditions then results in the expression:

$$Y^{\infty}_{F} + \alpha = \left[2l_{O_2} + \mu^2_{O_2}(1-\beta)^2\right]^{1/2} + \left[2l_F + \mu^2_F(\alpha+\beta)^2\right]^{1/2}, \tag{A.12}$$

$$\mu_{O_2} = \frac{\left(\hat{T}^{rad}_{st,BS} - \hat{T}^{\infty}_{O_2}\right)}{\left(\hat{T}_{st,BS} - \hat{T}^{\infty}_{O_2}\right)}, \tag{A.13}$$

$$\mu_F = \frac{\left(\hat{T}_{st,BS}^{rad} - \hat{T}_F^{\infty}\right)}{\left(\hat{T}_{st,BS} - \hat{T}_F^{\infty}\right)}, \tag{A.14}$$

$$\text{and } \beta = \hat{T}_{O_2}^{\infty} - \hat{T}_F^{\infty}. \tag{A.15}$$

Equation (A.12) can be used directly to determine $\hat{T}_{st,BS}^{rad}$ using an iterative method. However, it is unclear from this expression exactly how the flame temperature is affected by radiation losses. A simplification proposed by Sohrab et al. is to assume that l_{O_2} is negligible, i.e. there is no radiation loss from the oxidizer stream. This assumption allows Equation (A.12) to be solved explicitly for $\hat{T}_{st,BS}^{rad}$ resulting in:

$$\hat{T}_{st,BS}^{rad} = \hat{T}_{st,BS} - \frac{Y_F^{\infty}\alpha(\alpha+\beta)}{\left(Y_F^{\infty}+\alpha\right)\left(Y_F^{\infty}-\alpha\right)}\frac{\Delta h_c}{c_p}\left\{\left[1+\frac{2l_f\left(Y_F^{\infty}-\alpha\right)}{\left(Y_F^{\infty}+\alpha\right)(\alpha+\beta)^2}\right]^{1/2}-1\right\}, \tag{A.16}$$

which is equivalent to Equation (23). The second term on the RHS of Equation (A.16) can be interpreted as a temperature reduction due to radiation losses.

The assumption that l_{O_2} is negligible may be questionable with the presence of soot particles in the oxidizer stream due to vitiation. In the framework of a counterflow diffusion flame, Equation (A.16) is appropriate due to the relatively small value of κ on the oxidizer side of the reaction. However, in cases with significant oxidizer stream vitiation with soot, Equation (A.12) may be more appropriate.

Bibliography

[1] DiNenno, *The SFPE Handbook of Fire Protection Engineering*, National Fire Protection Association (2002).

[2] McGrattan, K., "Fire Dynamics Simulator (Version 4) Technical Reference Guide," NIST Special Publication 1018, National Institute of Standards and Technology (2006).

[3] McCaffrey, B., "Flame Height," *The SFPE Handbook of Fire Protection Engineering*, National Fire Protection Association, pp. 2-1 – 2-8 (2002).

[4] Rasbash, D. J., and Drysdale, D. D., "Fundamentals of Smoke Production," *Fire Safety Journal*, Vol. 5 (1982) pp. 77-86.

[5] Karlsson, B., and Quintiere, J. G., *Enclosure Fire Dynamics*, (2000).

[6] Quintiere, J. G., "Fire Behavior in Building Compartments," *Proceedings of the Combustion Institute*, Vol. 29 (2002) pp. 181-193.

[7] Gottuk, D. T., Roby, R. J., and Beyler, C. L., "The Role of Temperature on Carbon Monoxide Production in Compartment Fires," *Fire Safety Journal*, Vol. 24 (1995) pp. 315-331.

[8] Gottuk, D. T., and Roby, R. J., "Effect of Combustion Conditions on Species Production," *The SFPE Handbook of Fire Protection Engineering, Third Edition*, National Fire Protection Association, pp. 2-54 – 2-82, 2002.

[9] Pitts, W. M., "Reactivity of Product Gases Generated in Idealized Enclosure Fire Environments," *Twenty-Fourth Symposium (International) on Combustion*, The Combustion Institute, (1992) pp. 1736-1746.

[10] Williams, F. A., "A Review of Some Theoretical Considerations of Turbulent Flame Structure," *Analysis and Numerical Methods for Investigation of Flow Fields with Chemical Reactions, Especially Related to Combustion, AGARD Conference Proceedings*, Vol. 164 (1975) pp. III-1 – III-25.

[11] Lutz, A., Kee, R., Grcar, J., and Rupley, F., "OPPDIF: A Fortran Program For Computing Opposed-Flow Diffusion Flames," Sandia National Laboratories, SAND96-8243 (1997).

[12] Cha, C. M., and Pitsch, H., "Higher-Order Conditional Moment Closure of Local Extinction and Reignition in Turbulent Combustion," *Combustion Theory and Modelling*, Vol. 6 (2002) pp. 425-437.

[13] Bastiaans, R. J. M., Martin, S. M., Pitsch, H., van Oijen, J. A., and de Goey, L. P. H., "Flamelet Analysis of Turbulent Combustion," *Computational Science – ICCS 2005,* Springer Berlin Heidelberg, (2005) pp. 64-71.

[14] Morehart, J. H., Zukoski, E. E., and Kubota, T., "Chemical Species Produced in Fires Near the Limit of Flammability," *Fire Safety Journal*, Vol. 19 (1992) pp. 177-188.

[15] Utiskul, Y., "Extensive Study of Wall-vent Compartment Fire Behavior Under Limited Ventilation," PhD Thesis, University of Maryland, (2006).

[16] Beyler, C. L., "Major Species Production by Solid Fuels in a Two Layer Compartment Fire Environment," *Fire Safety Science - Proceedings of the First International Symposium,* (1985) pp. 431-440.

[17] Beyler, C. L., "Major Species Production by Diffusion Flames in a Two Layer Compartment Fire Environment," *Fire Safety Journal*, Vol. 10 (1986) pp. 47-56.

[18] Takeda, H., and Kazuo, A., "Critical Phenomenon in Compartment Fires with Liquid Fuels," *Proceedings of the Combustion Institute,* Vol. 18 (1981) 519-527.

[19] Tolocka, M. P., Richardson, P. B., and Miller, J. H., "The Effect of Global Equivalence Ratio and Postflame Temperature on the Composition of Emissions from Laminar Ethylene/Air Diffusion Flames," *Combustion and Flame,* Vol. 118 (1999) pp. 521-536.

[20] Tuovinen, H., "CFD Modelling of Under-Ventilated Fires," Swedish National Testing and Research Institute, Fire Technology, SP Report 1996:41.

[21] Zukoski, E. E., Morehart, J. H., Kubota, T., and Toner, S. J., "Species Production and Heat Release Rates in Two-Layered Natural Gas Fires," *Combustion and Flame,* Vol. 83 (1991) pp. 325-332.

[22] Tuovinen, H., and Simonson, M., "Incorporation of Detailed Chemistry into CFD Modelling of Compartment Fires," Swedish National Testing and Research Institute, Fire Technology, SP Report 1999:03.

[23] Tuovinen, H., "CO Formation from Soot and CO_2 in the Hot Gas Layer," Swedish National Testing and Research Institute, Fire Technology, SP Report 2002:08.

[24] Koseki, H., and Mulholland, G. W., "The Effect of Diameter on the Burning of Crude Oil Pool Fires," *Fire Technology,* (1991) pp. 54-65.

[25] Koseki, H., "Radiation Properties and Flame Structure of Large Hydrocarbon Pool Fires," *Thirteenth Meeting of the UJNR Panel on Fire Research and Safety*, National Institute of Standards and Technology, (1997) pp. 41-50.

[26] Babrauskas, V., "Burning Rates," *The SFPE Handbook of Fire Protection Engineering*, National Fire Protection Association, pp. 3-1 – 3-15 (2002).

[27] Heskestad, G., "Fire Plumes," *The SFPE Handbook of Fire Protection Engineering*, National Fire Protection Association, pp. 2-9 – 2-19 (2002).

[28] Gengembre, E., Cambray, P., Karmed, D., and Bellet, J. C., "Turbulent Diffusion Flames with Large Buoyancy Effects," *Combustion Science and Technology*, Vol. 41 (1984) pp. 55-67.

[29] Weckman, E. J., and Strong, A. B., "Experimental Investigation of the Turbulence Structure of Medium-Scale Methanol Pool Fires," *Combustion and Flame*, Vol. 105 (1996) pp. 245-266.

[30] Tieszen, S. R., O'Hearn, T. J., Schefer, R. W., Weckman, E. J., and Blanchat, T. K., "Experimental Study of the Flow Field in and Around a One Meter Diameter Methane Fire," *Combustion and Flame*, Vol. 129 (2002) pp. 378-391.

[31] Shabbir, A., and George, W. K., "Experiments on a Round Turbulent Buoyant Plume," *Journal of Fluid Mechanics*, Vol. 275 (1994) pp. 1-32.

[32] Heskestad, G., "Dynamics of the Fire Plume," *Royal Society of London, Series A*, Vol. 356 (1998) pp. 2815-2833.

[33] Tieszen, S. R., "On the Fluid Mechanics of Fires," *Annual Review of Fluid Mechanics*, Vol. 33 (2001) pp. 67-92.

[34] Liñán, A., "The Asymptotic Structure of Counterflow Diffusion Flames for Large Activation Energies," *Acta Astronautica*, Vol. 1 (1974) 1007.

[35] Williams, F. A., "A Review of Flame Extinction," *Fire Safety Journal*, Vol. 3 (1981) pp. 163-175.

[36] Sohrab, S. H., Liñán, A., and Williams, F. A., "Asymptotic Theory of Diffusion-Flame Extinction with Radiant Loss from the Flame Zone," *Combustion Science and Technology*, Vol. 27 (1982) pp. 143-154.

[37] Peters, N., "Local Quenching Due to Flame Stretch and Non-Premixed Turbulent Combustion," *Combustion Science and Technology*, Vol. 30 (1983) 1-17.

[38] Peters, N. "Laminar Flamelet Concepts in Turbulent Combustion," *Twenty-First Symposium (International) on Combustion,* The Combustion Institute, (1986) pp. 1231-1250.

[39] Kim, J. S., and Williams, F. A., "Extinction of Diffusion Flames with Nonunity Lewis Numbers," *Journal of Engineering Mathematics*, Vol. 31 (1997) pp. 101-118.

[40] Law, C. K., and Chung, S. H., "Steady State Diffusion Flame Structure with Lewis Number Variations," *Combustion Science and Technology*, Vo. 29 (1982) pp. 129-145.

[41] Chung, S. H., and Law, C. K., "Structure and Extinction of Convective Diffusion Flames with General Lewis Numbers," *Combustion and Flame,* Vol. 52 (1983) pp. 59-79.

[42] Williams, F. A., "Progress in Knowledge of Flamelet Structure and Extinction," *Progress in Energy and Combustion Science,* Vol. 26 (2000) pp. 657-682.

[43] Wang, H. Y., Chen, W. H., Law, C. K., "Extinction of Counterflow Diffusion Flames with Radiative Heat Loss and Nonunity Lewis Numbers," *Combustion and Flame,* Vol. 148 (2007) pp. 100-116.

[44] Puri, I. K., and Seshadri, K., "Extinction of Diffusion Flames Burning Diluted Methane and Diluted Propane in Diluted Air," *Combustion and Flame,* Vol. 65 (1986) 137-150.

[45] Papas, P., Fleming, J. W., and Sheinson, R. S., "Extinction of Non-Premixed Methane- and Propane-Air Counterflow Flames Inhibited with CF_4, CF_3H, and CF_3Br," *Twenty-Sixth Symposium (International) on Combustion,* The Combustion Institute, (1996) pp. 1405-1411.

[46] Bundy, M., Hamins, A., and Ki Yong Lee, "Suppression Limits of Low Strain Rate Non-Premixed Methane Flames," *Combustion and Flame,* Vol. 133 (2003) pp. 299-310.

[47] Logue, J. M., "Characteristics of Low Strain Near Extinction Flames in μG and 1G," MS Thesis, University of Maryland (2003).

[48] Atreya, A., Agrawal, S., Sacksteder, K. R., and Baum, H. R., "Observations of Methane and Ethylene Diffusion Flames Stabilized Around a Blowing Porous Sphere Under Microgravity Conditions," *32rd Aerospace Sciences Meeting and Exhibit,* Reno, Nevada (1994).

[49] Pickett, K., Atreya, A., and Agrawal, S., "Radiation from Unsteady Spherical Diffusion Flames in Microgravity," *33rd Aerospace Sciences Meeting and Exhibit,* Reno, Nevada (1995).

[50] Atreya, A., Agrawal, S., Shamim, T., Pickett, K., Sacksteder, K. R., and Baum, H. R., "Radiant Extinction of Gaseous Diffusion Flames," 3rd Micro-Gravity Workshop (1995).

[51] Dietrich, D. L., Haggard Jr., J. B., Dryer, F. L., Nayagam, V., Shaw, B. D., and Williams, F. A., "Droplet Combustion Experiments in Spacelab," *Twenty-Sixth Symposium (International) on Combustion*, The Combustion Institute, (1996) pp. 1201-1207.

[52] Colantonio, R. O., and Nayagam, V., "Radiative Heat Loss Measurements During Microgravity Droplet Combustion," *Proceedings of the 1997 Technical Meeting of the Central States of the Combustion Institute*, (1997).

[53] Sung, C. J., Zhu, D. L., Tse, S. D., and Law, C. K., "On Burner-Supported, Spherical Diffusion Flames under Micro-Buoyancy Conditions," *36th Aerospace Sciences Meeting and Exhibit*, Reno, Nevada (1998).

[54] Atreya, A., and Agrawal, S., "Effect of Radiative Heat Loss on Diffusion Flames in Quiescent Microgravity Atmosphere," *Combustion and Flame*, Vol. 115 (1998) pp. 372-382.

[55] Mills, K., and Matalon, M., "Extinction of Spherical Diffusion Flames in the Presence of Radiant Loss," *Twenty-Seventh Symposium (International) on Combustion*, The Combustion Institute, (1998) pp. 2535-2541.

[56] Nayagam, V., Haggard Jr., J. B., Colantonio, R. O., Zhang, B. L., and Williams, F. A., "Microgravity n-Heptane Droplet Combustion in Oxygen-Helium Mixtures at Atmospheric Pressure," *AIAA Journal*, Vol. 36, No. 8 (1998) pp. 1369-1378.

[57] Tse, S. D., Zhu, D. L., Sung, C. J., and Law, C. K., "Microgravity Burner-Generated Spherical Diffusion Flames: Experiment and Computation," *37th AIAA Aerospace Sciences Meeting and Exhibit*, Reno, Nevada (1999).

[58] Yoo, S. W., Christiansen, E. W., and Law, C. K., "Oscillatory Extinction of Spherical Diffusion Flames: Micro-Buoyancy Experiment and Computation," *Proceedings of the Combustion Institute*, Vol. 29 (2002) pp. 29-36.

[59] Chernovsky, M. K., Atreya, A., and Sacksteder, K. R., "The Effect of Inert Substitution on Transient Spherical Diffusion Flames in Microgravity," *Proceedings of the 2006 Technical Meeting of the Central States Section of the Combustion Institute*, (2006).

[60] Santa, K. J., Chao, B. H., Sunderland, P. B., Taylor, J. L., Urban, D. L., Stocker, D. P., and Axelbaum, R. L., "Radiative Extinction of Gaseous Spherical Diffusion Flames in Microgravity,"*44th AIAA Aerospace Sciences Meeting and Exhibit*, Reno, Nevada (2006).

[61] Chernovsky, M. K., Atreya, A., and Im, H. G., "Effect of CO_2 Diluent on Fuel Versus Oxidizer Side of Spherical Diffusion Flames in Microgravity," *Proceedings of the Combustion Institute,* Vol. 31 (2007) pp. 1005-1013.

[62] Hamins, A., Bundy, M., Oh, C. B., and Kim, S. C., "Effect of Buoyancy on the Radiative Extinction Limit of Low-Strain-Rate Nonpremixed Methane-Air Flames," *Combustion and Flame,* Vol. 151 (2007) pp. 225-234.

[63] Sung, C. J., Zhu, D. L., and Law, C. K., "On Micro-Buoyancy Spherical Diffusion Flames and a Double Luminous Zone Structure of the Hydrogen/Methane Flame," *Twenty-Seventh Symposium (International) on Combustion,* The Combustion Institute, (1998) 2559-2566.

[64] Bai, H., Ibarreta, A. F., Sung, C. J., and T'ien, J. S., "Structure of Low-Stretch Methane Nonpremixed Flames," *Combustion and Flame,* Vol. 149 (2007) pp. 173-190.

[65] Cha, M. S., and Ronney, P. D., "Propagation Rates of Non-Premixed Edge Flames," *Combustion and Flame,* Vol. 146 (2006) pp. 312-328.

[66] Du, J., and Axelbaum, R. L., "The Effects of Flame Structure on CH4-O2-N2 Diffusion Flames," *Twenty-Sixth Symposium (International) on Combustion,* The Combustion Institute, (1996) pp. 1137-1142.

[67] Seiser, R., Pitsch, H., Seshadri, K., Pitz, W. J., and Curran, H. J., "Extinction and Autoignition of n-Heptane in Counterflow Configuration," *Proceedings of the Combustion Institute,* Vol. 28 (2000) pp. 2029-2037.

[68] Chen, R., and Axelbaum, R. L., "Scalar Dissipation Rate at Extinction and the Effects of Oxygen-Enriched Combustion," *Combustion and Flame,* Vol. 142 (2005) pp. 62-75.

[69] Williamson, J. W., Marshall, A. W., and Trouvé, A., "Developing Extinction Criteria for Fires," *5th Joint Meeting of the US Sections of the Combustion Institute,* Abstract and Presentation, San Diego, California (2007).

[70] Williams, B. A., "Brief Communication – Sensitivity of Calculated Extinction Strain Rate to Molecular Transport Formulation in Nonpremixed Counterflow Flames," *Combustion and Flame,* Vol. 124 (2001) pp. 330-333.

[71] Gore, J. P., Lim, J., Takeno, T., and Zhou, X. L., "A Study of the Effects of Thermal Radiation on the Structure of Methane/Air Diffusion Flames Using Detailed Chemical Kinetics," *Proceedings of the 5th ASME/JSME Joint Thermal Engineering Conference,* San Diego, California (1999).

[72] Chelliah, H. K., Law, C. K., Ueda, T., Smooke, M. D., and Williams, F. A., "An Experimental and Theoretical Investigation of the Dilution, Pressure and Flow-Field Effects on the Extinction Condition of Methane-Air-Nitrogen Diffusion Flames," *Twenty-Third Symposium (International) on Combustion,* The Combustion Institute, (1990) pp. 503-511.

[73] Christiansen, E. W., Tse, S. D., and Law, C. K., "A Computational Study of Oscillatory Extinction of Spherical Diffusion Flames," *Combustion and Flame,* Vol. 134 (2003) pp. 327-337.

[74] Bai, X. S., Fuchs, L., and Mauss, F., "Laminar Flamelet Structure at Low and Vanishing Scalar Dissipation Rate," *Combustion and Flame,* Vol. 120 (2000) pp. 285-300.

[75] Maruta, K., Yoshida, M., Guo, H., Ju, Y., and Niioka, T., "Extinction of Low-Stretched Diffusion Flame in Microgravity," *Combustion and Flame,* Vol. 112 (1998) pp. 181-187.

[76] Chan, S. H., Yin, J. Q., and Shi, B. J., "Structure and Extinction of Methane-Air Flamelet with Radiation and Detailed Chemical Kinetic Mechanism," *Combustion and Flame,* Vol. 112 (1998) pp. 445-456.

[77] Simmons, R. F., and Wolfhard, H. G., "Some Limiting Oxygen Concentrations for Diffusion Flames in Air Diluted with Nitrogen," *Combustion and Flame,* Vol. 1 (1957) pp. 155-161.

[78] Norton, T. S., Smyth, K. C., Miller, J. H., and Smooke, M. D., "Comparison of Experimental and Computed Species Concentration and Temperature Profiles in Laminar, Two-Dimensional Methane/Air Diffusion Flames," *Combustion Science and Technology,* Vol. 90 (1993) pp. 1-34.

[79] Ishizuka, S., Tsuji, H., "Experimental Study of Effect of Inert Gases on Extinction of Laminar Diffusion Flames," *International Proceedings of the Combustion Institute,* Vol. 18 (1981) pp. 695-703.

[80] Leonard, S., Mulholland, G. W., Puri, R., and Santoro, R. J., "Generation of CO and Smoke During Underventilated Combustion," *Combustion and Flame,* Vol. 98, (1994) pp. 20-34.

[81] Donnerhack, S., Peters, N., "Stabilization Heights in Lifted Methane-Air Jet Diffusion Flames Diluted with Nitrogen," *Combustion Science and Technology,* Vol. 41 (1984) pp. 101-108.

[82] Donbar, J. M., Driscoll, J. F., and Carter, C. D., "Reaction Zone Structure in Turbulent Nonpremixed Jet Flames-From CH-OH PLIF Images," *Combustion and Flame,* Vol. 122 (2000) pp. 1-19.

[83] Donbar,, J. M., Driscoll, J. F., and Carter, C. D., "Strain Rates Measured along the Wrinkled Flame Contour Within Turbulent Non-Premixed Jet Flames," *Combustion and Flame*, Vol. 125 (2001) 1239-1257.

[84] Gummalla, M, Vlachos, D. G., and Delichatsios, M. A., "Bifurcations and Structure of Surface Interacting Methane-Air Diffusion Flames," *Combustion and Flame*, Vol. 120 (2000) pp. 333-345.

[85] Chao, B. H., Law, C. K., and T'ien, J. S., "Structure and Extinction of Diffusion Flames with Flame Radiation," *Twenty-Third Symposium (International) on Combustion*, The Combustion Institute, (1990) pp. 523-531.

[86] Givi, P., Jou, W. -H., and Metcalfe, R. W., "Flame Extinction in a Temporally Developing Mixing Layer," *Twenty-First Symposium (International) on Combustion*, The Combustion Institute, (1986) pp. 1251-1261.

[87] Yi Wang, and Trouvé, A., "Direct Numerical Simulation of Non-Premixed Flame-Wall Interactions," *Combustion and Flame*, Vol. 144 (2006) pp. 461-475.

[88] Pitsch, H., "Improved Pollutant Predictions in Large-Eddy Simulations of Turbulent Non-Premixed Combustion by Considering Scalar Dissipation Rate Fluctuations," *Proceedings of the Combustion Institute*, Vol. 29 (2002) pp. 1971-1978.

[89] Pitsch, H., Riesmeier, E., Peters, N., "Unsteady Flamelet Modeling of Soot Formation in Turbulent Diffusion Flames," *Combustion, Science, and Technology*, Vol. 158 (2000) pp. 389-406.

[90] Kronenburg, A., and Kostka, M., "Modeling Extinction and Reignition in Turbulent Flames," *Combustion and Flame*, Vol. 143 (2005) pp. 342-356.

[91] Ihme, M., Cha, C. M., Pitsch, H., "Prediction of Local Extinction and Re-Ignition Effects in Non-Premixed Turbulent Combustion Using a Flamelet/Progress Variable Approach," *Proceedings of the Combustion Institute*, Vol. 30 (2005) pp. 793-800.

[92] Mizukami, T., Utiskul, Y., and Quintiere, J. G., "Application of Zone models for Under-ventilated Compartment Fires," *International Mechanical Engineering Congress & Exposition (ASME) Conference*, Chicago, IL (2006).

[93] Mizukami, T., Utiskul, Y., and Quintiere, J. G., "Application of Zone models for Under-ventilated Compartment Fires," *31st International Symposium Combustion Institute*, Poster and Abstract**,** Heidelberg, Germany (2006).

[94] Beyler, C., "Flammability Limits of Premixed and Diffusion Flames," *The SFPE Handbook of Fire Protection Engineering*, National Fire Protection Association, pp. 2-147 – 2-159 (2002).

[95] Yeung, P. K., Girimaji, S. S., and Pope, S. B., "Straining and scalar dissipation on material surfaces in turbulence- Implications for flamelets," *Combustion and Flame*, Vol. 79 (1990) pp. 340-365.

[96] Dobrotka, S., "Counter-Flow Slot Burner Design and Fabrication," Final Report 2nd Practical Semester, University of Maryland (2005).

[97] Poinsot, T., Veynante, D., *Theoretical and Numerical Combustion*, (2001).

[98] Santoro, R. J., Yeh, T. T., Horvath, J. J., Semerjian, H. G., "The Transport and Growth of Soot Particles in Laminar Diffusion Flames," *Combustion Science and Technology*, Vol. 53 (1987) pp. 89-115.

[99] Lignell, D. O., Chen, J. H., Smith, P. J., Lu, T., Law, C. K., "The Effect of Flame Structure on Soot Formation and Transport in Turbulent Nonpremixed Flames using Direct Numerical Simulation," *Combustion and Flame*, Vol. 151 (2007) pp. 2-28.

[100] Grosshandler, W. L., "Radiant Heat Transfer in Nonhomogeneous Gases – A Simplified Approach," *International Journal of Heat and Mass Transfer*, Vol. 23 (1980) pp. 1447.

[101] Narayanan, P., and Trouvé, A., "Radiation-Driven Flame Weakening Effects in Sooting Turbulent Diffusion Flames," *Proceedings of the Combustion Institute*, (2008).

[102] Trouvé, A., "CFD Modeling of Large-Scale Pool Fires," *Fire Safety Science*, Vol. 9 (2008).